

Evaluation of the neurotoxicity of pentachlorophenol and its active metabolites on SH-SY5Y neuroblastoma cells

by

Desiree Linda Fraser

Dissertation submitted in fulfilment of the requirements for the degree

Magister Scientiae

in

Physiology

in the

Faculty of Health Sciences

at the

University of Pretoria

Supervisor

Prof V Steenkamp

Co-supervisor

Dr BA Stander

2017

Declaration

University of Pretoria

Faculty of Health Sciences

Department of Physiology

I, Desiree Linda Fraser,

Student number: 12168450

Subject of the work: Evaluation of the neurotoxicity of pentachlorophenol and its active metabolites on SH-SY5Y neuroblastoma cells

Declare that,

1. I understand what plagiarism entails and am aware of the University's policy in this regard.
2. I declare that this project (e.g. essay, report, project, assignment, dissertation, thesis etc.) is my own, original work. Where someone else's work was used (whether from a printed source, the internet or any other source) due acknowledgement was given and reference was made according to the departmental requirements.
3. I did not make use of another student's previous work and submitted it as my own.
4. I did not allow and will not allow anyone to copy my work with the intention of presenting it as his or her own work.

Signature _____

Acknowledgements

“Great are the works of the Lord, studied by all who delight in them” – Psalm 111:2

“For from Him and through Him and for Him are all things. To Him be the glory forever! Amen.” – Romans 11:36

First and foremost, thank you to my Lord and Saviour Jesus Christ. I would never have been able to make it through my studies without Him. He has never let me down.

I would also like to extend my sincerest gratitude to the following people:

My supervisor, Prof Steenkamp – thank you for your valuable input and all the knowledge you have passed on to me, and for your dedication to me as a student.

My co-supervisor, Andre – thank you for the time you made to help me with so many things, and for your patience with me, even with the silliest of questions. I couldn't have asked for a better co-supervisor.

To Prof Duncan Cromarty and Dr Werner Cordier for their advice and assistance.

To my labmate, Trophie, who helped me more times than I can count. Thank you for all of your help, for all the laughs, listening to all my nonsense, for your company during long nights in the lab, and solace during stress and despair.

To all my labmates in Physiology and Pharmacology, who endured the stress of labwork and postgrad with me. Thank you for making it an amazing journey.

To Prof du Toit, who was the first to believe in me enough to begin my postgraduate journey – thank you for giving me the opportunity in honours.

To my amazing parents – words cannot express my gratitude for all of your unwavering support throughout my academic career. I would never have come this far without you. Also, to my brother, Kevin – thank you for putting up with all my complaints, random sleep deprived thoughts, and terrible science puns.

Abstract

Pentachlorophenol (PCP) is an organochloride pesticide that is ubiquitous within the environment due to its chemical stability. It is classified as a persistent organic pollutant, and has been predominantly used in the wood preservation industry. Workers and populations living close to PCP usage and production are exposed to it via inhalation and dermal absorption, and ingestion of contaminated food and water. It is lipophilic and is able to accumulate within various bodily systems, including the brain. Adverse effects of PCP have been reported to varying degrees in the immune, hepatic, and endocrine systems. Although neurological symptoms have been associated with PCP exposure, knowledge of mechanisms of neurotoxicity is limited. Elucidation of molecular mechanisms at a cellular level within neuronal cells is required to contribute toward the current gap in the knowledge of PCP neurotoxicity. The aim of the study was to evaluate the effects of PCP and its active metabolites, tetrachloro-1,4-benzoquinone (TCBQ) and tetrachlorohydroquinone (TCHQ) in human neuroblastoma SH-SY5Y cells.

Effects on cell proliferation were assessed using the sulforhodamine B (SRB) assay. Flow cytometric analysis was employed to investigate effects on cell cycle using propidium iodide (PI), mode of cell death using Annexin V-FITC and PI, reactive oxygen species (ROS) using dichlorofluorescein, and mitochondrial membrane potential ($\Delta\psi_m$) using JC-1 fluorescence. Caspase-3 activity was assessed with Ac-DEVD-AMC, and glutathione (GSH) with monochlorobimane fluorescence. Effects on acetylcholinesterase (AChE) were assessed *in vitro* using the Ellman esterase assay, as well as *in silico* via molecular docking and molecular dynamics simulation.

The IC_{50} concentrations of PCP, TCBQ and TCHQ were 80.0, 35.4, and 63.7 μM , respectively. Cell cycle disruptions were revealed in the form of a G1 block and a G2/M block as a result of PCP and TCHQ exposure, respectively, while TCBQ resulted in a prolonged S phase traverse. The predominant mode of cell death of PCP was necrosis, while TCBQ induced apoptosis. Exposure to TCHQ resulted in one of two fates, being either predominantly apoptotic or necrotic cell death. Decreased $\Delta\psi_m$ was an early event for all compounds, however, differed in their involvement of inducing ROS. Oxidative stress was an evident mechanism of PCP and TCBQ toxicity, as increased ROS was accompanied by lowered GSH, while

reductive stress leading to subsequent oxidative stress was indicated by increased ROS and GSH for TCHQ. All compounds yielded increased caspase-3 activity. The fate of TCHQ exposed cells was postulated as a switch from apoptosis to necrosis due to overwhelming ROS insult on apoptotic machinery, surpassing a threshold for apoptosis capability. Inhibition of AChE was observed by only TCHQ *in vitro*, the Ellman IC₅₀ of which was 79.7 μM. *In silico* assessment supported a hypothesis of TCHQ inhibition of AChE, with TCHQ-acetate bound ligands binding AChE receptors with binding energies corresponding to the Ellman IC₅₀. Binding stability was confirmed by molecular dynamics.

Pentachlorophenol and its active metabolites exhibited different mechanisms of toxicity toward neuronal cells, leading to different modes of cell death. A new hypothesis for the molecular mechanism of TCHQ AChE inhibition was developed, and sets a platform for further investigation.

Key words: *Neurotoxicity, acetylcholinesterase inhibition, pentachlorophenol (PCP), tetrachloro-1,4-benzoquinone (TCBQ), tetrachlorohydroquinone (TCHQ)*

Table of contents

Abstract.....	i
List of figures.....	vi
List of tables.....	x
List of abbreviations.....	xi
Chapter 1: Literature review.....	1
1.1 Pesticides.....	1
1.2 Pentachlorophenol.....	2
1.3 Pentachlorophenol usage and regulations.....	5
1.4 Pharmacokinetics of pentachlorophenol.....	7
1.5 Effects of pentachlorophenol and its active metabolites in the body.....	9
1.6 Neurotoxicity.....	10
1.6.1 <i>In vitro</i> methods used to assess neurotoxicity.....	11
1.6.2 Processes involved in neurotoxicity.....	12
1.7 <i>In silico</i> ligand binding analysis.....	24
1.8 Study rationale.....	27
1.9.1 Aim.....	28
1.9.2 Objectives.....	28
Chapter 2: Methods and materials.....	30
2.1. Cell maintenance.....	30
2.2. Cell seeding and exposure.....	31
2.3. Detection of cytotoxicity.....	31
2.4. Cell cycle analysis.....	34
2.5. Mode of cell death.....	36
2.6. Caspase activity.....	37
2.7. Cell morphology.....	39
2.8. Reactive oxygen species production.....	40

2.9. Mitochondrial membrane potential	41
2.10. Intracellular reduced glutathione content	42
2.11. Acetylcholinesterase inhibitory activity	43
2.11.1. Ellman esterase assay	43
2.11.2. Molecular docking	45
2.11.3. Molecular dynamics simulation.....	46
2.12. Statistical analysis	46
Chapter 3: Results.....	48
3.1. Cell proliferation	48
3.2. Cell cycle analysis	51
3.3. Mode of cell death	60
3.4. Caspase activity	63
3.5. Cell morphology	64
3.6. Reactive oxygen species	68
3.7. Mitochondrial membrane potential	70
3.8. Reduced glutathione content	72
3.9. Acetylcholinesterase activity	73
3.9.1. Ellman esterase assay.....	73
3.9.2. Molecular docking	75
3.9.3. Molecular dynamics simulation.....	85
Chapter 4: Discussion	86
4.1. Detection of cytotoxicity	86
4.2. Cell cycle	87
4.3. Mode of cell death	93
4.4. Reactive oxygen species, mitochondrial membrane potential, and reduced glutathione content	100
4.5. Acetylcholinesterase activity	105

4.5.1. Ellman esterase assay.....	105
4.5.2. <i>In silico</i> assessment.....	106
Chapter 5: Conclusion.....	111
Chapter 6: Limitations to the study and future research.....	113
References.....	114
Appendix I: Ethical approval.....	146
Appendix II: Reagents and preparation.....	147

List of figures

Figure 1: Metabolism of pentachlorophenol (PCP). ²⁸ The active metabolites of PCP are tetrachloro-1,4-benzoquinone (TCBQ) and tetrachlorohydroquinone (TCHQ). Reactive oxygen species are a by-product of PCP metabolism.	4
Figure 2: Mechanisms of cell death. Multiple pathways may lead to apoptosis or necrosis, involving cascades of cell death related events and their crosstalk. Arrows indicate flow of events	14
Figure 3: Cell cycle phases and checkpoints. Cells in G1 phase undergo early preparation for mitosis, and transition through the G1/S checkpoint to S phase where DNA replication occurs. Cells then enter into G2, where further preparations for mitosis occur. Cells then pass through the G2/M checkpoint into M phase where mitosis occurs.....	15
Figure 4: Depiction of acetylcholinesterase (AChE) action. Acetylcholine (ACh) is cleaved in the AChE active site gorge into acetate and choline. Inhibitor molecules capable of entering and binding the active site may inhibit ACh cleavage.....	23
Figure 5: Schematic summary of project.	29
Figure 6: Experimental plate layout used for the SRB assay when conducted in a 96-well microplate.....	34
Figure 7: Quadrant compartmentalisation found in a scatter plot of Annexin V-FITC and PI fluorescence, indicating mode of cell death.....	37
Figure 8: Depiction of Ellman esterase assay reaction. ²⁰⁸	43
Figure 9: Dose-response curves of cells treated with A) PCP, B) TCBQ, and C) TCHQ.	49
Figure 10: Dose-response curve in cells treated with DDT.....	50
Figure 11: Histograms depicting stages in the cell cycle after 12 h exposure to A) DMSO (vehicle control), B) PCP, C) TCBQ, and D) TCHQ.	52
Figure 12: Average percent events for each cell cycle phase after 12 h exposure to PCP, TCBQ, or TCHQ. Significance of changes relative to vehicle control of the same cell cycle phase are indicated as ** = $p < 0.01$, *** = $p < 0.001$	53
Figure 13: Histograms depicting stages in the cell cycle after 24 h exposure to A) DMSO (vehicle control), B) PCP, C) TCBQ, and D) TCHQ.	54

Figure 14: Average percent events for each cell cycle phase after 24 h exposure to PCP, TCBQ, or TCHQ. Significance of changes relative to vehicle control of the same cell cycle phase are indicated as * = $p < 0.05$, ** = $p < 0.01$, *** = $p < 0.001$. . 55

Figure 15: Histograms depicting stages in the cell cycle after 48 h exposure to A) DMSO (vehicle control), B) PCP, C) TCBQ, and D) TCHQ. 56

Figure 16: Average percent events for each cell cycle phase after 48 h exposure to PCP, TCBQ, or TCHQ. Significance of changes relative to vehicle control of the same cell cycle phase are indicated as * = $p < 0.05$, ** = $p < 0.01$, *** = $p < 0.001$. . 57

Figure 17: Histograms depicting stages in the cell cycle after 48 h exposure to A) DMSO (vehicle control), B) 60 μM , C) 70 μM , and D) 90 μM PCP. 58

Figure 18: Average percent events for each cell cycle phase after 48 h exposure to 60, 70, 80, or 90 μM PCP. Significance of changes are relative to the vehicle control. ** = $p < 0.01$ and *** = $p < 0.001$ 59

Figure 19: Annexin V-FITC/PI staining scatter plots after 48 h exposure to A) DMSO (vehicle control), B) PCP, C) TCBQ, and D) TCHQ. FL3 log indicates PI fluorescence, and FL1 log indicates Annexin V-FITC fluorescence..... 61

Figure 20: Percent of various states following 48 h exposure to vehicle control (DMSO), PCP, TCBQ and TCHQ (1 and 2 indicate different fates). Significance is indicated by * = $p < 0.05$, ** = $p < 0.01$, and *** = $p < 0.001$ 62

Figure 21: Fold change in caspase-3 activity relative to vehicle control (DMSO) following 48 h exposure to PCP, TCBQ, TCHQ or staurosporine (positive control). Significance of changes compared to vehicle control are indicated as *** = $p < 0.001$ 63

Figure 22: Light microscopy images of SH-SY5Y cells following 48 h exposure to A) DMSO (vehicle control), B) PCP, C) TCBQ, D) TCHQ, and E) DDT (100x magnification). 66

Figure 23: Fluorescence microscopy images of SH-SY5Y cells at 400x magnification following 48 h exposure to A) DMSO, B) PCP, C) TCBQ and D) TCHQ. Fluorescent dyes used were Hoechst 33342, acridine orange and PI. Merge indicates superimposed images of the three dyes. 67

Figure 24: Fold change in reactive oxygen species (ROS) relative to vehicle control (DMSO) following 4, 24, or 48 h exposure to PCP, TCBQ, TCHQ, or AAPH (positive control). Significance of changes compared to the vehicle control of the same time point are indicated as ** = $p < 0.01$, and *** = $p < 0.001$ 69

Figure 25: Fold change in mitochondrial membrane potential ($\Delta\psi_m$) relative to DMSO (vehicle control) following 4, 24, or 48 h exposure to PCP, TCBQ, TCHQ or rotenone (positive control). Significance of changes compared to the vehicle control of the same time point are indicated as * = $p < 0.05$, ** = $p < 0.01$, and *** = $p < 0.001$ 71

Figure 26: Change in GSH levels relative to DMSO (vehicle control) following 48 h exposure to PCP, TCBQ, TCHQ, or NEM (positive control). Significance of changes compared to the vehicle control are indicated as ** = $p < 0.01$ 72

Figure 27: Effect of cytotoxic IC_{50} concentrations of PCP, TCBQ, and TCHQ, (concentrations determined from the SRB assay), on AChE activity. Significance is indicated by † = $p < 0.01$ when compared to negative control (N/C), and ** = $p < 0.01$ and *** = $p < 0.001$ when compared to DMSO (vehicle control). 74

Figure 28: Inhibitory activity of TCHQ on AChE. The Ellman IC_{50} was determined as $79.7 \pm 7.7 \mu M$ 74

Figure 29: Box plots showing binding energies of ligands docked to 47 AChE receptor molecules. Whiskers indicate maximum and minimum, box edges indicate first and third quartiles and horizontal lines inside boxes indicate medians of binding energy..... 78

Figure 30: Docked ligands in AChE receptors with surrounding amino acid and ribbon structures. Ligands in receptors are: A) PCP-Ac in 1ut6, B) Ac-TCHQ-Ac in 1qti, C) TCHQ-Ac in 1zgc and D) Ch-TCHQ-Ch in 1acj..... 80

Figure 31: Docked ligands in AChE receptors. Receptor surfaces are shown for visualisation of ligand positioning within the active site gorge. Ligands in receptors are: A) PCP-Ac in 1ut6, B) Ac-TCHQ-Ac in 1qti, C) TCHQ-Ac in 1zgc and D) Ch-TCHQ-Ch in 1acj. 81

Figure 32: Docked ligands (blue) superimposed with ACh (green). Ligand and ACh surfaces are shown for overlap visualisation. Ligands in receptors are: A) PCP-Ac in 1ut6, B) Ac-TCHQ-Ac in 1qti, C) TCHQ-Ac in 1zgc and D) Ch-TCHQ-Ch in 1acj. ... 82

Figure 33: Docked ligands (beige) superimposed with receptor's original ligand (blue). Docked ligands superimposed with original ligands are: A) PCP-Ac with tacrine derivative, B) Ac-TCHQ-Ac with galanthamine, C) TCHQ-Ac with (RS)-tacrine(10)-huprydone and D) Ch-TCHQ-Ch with tacrine. 83

Figure 34: Visualisation of ligand PCP-Ac docked to receptor 1ut6, superimposed with ACh. Atoms of AChE are shown, with focus on the ligands. 84

Figure 35: Visualisation of ligand PCP-Ac docked to receptor 1ut6, superimposed with ACh. Surface of AChE is shown to visualise ligand atoms within the active site gorge.	84
Figure 36: Theorised molecular mechanism of TCHQ inhibition of AChE.	107
Figure 37: Summary of pathways of PCP, TCBQ and TCHQ.	112

List of tables

Table 1: Percent changes between cell states compared to DMSO following 48 h exposure to PCP, TCBQ, TCHQ (1 and 2 indicate different fates), and the positive control (DDT).	62
Table 2: Simplified and IUPAC names of ligands suspected to be implicated in AChE inhibition.	75
Table 3: Chemical structures and simplified names of PCP and TCHQ structural analogues hypothesised to be involved in AChE inhibition. Red = acetate addition, blue = choline addition.....	76
Table 4: Summary of average binding energies from two molecular dynamics simulations.....	85
Table 5: Summary of literature for PCP induced mode of cell death in different cell lines.....	96

List of abbreviations

°C	Degrees Celsius
%	Percent
α	Alpha
Δψ _m	Mitochondrial membrane potential
μg	Microgram
μL	Microliter
μM	Micromolar
3D	Three dimensional
Ac-DEVD-AMC	N-Acetyl-Asp-Glu-Val-Asp-7-amido-4-Methylcoumarin
ACh	Acetylcholine
AChE	Acetylcholinesterase
AMBER	Assisted Model Building with Energy Refinement
APC	Anaphase promoting complex
ATCC	American Type Tissue Culture
ATCh	Acetylthiocholine
ATChI	Acetylthiocholine iodide
atm	Atmospheric pressure
ATM	Ataxia telangiectasia mutated
ATP	Adenosine triphosphate
ATR	Ataxia telangiectasia and Rad3-related protein
Bach1	BTB and CNC homolog 1
Bak	Bcl-2 homologous antagonist/killer
Bax	Bcl-2-associated X protein
BFA	Bioconcentration factor
Bid	BH3 interacting-domain death agonist
BSA	Bovine serum albumin
Ca ²⁺	Calcium
CaCl ₂	Calcium chloride

CAD	Caspase-activated DNase
CAK	CDK activating kinase
CDC	Cell division cycle
CDK	Cyclin dependent kinase
CGN	Cerebellar granule neuron
Chk	Checkpoint kinase
CKI	Cyclin-dependent kinase inhibitor
CNS	Central nervous system
CO ₂	Carbon dioxide
cyt <i>c</i>	Cytochrome <i>c</i>
DCF	2,7-Dichlorofluorescein
DCFDA	2,7-Dichlorofluorescein diacetate
DDT	Dichlorodiphenyltrichloroethane
DISC	Death-inducing signalling complex
DMEM	Dulbecco's Modified Eagle Medium
DMSO	Dimethyl sulfoxide
DNA	Deoxyribonucleic acid
DR5	Death receptor 5
DSB	Double strand break
DTNB	5,5'-dithiobis(2-nitrobenzoic acid)
E2F	Elongation factor 2
EDTA	Ethylenediaminetetraacetic acid
EPA	Environmental Protection Agency
ER	Endoplasmic reticulum
ERK	Extracellular signal-regulated kinase
EU	European Union
FADD	Fas-associated protein with death domain
Fas	Apoptosis stimulating fragment
FCS	Foetal calf serum

FITC	Fluorescein isothiocyanate
FLIP _L	FLICE-Like inhibitory protein
fs	Femtosecond
g	Gram
<i>g</i>	Centrifugal force
G1	Gap phase 1 of interphase
G2	Gap phase 2 of interphase
GADD45	Growth Arrest and DNA Damage-inducible 45
GLU	Glutamic acid
GMO	Genetically modified organism
GPU	Graphics processing unit
GSH	Glutathione
GSSG	Glutathione disulfide
HCl	Hydrochloric acid
HEPES	4-(2-hydroxyethyl)-1-piperazineethanesulfonic acid
HIS	Histidine
HMGB	High mobility group protein
H ₂ O ₂	Hydrogen peroxide
IAP	Inhibitor of apoptosis protein
IC ₅₀	Concentration at which cell growth is inhibited by half
IgF-Bp3	Insulin-like growth factor-binding protein 3
IUPAC	International Union of Pure and Applied Chemistry
JC-1	5,5,'6,6'-tetrachloro-1,1,3,3'-tetraethylbenzimidazolylcarbocyanine iodide
JNK	c-Jun N-terminal kinase
K	Kelvin
KCl	Potassium chloride
Keap1	Kelch-like ECH-associated protein 1
kg	Kilogram
kJ	Kilojoules

K _m	Michaelis constant (Concentration of a substrate for which the rate of reaction is half of V _{max})
L	Liter
LC ₅₀	Lethal concentration at which 50% of a population is killed in a given time frame
LD ₅₀	Lethal dose at which 50% of a population is killed in a given time frame
LINCS	Linear Constraint Solver
M	Molar
m ³	Cubic metre
mM	Milimolar
M phase	Mitotic phase of cell cycle
MAD	Mitotic arrest deficient
MAPK	Mitogen-activated protein kinase
MCB	Monochlorobimane
MCM	Minichromosome maintenance protein complex
MD	Molecular dynamics
MEA	Multilateral environmental agreements
mg	Milligram
MgCl ₂ .6H ₂ O	Magnesium chloride hexahydrate
min	Minutes
mL	Milliliter
mRNA	Messenger RNA
NaCl	Sodium chloride
NADPH	Nicotinamide adenine dinucleotide phosphate
Na-PCP	Sodium-pentachlorophenol
NEM	n-ethylmaleimide
NF-κB	Nuclear factor kappa-light-chain-enhancer of activated B cells
NIP	National Implementation Plan
nm	Nanometer
NOAEL	No-observed-adverse-effects level

Nrf2	Nuclear factor (erythroid-derived 2)-like 2
NS	Nervous system
PARP-1	Poly (ADP-ribose) polymerase 1
PBS	Phosphate buffered saline
PCP	Pentachlorophenol
PDB	Protein Data Bank
PDI	Protein disulfide isomerase
PHE	Phenylalanine
PI	Propidium iodide
PMSF	Phenylmethylsulfonyl fluoride
POP	Persistent organic pollutant
ps	Picosecond
PS	Phosphatidylserine
QSAR	Quantitative structure–activity relationship
Rad3	DNA repair helicase
RB	Retinoblastoma
RNA	Ribonucleic acid
RNase	Ribonuclease
ROS	Reactive oxygen species
SAICM	Strategic Approach to International Chemicals Management
SMAC	Second mitochondria-derived activator of caspases
SMILES	Simplified molecular-input line-entry system
SOD	Superoxide dismutase
S phase	DNA synthesis phase of interphase
SRB	Sulforhodamine B
TCA	Trichloroacetic acid
TCBQ	Tetrachloro-1,4-benzoquinone
TCHQ	Tetrachlorohydroquinone
TNB	5-thio-2-nitrobenzoate

TNF	Tumour necrosis factor
TRP	Tryptophan
TYR	Tyrosine
U	Enzyme unit
UbcH7	Ubiquitin-conjugating enzyme H7
UN	United Nations
WHO	World Health organisation
V _{max}	Maximum rate of reaction
v/v	Volume/volume ratio

Chapter 1: Literature review

1.1 Pesticides

Humans have generated and used many multitudes of approaches to pest control since the first agricultural revolution.¹ As the human population began to increase exponentially, it became increasingly crucial to produce a maximum yield of crops in order to sustain continued growth, and thus emerged the industry of crop protection via pesticides, which has continued to evolve along with human population expansion.² The first generation of chemical pesticides included highly toxic compounds such as hydrogen cyanide and arsenical compounds.³ Use of these was discontinued due to toxicity and inefficacy, and thus followed a second generation of synthetically manufactured organic compounds (compounds containing carbon).⁴ Categories that fall within this second generation include organophosphates and organochlorides, each of which contain large subsets of compounds with varying degrees of effectiveness, toxicity, mechanisms of action, and accompanying regulations.⁵ These pesticides have the potential to be extremely harmful to the environment and human health, a well-known example of which is the organochloride, dichlorodiphenyltrichloroethane (DDT), which has been banned in most countries due to its various modes of toxicity, including potent endocrine disruption.⁶ Due to the growing understanding of the dangers of pesticides used in agriculture and related industries, there have been a number of companies, congresses and treaties established that review evidence of the risks of individual pesticides, and put into motion suggestions of safety regulations, restrictions or bans that countries' industries should follow.⁷⁻⁹ These processes can however be very lengthy, and a large wealth of information is required before decisions are made. Data for these decisions can come either directly from the company's research department, or from independent studies.

Pesticides may be classified according to their chemical structures, with some of the major groups including organophosphates, organochlorides, pyrethroids, carbamates, and growth regulators.⁵ Organophosphate pesticides have a hydrocarbon base and contain a phosphate group. They act on the central nervous system (CNS) of insects and other living organisms by irreversibly inhibiting

acetylcholinesterase (AChE) activity, thereby causing parasympathetic overstimulation and damage to neuronal functioning, ultimately leading to death at high enough concentrations.¹⁰ Organochloride pesticides are chlorinated hydrocarbon molecules that can act against all pest classes with multiple mechanisms of action.¹¹ Pyrethroids are synthetic analogues of the compound pyrethrin which is found naturally in the flower *Chrysanthemum cinerariaefolium*. Pyrethroids are used as insecticides, and act as neurotoxins by interrupting the closure of axonal membrane sodium channels.¹² Carbamate pesticides are compounds derived from carbamic acid, which act similarly to organophosphates, however the reaction with AChE is reversible.¹³

The magnitude of pesticide usage has changed over the years with the emergence of genetically modified (GMO) crops, where seeds are genetically altered to be more resilient to either pesticides or pests themselves.¹⁴ Genetic modification to seeds may result in crop resistance to herbicidal pesticides, allowing for greater application levels of compounds acting against unwanted plant growth.¹⁵ Alternatively, or additionally, seeds may be modified in such a way that the plants may be more resilient to pests themselves, resulting in a lower need for application of insecticides, and thus lower levels of this type of pesticide per plantation acre are necessary. Although the relative levels of insecticide used on crops may be decreasing due to GMO advancement, this does not necessarily translate into a decrease in absolute pesticide levels as the continually expanding human population requires the continual growth of agricultural yield, and thus ever growing plantation sizes.¹⁶

1.2 Pentachlorophenol

Pentachlorophenol (PCP) is an organochloride, which has been commonly used as a pesticide in the agricultural, textile, and wood preservation industries, as well as in disease vector control.¹⁷ In 1989, the World Health Organisation (WHO) stated that approximately 30 000 tonnes of PCP was manufactured per year. Production has largely diminished in the last few decades due to the increasing discoveries of the various dangers of PCP.¹⁸ The WHO has classified it as highly hazardous, and its use is largely restricted in many first world countries.¹⁹ Although new environmental insults in compliant areas are limited due to its restriction, it is still problematic as it is

considered to be a persistent organic pollutant (POP) due to its chemical structure being highly stable and not easily degradable.²⁰ It is lipophilic, and accumulates in fats within food substances, and is thus increased in concentration at each trophic level.²⁰ In addition, many third world countries do not take heed of toxicity warnings, and continue to use PCP regardless, particularly in wood preservation, as it is often cheaper and easier to use than alternative compounds.²¹ This results in exposure levels of workers to PCP in these industries to be dangerously high.²² Even individuals who are not closely affiliated with high exposure levels may be in danger of PCP exposure due to its ubiquitous environmental pollutant status in soil, water, air and food.¹⁸

Pentachlorophenol has a chemical formula of C_6Cl_5OH , and contains an aromatic ring (Figure 1). The hydroxyl group is commonly substituted with sodium, forming sodium pentachlorophenol (Na-PCP), which is highly soluble in water.²³ Pentachlorophenol is produced either by the chlorination of phenols, or by hydrolysis of hexachlorobenzene.²⁴ During manufacturing, impurities can arise, including variations of polychlorinated phenolic substances, particularly dioxins. Pure PCP is volatile, and is readily soluble in many organic solvents, as well as having a water solubility of 10-20 mg/mL.^{18,25} Levels of PCP have been reported for various different environmental sources, and have been described by the International Programme on Chemical Safety.¹⁷ Levels in general urban air may range between 5.7-7.8 ng/m³ (0.02-0.03 pM), groundwater $\leq 23 \mu\text{g/L}$ (0.08 μM), and surface water 31.9 $\mu\text{g/L}$ (0.12 μM). These values increase the closer sampling is from the origin of PCP use or production. High levels of PCP in soil and plants range between 100 $\mu\text{g/kg}$ to 45.6 mg/kg. Animals such as fish and birds become contaminated when they come into contact with PCP, particularly in areas of high PCP use such as in wood preservation activities. In 2007, samples of guar gum which originated from India were found to be contaminated with excessively high levels of PCP.²⁶ Guar gum is used as a stabiliser in many food substances, and the detection of levels of PCP greater than 1 000 times that of acceptable concentrations in these samples raised great concern for contamination.²⁷

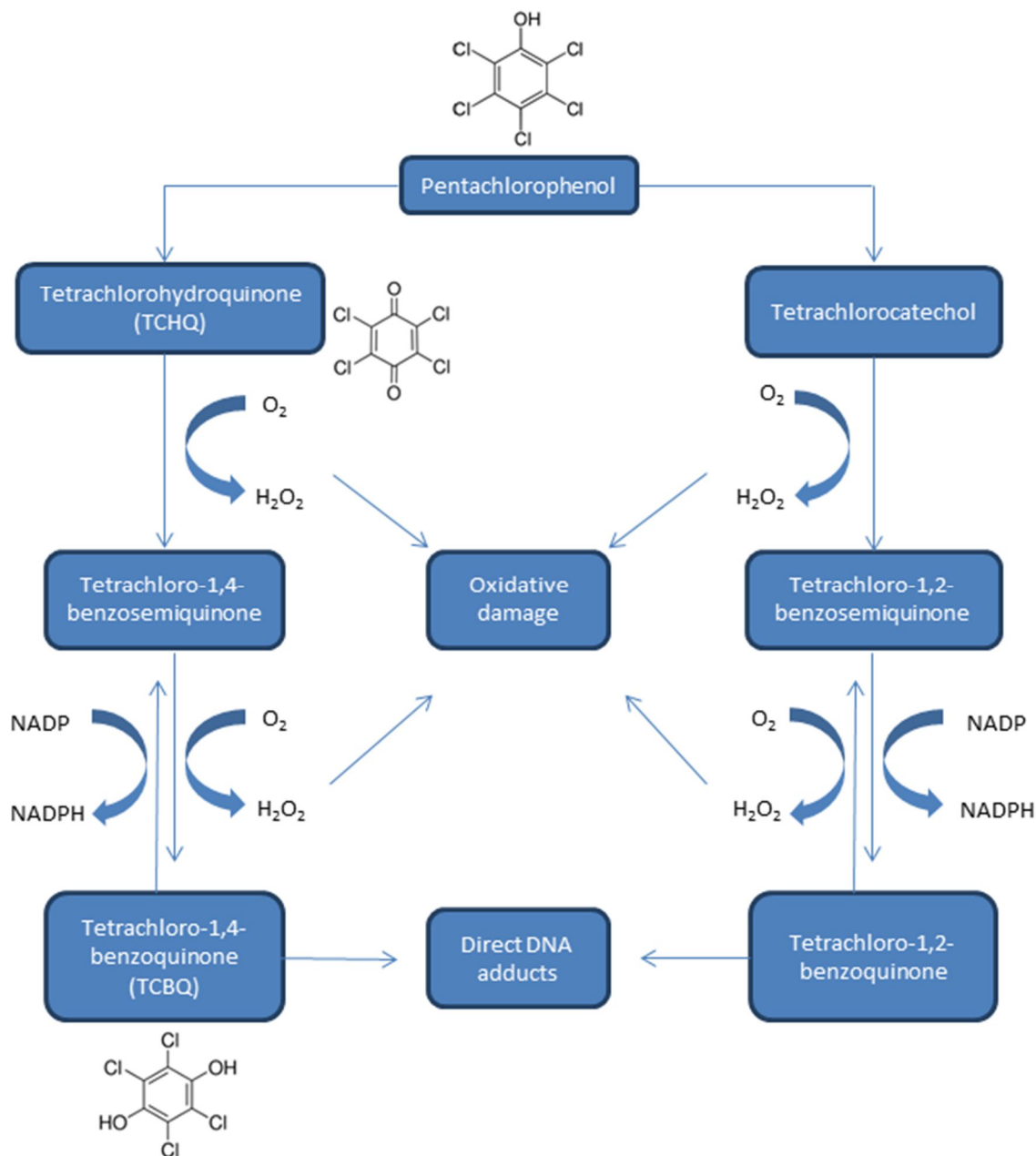


Figure 1: Metabolism of pentachlorophenol (PCP).²⁸ The active metabolites of PCP are tetrachloro-1,4-benzoquinone (TCBQ) and tetrachlorohydroquinone (TCHQ). Reactive oxygen species are a by-product of PCP metabolism. NADP - nicotinamide adenine dinucleotide phosphate (oxidised), NADPH -Nicotinamide adenine dinucleotide phosphate (reduced), O₂ - oxygen, H₂O₂ – hydrogen peroxide.

1.3 Pentachlorophenol usage and regulations

Pesticide safety has gained much attention over the past 65 years, with many organisations being established in order to evaluate and put forward regulatory protocols for potentially harmful pesticides.^{5,7,8,29-31} South Africa is a signatory to a number of these, including the Stockholm Convention on Persistent Organic Pollutants (POPs),⁷ (signed in 2001, effective from 2004), the Rotterdam Convention on the Prior Informed Consent Procedure for Certain Hazardous Chemicals,⁸ and the Basel Convention.⁹ These are known as multilateral environmental agreements (MEA's). Pentachlorophenol is currently banned in only six countries, namely, Switzerland, Sweden, New Zealand, Austria, Indonesia and India,¹⁹ but is registered for use (with varying restrictions) in South Africa, Cameroon, Northern America and Canada.⁵

The Stockholm Convention on POPs⁷ stems from work by the POPs Review committee, which comprises experts nominated by the United Nations (UN) and aims to protect the environment as well as human health by restricting the production and use of chemicals that are deemed POPs. South Africa, being one of the first UN members, is a signatory, and must comply with these restrictions.³² South Africa has put forward a National Implementation Plan (NIP)³⁰, which illustrates how they will implement and enforce regulations stipulated by the convention. This plan focuses on a number of organochlorides, however PCP is not included despite its clear environmental POP status. This may be because PCP was only introduced into the Stockholm Convention in 2015,⁷ thus the NIP needs to be amended.

Pentachlorophenol is listed under Annex III of the Rotterdam Convention.⁸ Chemicals listed under this Annex are subject to Prior Informed Consent regulations, to which signatories of the convention, as well as all EU nations must adhere. This regulates the international trade of pesticides, including PCP, particularly regarding the import and export of it between EU and non-EU countries. Within this, the European Chemicals Agency has placed restrictions on PCP such that it may not be used, sold or bought as a substance, and when found in other substances, may not amount to more than 0.1% as a constituent.³³ These regulations limit the import and export of PCP where EU nations are involved, however, policies in non-EU nations are not as

clear and stringent. South Africa is a signatory of the Rotterdam convention, and has a current status of an interim decision of no consent to import.⁸

The Strategic Approach to International Chemicals Management (SAICM) has stated that insufficient progress has been made with regard to hazardous chemicals by these treaties, particularly in developing countries.²⁹ In partnership with the United Nations Environmental Programme, efforts have been, and are currently being made to gather information on toxic chemicals and develop better, more coherent management strategies. They aim to achieve these goals by 2020.

In September 2015, the South African Department of Environmental Affairs put forward a request for companies that produce, sell and export chemicals to provide information on certain chemicals contained within a request list, one of which was PCP.³⁰ The information is required to develop appropriate management strategies of these chemicals, such that their use and distribution is in alignment with the MEA's. Pesticides used in South Africa must be registered under South African National Pesticide Registration Authority,³⁴ however this register is not readily available to the public, which may contribute to further unregulated use of PCP.

In Northern America, PCP is currently under registration review (re-evaluation of registered pesticides every 15 years) for the US Environmental Protection Agency (EPA) at the office of Pesticide Programs.³¹ This review aims to evaluate if PCP meets Federal Insecticide, Fungicide, and Rodenticide Act criteria.¹⁴ To be registered, a pesticide must produce no unreasonable harm to humans or the environment when used as stipulated. This agency regulates the sale and distribution of all pesticides in the USA, however an agency specific to South Africa of equivalent calibre with similar stringent regulations is not established, thus despite the accumulating body of evidence that PCP is in fact harmful on various levels, its use in Africa is not highly regulated.³⁵ Ongoing efforts to develop effective techniques for the environmental remediation of PCP are currently under investigation, and range from chemical and enzymatic remediation agents to synthetically engineered techniques such as nanoparticles involved in PCP degradation.³⁶⁻³⁸

1.4 Pharmacokinetics of pentachlorophenol

I. Absorption

Pentachlorophenol can enter into human circulation via inhalation, dermal absorption, or consumption of contaminated food or drinking water.³⁹ Exposure levels in humans are dependent on the context to which an individual is exposed. Workers occupationally exposed to PCP have above acceptable levels of PCP in their body, which mostly arise due to contaminated air inhalation and skin contact, while others may be exposed to lower levels, mainly via ingestion of contaminated food or drinking water.²² This contamination occurs most commonly in areas either near to where PCP is manufactured, or where it is used on a large scale. Both of the afore mentioned circumstances can be considered as chronic exposure if exposed over months or years. Chronic exposure may continually cause damage to human bodily functioning, as recovery of the exposure effects does not occur, and is further compounded by PCP accumulation within the body.⁴⁰ It is estimated that daily human ingestion of PCP via contaminated food accounts for between 0.1-6 µg/day.¹⁷ Inhalation of PCP in indoor wood treated areas may range between 10-160 µg/m³ (0.038 – 0.601 nM), while in untreated areas, inhalation levels¹⁷ are lower than 0.1 µg/m³. Oral ingestion LD₅₀ values of PCP in rats can range from 27-211 mg/kg body weight.⁴¹ The LC₅₀ for PCP inhalation in rats has been reported at 0.2-2.1 mg/L (0.75 – 7.88 µM),⁵ with dermal LD₅₀ ranging between 96-330 mg/kg.⁴¹ Dermal absorption may be enhanced if the skin is pre-exposed to certain chemicals. In particular, Qiao *et al.* found that pre-exposure to the carcinogen, benzopyrene, resulted in highly increased dermal absorption rates of PCP.⁴² In addition to external sources, PCP can occur in circulation if other chlorinated phenols are introduced into the body and metabolised to PCP. Substances that can be metabolised to PCP include hexachlorobenzene, pentachloronitrobenzene, and benzene hexachloride isomers.¹⁷

II. Distribution

In humans, the highest levels of PCP are found in the kidneys and liver, whilst also occurring in fats, muscles and the CNS.¹⁸ Distribution of substances in body tissues is described by the substance's bioconcentration factor (BFA), which is the

concentration of the substance divided by the surrounding concentration. The BFA of PCP in the liver is considered at 5.7, the brain at 3.3, and blood and spleen tissue both at 1.4.⁴³

III. Metabolism

Once PCP has been introduced into the body, it is partially metabolised in the liver into two main active metabolites of interest: tetrachloro-1,4-benzoquinone (TCBQ), and tetrachlorohydroquinone (TCHQ) (Figure 1).⁴⁴ Although precise enzymatic pathways of PCP metabolism are not well characterised in humans, its dechlorination appears to be a function of cytochrome P450, and has been shown to induce CYP1A1 activity.²⁸ A moderate amount of PCP is excreted via urine without being metabolically altered.¹⁷ Pentachlorophenol is also conjugated with glucuronic acid to a small extent.⁴⁵ Specifically, PCP is initially metabolised into either TCHQ for the first branch pathway, or tetrachlorocatechol for the alternative branch pathway. In the first branch, TCHQ is oxidised to tetrachloro-1,4-benzosemiquinone and further oxidised to TCBQ, the by-product of which is hydrogen peroxide (H₂O₂). The latter is known to cause oxidative stress and deoxyribonucleic acid (DNA) damage. In the second pathway, tetrachlorocatechol is also oxidised via similar reactions to tetrachloro-1,2-benzosemiquinone and tetrachloro-1,2-benzoquinone (Figure 1).²⁸

IV. Excretion

Ahlborg *et al.* found that 41-43% of unaltered PCP is excreted via urine in rats.⁴⁶ The TCBQ concentration in urine can range from 5-24% in rats and mice. Tetrachlorohydroquinone has been found in the urine of occupationally exposed workers.²² Pentachlorophenol levels in urine of exposed workers is approximately 1 mg/L (3.75 µM), while levels in the non-chronically exposed population have been reported at 0.01 mg/L (0.038 µM).¹⁸ A minor amount of PCP is eliminated in faeces.⁴⁷ Excretion half-lives of PCP in humans are still controversial, with some studies indicating slower half-lives than others.^{40,48} Elimination half-lives cannot be extrapolated from rat models as rats have been shown to have much faster elimination rates of PCP, regardless of which human study half-life it is referenced

against.⁴⁷ It is thought that humans metabolise PCP less readily than rats, and time for elimination when acutely exposed to PCP can be a few days, while the half-life elimination when chronically exposed can be a few weeks.⁴⁸ Human volunteers exposed to controlled amounts of PCP, were found to have an elimination half-life of 17 days, with a slow clearance rate of 0.07 mL/min.⁴⁵ This slow elimination is postulated to be due to strong binding to plasma proteins. In addition, a faster elimination rate of PCP was noted when subjects' pH was raised with sodium bicarbonate.⁴⁵

1.5 Effects of pentachlorophenol and its active metabolites in the body

Pentachlorophenol uncouples oxidative phosphorylation in the mitochondria, leading to excessive heat production, and accentuated metabolism. Lethal doses of PCP cause a highly increased respiratory rate followed by respiratory and cardiac arrest.³⁹ If PCP comes into contact with epithelial tissue it can cause irritation, manifesting as redness, swelling and tissue damage, particularly in the eyes. Neurological effects have been reported in the form of tremors, the loss of righting reflex (in rats), and an altered state of consciousness manifested by drowsiness, nausea, irritability and headaches.⁴⁹ A limited amount of literature exists regarding PCP toxicity at a neuronal level, with a study suggesting the possible involvement of oxidative stress in cytotoxicity, as well as cell cycle disruptions.⁵⁰ This study did not, however include investigation of the active metabolites, and thus does not provide an indication of neurotoxic effects in its entirety.

Adverse effects of PCP and its active metabolites have been demonstrated to varying degrees in the immune, hepatic, neurological and endocrine systems.^{28,51,52} It has been deemed a possible human carcinogen by the International Agency for Research on Cancer,²³ and has been linked to multiple types of cancer, including hematopoietic cancers such as non-Hodgkin's lymphoma, soft tissue sarcomas, and hepatocellular adenomas among others.^{53,54} It has been shown to be clastogenic (induces chromosomal damage) in mammalian cells *in vitro*, as well as in lymphocytes of exposed persons *in vivo*.⁵⁵ Pentachlorophenol is an endocrine disruptor, as it reduces levels of thyroid hormone and other hormones, thus impairing growth and reproduction processes in organisms.^{56,52} Hepatotoxicity has been

demonstrated by an increase in liver weight and increased activity of liver enzymes.⁵⁷ Shroeder *et al.* further demonstrated the mechanistic of hepatotoxicity where PCP and its metabolites, TCHQ and TCBQ exhibited cytotoxicity between 68 and 130 μM in HepG2 cells. Induction of hepatic CYP1A1 activity was noted for the compounds, and all compounds induced mitochondrial depolarisation, while only the metabolites produced reactive oxygen species (ROS).²⁸ Pentachlorophenol can also hamper porphyrin and normal renal metabolism,⁵⁷ and in rats, interferes with foetal development.⁵⁸ The no-observed-adverse-effects level (NOAEL) of PCP for fetotoxicity is between 5-30 mg/kg body weight per day.^{18,59} Immunotoxicity has been demonstrated in mice exposed to PCP that show an increased susceptibility to tumour formation,⁶⁰ as well as a decreased humoral immune response, however the latter may be due to impurities found within technical grade PCP.⁶¹

Tetrachlorohydroquinone is considered genotoxic as it causes DNA damage in the form of single strand breaks when binding DNA, as well as DNA mutations.⁶² It is more potently genotoxic than the accompanying by-product of its formation, H_2O_2 , and the combination of the two compounds as found in organic systems can also cause extensive oxidative stress.⁶³ Tetrachlorohydroquinone can also impair DNA repair mechanisms, thus contributing to its mutagenic abilities.⁶³ Tetrachloro-1,4-benzoquinone has been shown to cause oxidative damage as well as induce pro-inflammatory activity by promoting the release of the cytokine mediator molecule, high mobility group protein 1 (HMGB1).⁶⁴

Although there have been a number of studies elucidating effects of PCP in humans and in animal models, there is still much to be discovered of the effects and mechanisms of its major metabolites. As PCP is a compound that affects such a broad range of bodily systems and functions, there are many areas where extensive mechanistic research has not yet been satisfactorily covered, particularly with regard to its neurotoxic effects.

1.6 Neurotoxicity

Neurotoxicity can manifest via multiple pathways, which ultimately leads to either abnormal or diminished brain functioning as a result of neuronal cell death or

compromise.⁶⁵ Neurological effects of PCP poisoning can be seen by symptoms such as varying degrees of loss of consciousness, nausea, headaches, confusion, delusions, loss of balance and inhibition, behavioural abnormalities, as well as a decrease in sensorimotor abilities including muscle weakness, loss of muscle control and loss of sensation.⁴⁹ The presence of these symptoms indicates the ability of PCP to cross the blood brain barrier. The onset of neurotoxicity may appear immediately, or may be delayed, depending on the mode of action, as well as the amount and duration of toxin exposure.⁴⁹

1.6.1 *In vitro* methods used to assess neurotoxicity

Testing for toxicity of substances has evolved substantially with the continuing development of evaluation methods, as well as with the growing variety of models upon which testing can be performed. *In vitro* testing has allowed for in depth mechanisms to be unravelled in terms of toxicity as the models allow for controlled exposure to toxins.⁶⁶ One cell line commonly used in neurotoxicity evaluation is PC12, which is of neuronal embryonic rat origin. Although useful in the assessment of developmental neurotoxicity, it is not a good representation of mature neuronal cells in adult humans.⁶⁷ The SH-SY5Y human neuroblastoma cell line is also commonly employed for neurotoxicity testing. Despite some innate limitations, this cell line is commonly used to elucidate effects that substances would have on human neurons.⁶⁸ This cell line has been shown to exhibit similar biochemistry and morphology to human neuronal cells,⁶⁹ however the drawbacks of it should be noted. The SH-SY5Y cell line is cancerous, and therefore harbours differences to non-cancerous neurons in its relative hallmark mutations. The cells of this model are also undifferentiated, and therefore do not exhibit the same maturity markers, metabolism, or synaptic connections as mature neurons.⁷⁰ Other *in vitro* models include the differentiation of SH-SY5Y cells with retinoic acid, which yields cells more characteristic of mature neurons in terms of maturity markers and metabolism,⁷¹ or three-dimensional cell culture models which attempt to simulate *in vivo* architecture.⁷² The undifferentiated SH-SY5Y cell line has nonetheless been established as an *in vitro* model for neurotoxicity evaluation in research history, and

as such, this cell line was used in this study to determine neurotoxicity of PCP and its metabolites.

1.6.2 Processes involved in neurotoxicity

An essential mechanism to evaluate toxicity is the mode of cell death.⁷³ Toxic compounds can induce cell death through a number of pathways, two common endpoints of which are apoptosis and necrosis.⁷⁴

I. Apoptosis

Apoptosis is commonly known as programmed cell death, and can occur in two broad pathways, namely the intrinsic pathway, where cell death is initiated as the cell detects internal stress stimuli, or the extrinsic pathway, where apoptosis is initiated in response to signalling molecules originating from surrounding cells which bind cell surface receptors.⁷⁵ Apoptosis is characterised by the condensing of the nucleus and cytoplasm, with membrane blebbing, followed by the cell breaking into apoptotic bodies.⁷⁶ These are subsequently engulfed by phagocytes *in vivo*, which recognise the apoptotic cell by the externally presented phosphatidylserine (PS), which is absent on the outer surface membrane of healthy cells.⁷⁷ The process of apoptosis once initiated, is irreversible, and is tightly regulated.⁷⁸

The intrinsic pathway of apoptosis (Figure 2) is commonly activated upon mitochondrial membrane permeability alteration, either as the mitochondria swells and the membrane subsequently ruptures, or by the creation of pores in the mitochondrial membrane.⁷⁵ This causes apoptosis effectors to leak out of the mitochondria. Two pertinent molecules released from the mitochondria include second mitochondria-derived activator of caspases (SMAC), and cytochrome c (cyt c).^{79,80} Proteins such as SMAC deactivate inhibitor of apoptosis proteins (IAPs), which allows for the activation of caspases.⁸¹ Caspases are protease enzymes that can induce apoptosis by the degradation of cellular protein. At least thirteen caspase types have been discovered, seven of which are specifically involved in apoptosis.⁸² Apoptotic caspases may be divided into initiator and executioner classes, the latter of

which is activated by the former.⁸² The second mentioned mitochondrial derived apoptosis effector, cyt *c*, works for example by forming an apoptosome by binding and cleaving pro-caspase-9 into the active initiator caspase-9, which can activate executioner caspase-3, ultimately eventuating apoptosis.⁸³

The extrinsic pathway of apoptosis (Figure 2) can be activated by the binding of signalling molecules originating from surrounding cells to extracellular membrane receptors.⁷⁵ Apoptosis in this manner can occur through many mechanisms, such as via the binding of tumour necrosis factor- α (TNF α), (usually originating from activated macrophages) to TNF receptors, which activates death domain containing proteins and caspases, and ultimately results in cell death.⁸⁴ Another such mechanism is by the binding of apoptosis stimulating fragment (Fas) to the Fas receptor, causing the creation of death-inducing signalling complex (DISC), which contains caspases, and may either activate other caspases, or induce the mitochondria to release further apoptosis signals.⁸⁵ Extrinsic pathways often lead to the activation of caspase-8, and subsequently caspase-3, thus having a similar endpoint as the intrinsic pathway. Caspases, are not however always involved in apoptosis.⁷⁵

Upstream of this, p53 can respond to a number of different cell stress stimuli to induce either cell cycle arrest or apoptosis through a plethora of different pathways, implicating both intrinsic and extrinsic apoptosis.⁸⁶ Cell death via apoptosis can be less acutely damaging to surrounding cells than necrosis, as apoptotic bodies are formed, which are engulfed and removed by phagocytes before cellular contents are spilled to the external environment.⁷⁶ Abnormal rates of apoptosis can result in adverse consequences, where reduced apoptosis may contribute to cancer, while accentuated apoptosis results in atrophy of the area and thus possible diminished functioning.⁷⁶

II. Necrosis

Necrosis is a mode of cell death where the cell dies as a result of external trauma. It is initiated as substances bind extracellular receptors and the integrity of the plasma membrane is compromised (Figure 2).⁸⁷ The necrotic cell ultimately ruptures, expelling its contents, which initiates an inflammatory response and bars

phagocytosis of the harmful cell debris, thus potentiating the effect on surrounding cells.⁸⁸ Necrosis can be identified by the swelling of cellular components and cytoplasm, with membrane damage leading to cell rupture and release of harmful cell contents into the surrounding area.⁷⁵ Reactive oxygen species have been found to play roles in necrotic cell death by contributing to the damage of cellular contents such as proteins, enzymes, and DNA.⁸⁹

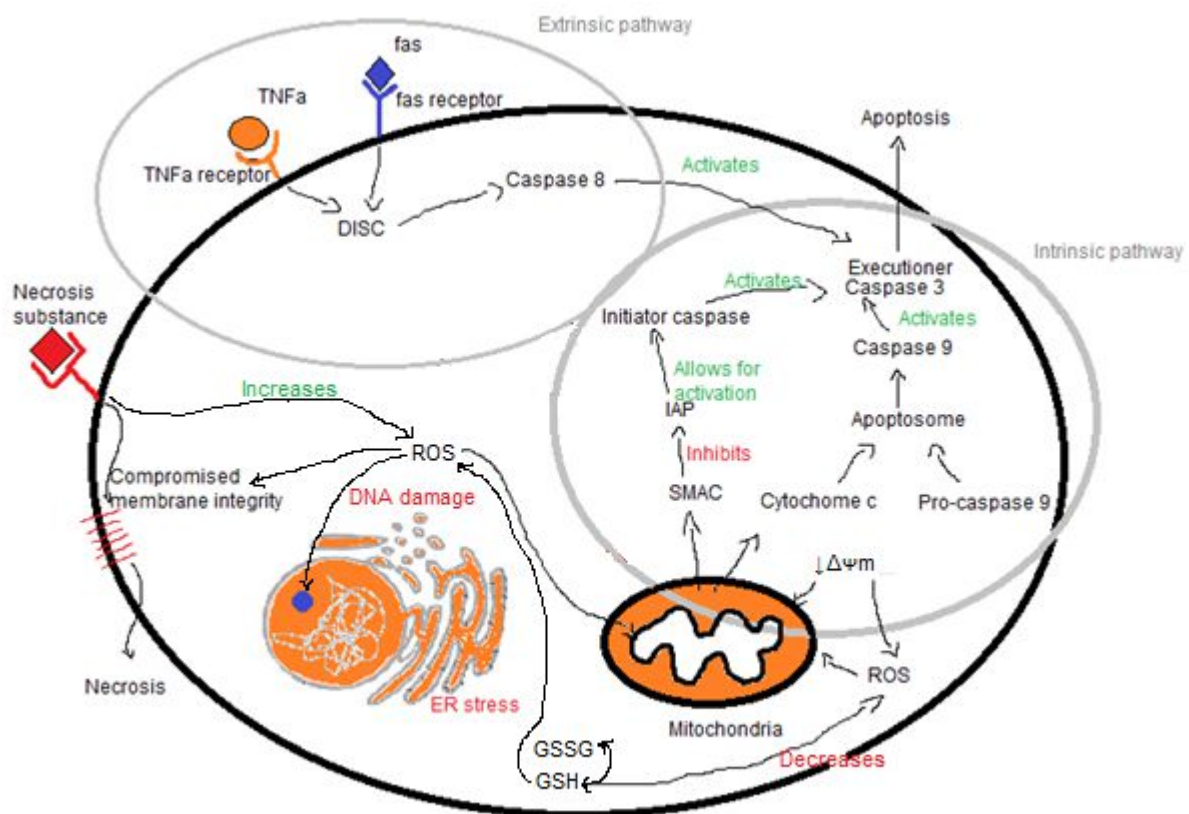


Figure 2: Mechanisms of cell death. Multiple pathways may lead to apoptosis or necrosis, involving cascades of cell death related events and their crosstalk. Arrows indicate flow of events. (image produced in Microsoft Paint version 6.1.).

SMAC - second mitochondria-derived activator of caspases, DISC - death-inducing signalling complex, ER – endoplasmic reticulum, $\Delta\psi_m$ – mitochondrial membrane potential, ROS – reactive oxygen species, TNF α – tumour necrosis factor α , GSH – reduced glutathione, GSSG – oxidised glutathione.

III. Cell cycle

The cell cycle (Figure 3) is a process through which a eukaryotic cell progresses through multiple phases which ultimately lead toward mitotic division.⁹⁰ A daughter cell emerging from the mitosis of a mature cell starts its cell cycle progression in the Gap 1 phase (G1).⁹⁰ In this phase, the cell undergoes maturation, whereupon it grows in size, and produces an assemblage of histones and messenger ribonucleic acid (mRNA) in early preparation for eventual mitosis.⁹¹ It is during the latter period of this phase where a cell is committed to mitosis, whereupon the cell will continue in its cell cycle progression towards mitotic (M) phase. Alternatively, a cell may enter into the G0 phase, a non-proliferative state of quiescence (reversible), senescence, or differentiated cells (irreversible).⁹² The destiny of a cell to become non-cycling or proliferative is determined by the G1/S checkpoint.⁹³ Here, the cell will be committed to mitosis if cyclin dependent kinase (CDK) forms a CDK-cyclin E complex, and cyclin-CDK-dependent transcription is activated, allowing for the progression into S phase.⁹³

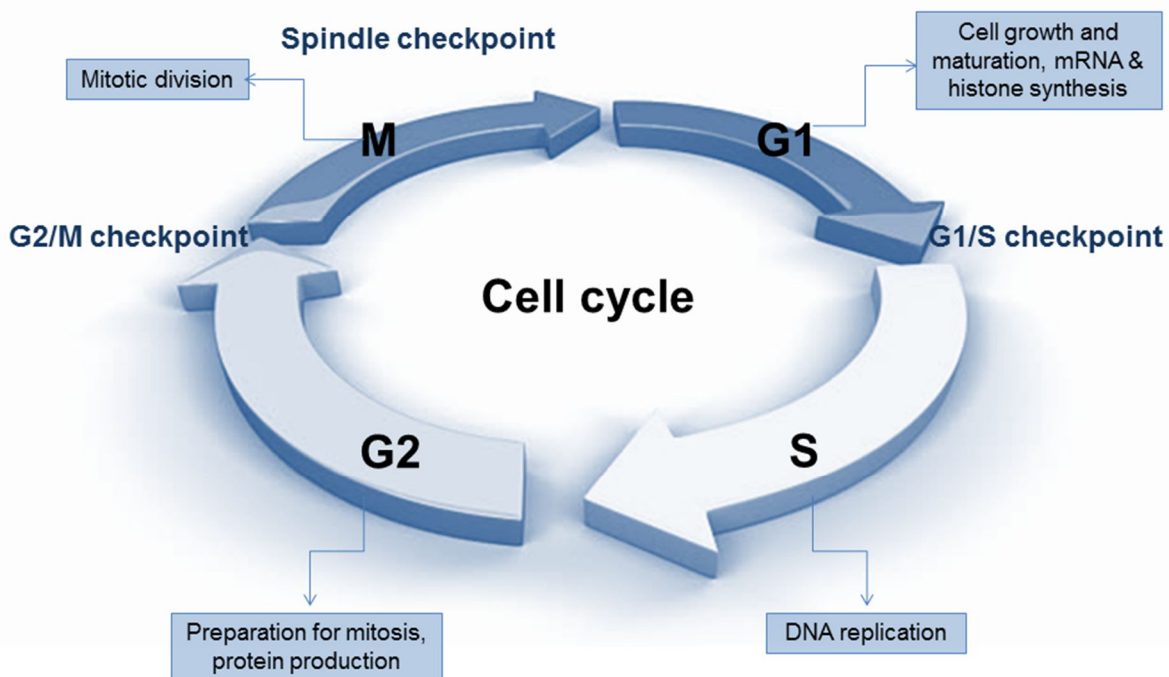


Figure 3: Cell cycle phases and checkpoints. Cells in G1 phase undergo early preparation for mitosis, and transition through the G1/S checkpoint to S phase where DNA replication occurs. Cells then enter into G2, where further preparations for mitosis occur. Cells then pass through the G2/M checkpoint into M phase where mitosis occurs (image produced in Microsoft PowerPoint 2010).

This second stage of the interphase of cell cycle, termed S phase, involves the duplication of DNA in preparation for mitosis, a process which is highly regulated and conserved in order to prevent the arise of mutations.⁹⁰ Following successful DNA replication, the cell will enter into the Gap 2 phase (G2), where further preparations for mitosis occur, involving the continuation of cell growth, and substantial protein production.⁹⁰ The cell will arrive at the G2/M checkpoint when a threshold level of cyclin B1/CDK1 complex has been reached.⁹⁴ This checkpoint will not be passed if DNA damage is present, the impasse of which is mediated by transcription factor p53 among a plethora of other signalling molecules.⁹⁵ Assuming no DNA damage occurs, the cell will then progress to M phase, where, through a complex and well established series of events, the cell is divided into two identical daughter cells, each possessing a full diploid (humans) set of chromosomes, and each of which will continue in its own cell cycle.⁹⁶

Cessation of cell proliferation, or cell death may arise following cell cycle disruption pertaining to any of the aforementioned phases, harbouring differing characteristics depending on the point of disruption.⁹⁷ Cell cycle blocks occur as the cell is unable to pass to subsequent phases, and are manifested by an accumulation of cells in the phase before the relevant checkpoint. Cell cycle arrest in the G1 phase often leads to a non-proliferative state, however assuming continued cellular activity, may not necessitate cell death, in which case cytostatic rather than cytotoxic effects are manifested.⁹⁸ The onset of resultant cell cycle arrest or cell death from a G1 block is frequently mediated by the activation of p53 and p21 in response to DNA damage.⁹⁹ This activation initiates either an attempt at DNA repair, or in the case of irreparable damage, apoptosis.¹⁰⁰ Progression to S phase is obstructed at the G1/S checkpoint upon the binding of transcription repressors such as retinoblastoma (RB) to elongation factor (E2F) transcription factors.¹⁰¹ The progression past this checkpoint will only occur once a cascade of cyclin phosphorylation reverses the transcription repression, and cyclin E complexes with CDK2. This may only be activated in the presence of cell division cycle 25A (CDC25A), a phosphatase which is ubiquitinated and degraded under G1 arrest conditions.¹⁰² It should be noted that cell cycle arrest in the G1 phase is not synonymous with quiescence or senescence, however cell cycle arrest may lead to these states. Quiescence primarily arises due to a depletion of growth factors, and is easily reversible, while senescence, as induced by CDK

inhibitors, exhibits cellular hypertrophy due to a continuation of growth stimulation under the influence of cell cycle arrest, and is analogous to a permanent state of quiescence.⁹⁸

S phase blocks are strong indicators of DNA damage that may occur during the process of DNA replication.¹⁰³ The presence of persisting Okazaki fragments in the lagging strand of DNA synthesis indicate incomplete DNA duplication, and thus the cell will not be permitted to progress to the next phase of the cell cycle.¹⁰⁴ The inability to repair replication errors that occur during DNA synthesis will also result in a cell's inability to progress with the cycle.¹⁰⁵ Cells in such states will ultimately fall out of the cell cycle into cell death, as denoted by sub-G1, where cellular contents and DNA are degraded in a cascade of events leading to apoptosis.¹⁰⁶

The occurrence of a G2/M block yields a great propensity for translation into cell death, and arises as a cell cannot pass the G2/M checkpoint in response to DNA damage accumulated in S phase.¹⁰⁷ Such instances result in the activation of checkpoint kinase 1 (Chk1) by DNA repair helicase (rad3), which in turn inhibits CDC25 and activates wee1. This causes the inhibition of CDK1 (previously named CDC2) binding cyclin B, and a resultant arrest in progression to M phase.^{108,109} Alternatively, a G2/M block may be indicative of an impasse reached at the spindle check point of metaphase during mitotic division.¹¹⁰ This checkpoint exists to prevent aneuploidy due to improper chromosomal spindle binding and separation, the regulation of which is largely dependent on mitotic arrest deficient (MAD) proteins, anaphase promoting complex (APC), CDC20, among a milieu of further spindle checkpoint factors.¹¹¹ A block at this point may suggest damage to microtubules essential for proper spindle functioning.¹¹² Cell death is often cell cycle dependent,¹¹³ and the characteristic cell cycle block of a toxin is often a strong indicator of the mechanisms leading to cell demise, as well as the point at which damage is inflicted.

IV. Cell cycle considerations in neurons

Regarding neuronal cells, the role of the cell cycle is different to that of most other somatic cell types, as mature neurons are fully differentiated, and thus are in a post-mitotic, non-proliferative state.¹¹⁴ Upon maturation, the neuron enters into a

permanently maintained cell cycle arrest by strict cell cycle regulation. It is thought that this is achieved primarily by the maintenance of RB bound to E2F, a complex which bars a quiescent cell from re-entering the cell cycle.¹¹⁵ A number of cyclin-dependent kinase inhibitors (CKIs) also appear to play a role,¹¹⁶ however the mechanisms are not well described. The dysregulation of E2F, accompanied by the upregulation of cyclin D-CDK4/6 causes RB phosphorylation, which liberates the two molecules from each other and initiates apoptosis before the G1/S checkpoint is passed, a process coined “abortive cell cycle re-entry”.¹¹⁴ Alternatively, this apoptosis fate may be eventuated due to cyclin E and CDK2 response to insuperable DNA damage, wherein apoptosis occurs after entry into S phase.¹¹⁷ In post-mitotic cells, the maintenance of a non-proliferative state is a highly dynamic and active process, and the disruption of cell cycle regulation can result in the re-entry of a post-mitotic neuron into the cell cycle, which leaves it highly vulnerable to cell death. This cell cycle re-entry and susceptibility to cell death is postulated to cause, or be implicated in neurodegenerative diseases, as well as contribute to more acute neuronal insults.¹¹⁸

Cell cycle proteins have been discovered to be expressed in post-mitotic neurons, and have been found to play a role in neuronal plasticity and DNA repair.¹¹⁹ Double strand breaks (DSB) commonly arise in DNA as a result of oxidative stress in the cell, which may originate as a normal by-product of oxidative phosphorylation, or due to high levels of aberrant ROS occurrence.¹²⁰ In proliferative cells, DSBs are rectified by DNA repair processes which rely on cell cycling,¹²¹ however since neurons do not abide putative cell cycling, neurons must rely on alternative, or at least, modified mechanisms for DNA repair.¹²² Cell cycle components discovered in post-mitotic neurons in response to DNA damage include G1 progression factors such as phosphorylated RB, cyclin C and D, and CDK4/6, which appear to stimulate non-homologous end joining of DSBs.¹¹⁴ Despite cell cycle proteins’ presence, cells undergoing DNA repair do not progress to S-phase, indicating that complete cell cycling is not re-established during this process.¹²³ The inhibition of S-phase progression is thought to be achieved by ataxia telangiectasia mutated (ATM),¹²⁴ the dysregulation of which may promote abortive cell cycle re-entry.¹²⁵

Neuroplasticity refers to the brain’s ability to continuously and dynamically change the structure and function of neurons throughout post developmental life. This

process is essential for brain functioning, learning, cognition, memory formation and other adaptations.¹²⁶ Cell cycle proteins that have been implicated in neuroplasticity include, but are not limited to, cyclins B, D and E, and CDKs 1, 2, 4 and 5. Their roles in plasticity appear to be centred around microtubule and cytoskeleton control in the neuron.^{127,128} One such mechanism thereof involves the inhibition of CDK 5 by cyclin E, which precludes the binding of p35 or p39, ensuing plasticity.¹²⁹ Conditions of synaptic connectivity loss have also been found to enhance the expression of cell cycle proteins in an apparent attempt to remodel and compensate for neuron loss.¹¹⁹ Unlike neuronal DNA repair processes that express mainly G1 components, the plethora of cell cycle associated proteins involved in neuroplasticity have putative origins from all cell cycle phases. The exact mechanisms by which cell cycle proteins are involved in neuroplasticity are currently poorly understood. It is known however that the disruption of the implicated proteins gives rise to abnormal plasticity functioning.¹¹⁹

Contrary to historical belief, neurogenesis still occurs in the adult brain, particularly in the subgranular zone of the dentate gyrus (which is found in the hippocampus), as well as in the subventricular zone.¹³⁰ The neurogenesis in this area implicates the striatum, which is responsible for cognition, planning, and reward systems among others.¹³¹ Unlike other brain areas, these regions within the CNS exhibit a cell cycle more characteristic of proliferative cells, and thus may be more susceptible to exogenous compounds that exert effects on the cell cycle.¹³² The hippocampus is responsible for memory formation, wherein about 700 new neurons are formed per day, and damage relating to cell cycle progression of neurons within this region may translate to impaired functioning of memory, learning and cognitive plasticity.¹³³

V. The role of reactive oxygen species, mitochondrial membrane potential and glutathione in cell death

Oxidative stress, changes in mitochondrial membrane potential ($\Delta\psi_m$), and glutathione play pivotal roles in toxicology, and their dynamic crosstalk contribute substantially to cell death.¹³⁴⁻¹³⁶ Reactive oxygen species are created as a normal by-product of oxidative phosphorylation in cellular metabolism, and are required for normal cell functioning. Under pathological conditions it is well known that excessive

increases in ROS can influence or cause cellular damage or cell death.¹³⁷ Oxidative stress occurs upon the imbalance of oxidant and antioxidant levels, and is often a result of targeted drugs or exogenous toxins such as pesticides or other xenobiotics.^{138,139} Excessive ROS can lead to cell death by oxidative damage to a host of cellular components, which can trigger a cascade of apoptotic signalling (Figure 2). Damage to DNA can include various forms of DNA mutations or DSB, while damage inflicted on proteins can result in impaired enzyme functioning, as well as disruption of non-enzyme proteins.¹⁴⁰ Oxidative stress may also cause damage to lipids, consequently compromising phospholipid membrane bilayers, and thus the integrity of membrane bound organelles, such as mitochondria.¹⁴¹

Reactive oxygen species mediated cell death may occur in a mitochondria-dependent or independent manner.¹⁴² Mitochondria-dependent cell death is commonly associated with the intrinsic apoptosis pathway, and is frequently triggered by oxidative damage to mitochondrial DNA, which causes impairment of cellular respiration and in turn creates more ROS.¹⁴³ This cycle, along with direct ROS action on the mitochondrial phospholipid bilayer, leads to a reduction in $\Delta\psi_m$, which translates to mitochondrial membrane permeabilization, and subsequent leakage of apoptotic factors (Figure 2).¹⁴⁴ Alternatively, increased ROS associated with $\Delta\psi_m$ collapse may not be the primary trigger, but a secondary outcome which exacerbates the situation. Mitochondrial dysfunction can arise from the disruption of cellular metabolism through the uncoupling of oxidative phosphorylation, a process known to occur due to PCP.¹⁴⁵ Reactive oxygen species involvement in mitochondria-independent cell death often pertains to the death receptor pathway. Activation of Fas receptors can cause ROS production by nicotinamide adenine dinucleotide phosphate (NADPH) oxidase, which subsequently ubiquitinates FLICE-like inhibitory protein (FLIP_L), an anti-apoptotic factor, marking it for destruction, ultimately leading to apoptosis.¹⁴⁶ Activation of TNF receptor 1, while normally associated with apoptosis, has been reported to induce necrosis in some cell lines, with an accompanied association of ROS accumulation and mitochondrial dysfunction.¹⁴⁷ In addition, necrotic cell death has been demonstrated to occur due to a burst of ROS in neurons with altered $\Delta\psi_m$.¹⁴⁸ Excessive ROS production has also been implicated in cell cycle and aberrant cell cycle re-entry in mature neurons.¹⁴⁹

Glutathione is the most prominent non-protein modulator of cellular redox and ROS regulation. It exists in two forms, namely reduced glutathione (GSH) and oxidised glutathione (glutathione disulphide) (GSSG), which serves to protect cells against oxidative stress.¹⁵⁰ Under normal circumstances, GSH is oxidised by ROS to GSSG, thus neutralising ROS and preventing it from exerting oxidative stress on other cellular components.¹⁵⁰ Reduced glutathione is then recycled by glutathione reductase which converts it back to GSH. Severe oxidative stress is usually accompanied by a depletion of GSH, as the redox maintenance system is overwhelmed by increased ROS levels, which often leads to the induction of apoptosis (Figure 2). Cell death may occur as results of unchecked ROS, or may be signalled more directly due to an altered GSH redox state.¹⁴³ Alternatively, GSH depletion may not be triggered by ROS, but may be due to the direct action of an exogenous compound on the GSH molecule itself, or due to dysregulation of GSH synthesis.¹⁵¹ These events will, however, lead to secondary ROS accumulation and oxidative stress. The severity of GSH depletion and oxidative stress can determine the fate of a cell, where moderate alterations will lead to apoptosis, while greater redox disruptions triggers a switch from apoptosis to necrosis if cellular apoptotic mechanisms are no longer able to cope with the inflicted damage.¹⁵²

VI. Acetylcholinesterase

Acetylcholine (ACh) is a cholinergic neurotransmitter involved in many neurological functions. In the peripheral nervous system, its release from motor neuron synapses in the neuromuscular junction and subsequent binding to receptors causes muscle contraction.¹⁵³ It occurs in the sympathetic nervous system as an intermediate neurotransmitter, and in the parasympathetic nervous system as an end neurotransmitter.¹⁵⁴ In the CNS, ACh functions as a neuromodulator, and controls processes in cholinergic areas of the brain.¹⁵⁵ Acetylcholinesterase is a hydrolase enzyme that catalyses the breakdown of ACh into acetate and choline (Figure 4), and thus regulates ACh levels and duration of action.¹⁵⁶ A common target for nerve agents is AChE, where its activity is inhibited, thus allowing for unchecked accumulation of ACh.¹⁵⁷ This results in disrupted neurotransmission due to a hyperstimulated cholinergic nervous system, leading to impaired brain functioning, as

manifested by neurological symptoms such as headache, confusion, anxiety, convulsion, or coma.¹⁵⁶ In addition, AChE inhibition can result in an exaggeration of parasympathetic functioning, which results in a plethora of symptoms mnemonically known as 'SLUDGE syndrome'. This includes hypersecretion (particularly of lacrimal, salivary and sweat glands), diarrhoea, vomiting, and muscle tetanus. In severe cases, death may occur due to failed respiration as a result of muscle paralysis of the lungs, or an accumulation of liquid in the lungs.¹⁵⁸ Pharmacological treatment for acute AChE-inhibitor poisoning focuses on the suppression of symptoms with the use of anticholinergic drugs such as atropine.¹⁵⁹ Many pesticides are AChE inhibitors, including carbamates, organophosphates and organochlorides.¹⁵⁶ As PCP is classified as an organochloride, it is expected to act as an AChE inhibitor. While it has yet to be empirically confirmed in humans, the respiratory failure and neurological symptoms associated with the clinical presentation of PCP poisoning suggest the possibility of cholinergic pathway involvement.⁴⁹

Acetylcholinesterase contains a deep active site gorge, and consists of an anionic and an esteratic subsite (Figure 4). The anionic subsite is predominantly populated by aromatic amino acids such as tryptophan, tyrosine and phenylalanine, which allow for the binding of aromatic-based inhibitors which bar the entry of ACh into the active site.¹⁶⁰ In particular, tryptophan 84 is highly conserved in AChE throughout different species and is crucial for AChE activity. Within the esteratic subsite, the amino acids, histidine 440, glutamate 327 and serine 200 are responsible for the catalytic action of the enzyme.¹⁶¹ The binding of exogenous compounds within this active site leads to competitive AChE inhibition, as they directly impede ACh access to the binding site, preventing hydrolysis of ACh (Figure 4).

The extent of an inhibitor's pathological impact depends largely on the reversibility of its binding. Irreversible inhibitors typically bind covalently with the enzymes, causing a permanent protein conformation change, which disallow normal enzymatic reaction processes to take place.¹⁶² As this change is permanent, enzyme functionality is not regained, leading to severe, pathological outcomes. This kind of inhibition is typically seen in nerve agents and pesticides, which inhibit AChE activity, such as organophosphates, however these are not exclusively classed as irreversible.¹⁵⁶ Conversely, reversible inhibitors bind and exert a transient effect before they are

cleared, and leave the enzyme intact to continue normal functioning. This kind of AChE inhibitor does not tend to lead to as severe adverse effects as in the case of irreversible inhibitors, and are in fact used in a therapeutic capacity for the treatment of diseases, the most common of which is Alzheimer's disease.¹⁶³ Such drugs include tacrine and galanthamine.

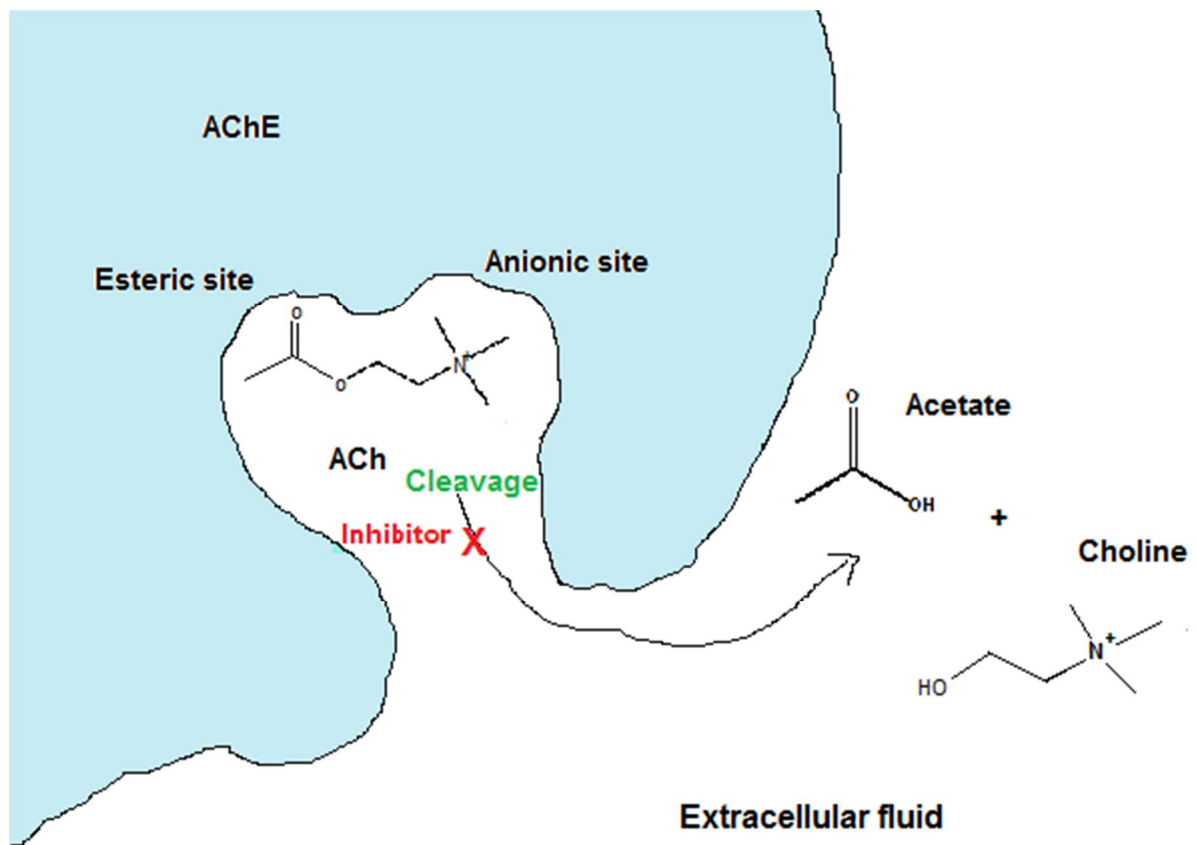


Figure 4: Depiction of acetylcholinesterase (AChE) action. Acetylcholine (ACh) is cleaved in the AChE active site gorge into acetate and choline. Inhibitor molecules capable of entering and binding the active site may inhibit ACh cleavage (image produced in Microsoft Paint version 6.1.).

Enzyme inhibitors can further be classed as competitive, non-competitive, or uncompetitive, and are determined by changes in maximum rate of reaction (V_{max}) and Michaelis constant (K_m) values in Lineweaver-Burk plots.¹⁶⁴ K_m values represent the concentration of a substrate for which the rate of reaction is half of V_{max} . Competitive inhibitors typically act by binding the active site of an enzyme, thus barring substrate entry, and serve to outcompete the substrate for a place in the

active site.¹⁶⁵ The extent of competitive inhibition thus depends on relative substrate concentration, where greater substrate concentrations may usurp inhibitor binding, thus competitive inhibition is indicated by a change in the K_m value.¹⁶⁴ The hallmark of this type of inhibition is that substrate and inhibitor binding is mutually exclusive. Non-competitive inhibitors harbour equal binding affinity as the substrate, and do not depend on substrate concentration, and are thus indicated by a change in V_{max} accompanied by a constant K_m value.¹⁶⁵ The binding of substrate and non-competitive inhibitors are not necessarily mutually exclusive, often conferring allosteric inhibition, where the inhibitor binds a site separate to that of the active site. Uncompetitive inhibition is indicated by a change in both V_{max} and K_m , and may only bind when the substrate-enzyme complex is already formed.¹⁶⁶ For all enzyme inhibitors, the binding affinity plays a key role in inhibition, where sufficient binding affinity is required to execute activity. In particular, the greater the binding affinity confers greater potential for inhibition and greater potency in the case of competitive inhibitors.¹⁶⁵ The absence of appropriate binding affinity and compatibility would result in inactivity against an enzyme. The characterisation of an AChE inhibitor's action at a molecular level is crucial not only to the understanding of such inhibition and the resultant systemic effects, but also to the development and advancement of treatments toward AChE inhibitor poisoning.

1.7 *In silico* ligand binding analysis

The use of *in silico* research techniques are rapidly being adopted among researchers of diverse disciplines, particularly within health related fields. It refers to research conducted via computational methods, and has great potential for application in the technological age as methods continue to become more sophisticated, accurate and advanced.¹⁶⁷ Furthermore, it is with the emergence of ever increasingly powerful high performance computing (supercomputers), which accede to the running of highly complex algorithms and simulations.¹⁶⁸ Such tools allow for in depth analysis of systems biology, with applications in medicine, drug discovery, and toxicology among others. When combined with *in vitro* or *in vivo* assessment, this yields a powerful research platform as it provides a holistic frame of insight into the topic of interest.¹⁶⁹ In drug discovery, potential drug targets for a

disease are determined, and a drug can be modelled as a ligand to target the determined receptor.¹⁷⁰ Further *in silico* assessment such as molecular docking is performed to help predict drug actions *in vivo*, and to optimise specificity to the target in order to reduce the potential of time and resource wasting in the case of drug failure further down the line of testing such as in late phase clinical trials.¹⁷¹

In silico toxicology can be applied in a broad nature wherein a large quantity of chemicals are screened in a high throughput manner for toxic potential, or in a more targeted approach, assessing specific toxicological concerns of individual compounds.¹⁷² Read-across and categorisation methods determine structural alerts, which flags molecules with structural attributes that indicate toxicity potential.¹⁷³ This is used in early stage screening and relies on the similarity principle, with the assumption that similar structures confer similar activity. Expert systems methods use artificial intelligence to apply mimicry of human reasoning in toxicological screening, the end decisions of which are drawn from formalisation of known facts and the application thereof to new data.¹⁷⁴ Quantitative structure–activity relationship (QSAR) modelling uses regression and categorisation algorithms to predict biological activity of compounds, which yields high throughput results, but does not take into account three dimensional (3D) protein conformation or receptor site interaction, and thus is considered ligand-based.¹⁷⁵ Structure-based methods are more commonly used for individual toxicological evaluation, wherein the 3D conformation of both ligand and receptor are considered. The more factors considered, the greater computational power required, thus more complex evaluation is usually reserved for targeted theory application.

Similar to pre-testing of *in silico* designed drugs, molecular docking can be used as a structure-based assessment of ligand-receptor interaction in a predicted toxicity scenario,¹⁷⁶ such as the inhibition of an affected enzyme like AChE by xenobiotic compounds. The aim of docking a ligand into a receptor is to produce the most favourable pose of the ligand within the binding site in terms of orientation and binding energy for the docking scoring function.¹⁷⁷ Ligands docked to receptors with low binding energies confer high binding affinity, indicating a high likelihood of receptor binding and consequential biological activity toward the enzyme, which may confer toxicity in a correctly predicted model.¹⁷⁸

Molecular dynamics (MD) use computer simulation to determine molecule interactions within a system over time. Laws of physics pertaining to inter-molecular energies and exerted forces are numerically solved during simulated interaction, which predicts time-dependent molecule trajectories.¹⁷⁹ One such application is the elucidation of ligand-receptor binding stability, the simulation of which predicts ligand movement and behaviour within a temperature, pressure, and solvent considered environment.¹⁸⁰ Molecular dynamics simulations require a large amount of computational power and are frequently run using high performance computing, which reduces the amount of time required for each simulation run.¹⁸¹ Due to the many factors considered, this too is usually reserved for individually selected applications. Protocols for MD simulation involve the creation of an environment most representative of *in vivo* situations. In biology, most molecular interactions and reactions occur in aqueous solution, thus a solvent environment model of water molecules and dissolved salts such as sodium, potassium and chlorine is added, each molecule of which has force exertions to be considered in the final simulation.¹⁸² Further appropriation of *in vivo* circumstances commonly applied in MD is the gradual application of temperature and pressure. The addition of these factors allows for thermodynamic force consideration in un-constrained ligand-receptor environmental interactions. Force fields are defined parameters for energy functions which are applied to simulation calculations.¹⁸³ A commonly used force field such as Assisted Model Building with Energy Refinement (AMBER) takes into account potential energies derived from different types of bonds, bond angles, torsions and the changes thereof, as well as other parameters.¹⁸⁴ Minimization of potential energy within a system by reduction of energetically unfavourable conformations is essential for successful simulation, as too great force clashes will result in the termination of the simulation.¹⁸⁵ Upon successful simulation, the average binding energy of the ligand over time is given, as well as rendered snap shots, which can be viewed in visual molecular dynamics tools for movement observation.¹⁸⁶

1.8 Study rationale

Ultimately, although neurological symptoms have been described for PCP, there are many gaps in the knowledge of the mechanisms of the neurotoxicity thereof. While existing literature provides some insight, much of it has been conducted on non-neuronal models, and those for which neuronal cells have been used have limitations in that only the parent compound was investigated,⁵⁰ which does not provide a complete picture. Elucidation of molecular mechanisms at a cellular level within neuronal cells is therefore required to contribute toward the current gap in the knowledge of PCP neurotoxicity. Empirical definition of molecular underpinnings and events at this level would aid not only the understanding thereof, but also assist future research with regard to treatment of PCP exposure, as well as justification for regulatory, and environmental remediation considerations.

1.9.1 Aim

The aim of the study was to evaluate the effects of PCP and its active metabolites, TCBQ and TCHQ on SH-SY5Y human neuroblastoma cells.

1.9.2 Objectives

An initial assessment of the effects of PCP and its metabolites on cell proliferation was performed in order to determine the concentration at which cell growth is inhibited by half (IC_{50}) concentrations of each compound on SH-SY5Y neuroblastoma cells that were used in subsequent experiments. This was determined using the sulforhodamine B (SRB) colorimetric assay.

Possible mechanisms of cell death in SH-SY5Y neuroblastoma cells were assessed in multiple domains, and entailed the following:

- Cell cycle analysis using flow cytometry and propidium iodide (PI) staining
- Mode of cell death using Annexin V-FITC and PI staining to differentiate between apoptosis and necrosis
- Caspase-3 activity using Ac-DEVD-AMC fluorescence
- ROS production with 2,7 dichlorofluorescein (DCF) fluorescence
- Mitochondrial membrane potential using 5,5',6,6'-tetrachloro-1,1',3,3'-tetraethylbenzimidazolocarbo-cyanine iodide (JC-1) dye
- Intracellular GSH content with a monochlorobimane (MCB) assay

Effects of compounds on ACh were assessed:

- AChE inhibitory activity using Ellman esterase assay
- *In silico* assessment of molecular mechanisms of inhibition via computational docking of metabolite ligands to AChE receptors
- *In silico* assessment of ligand binding stability via molecular dynamics

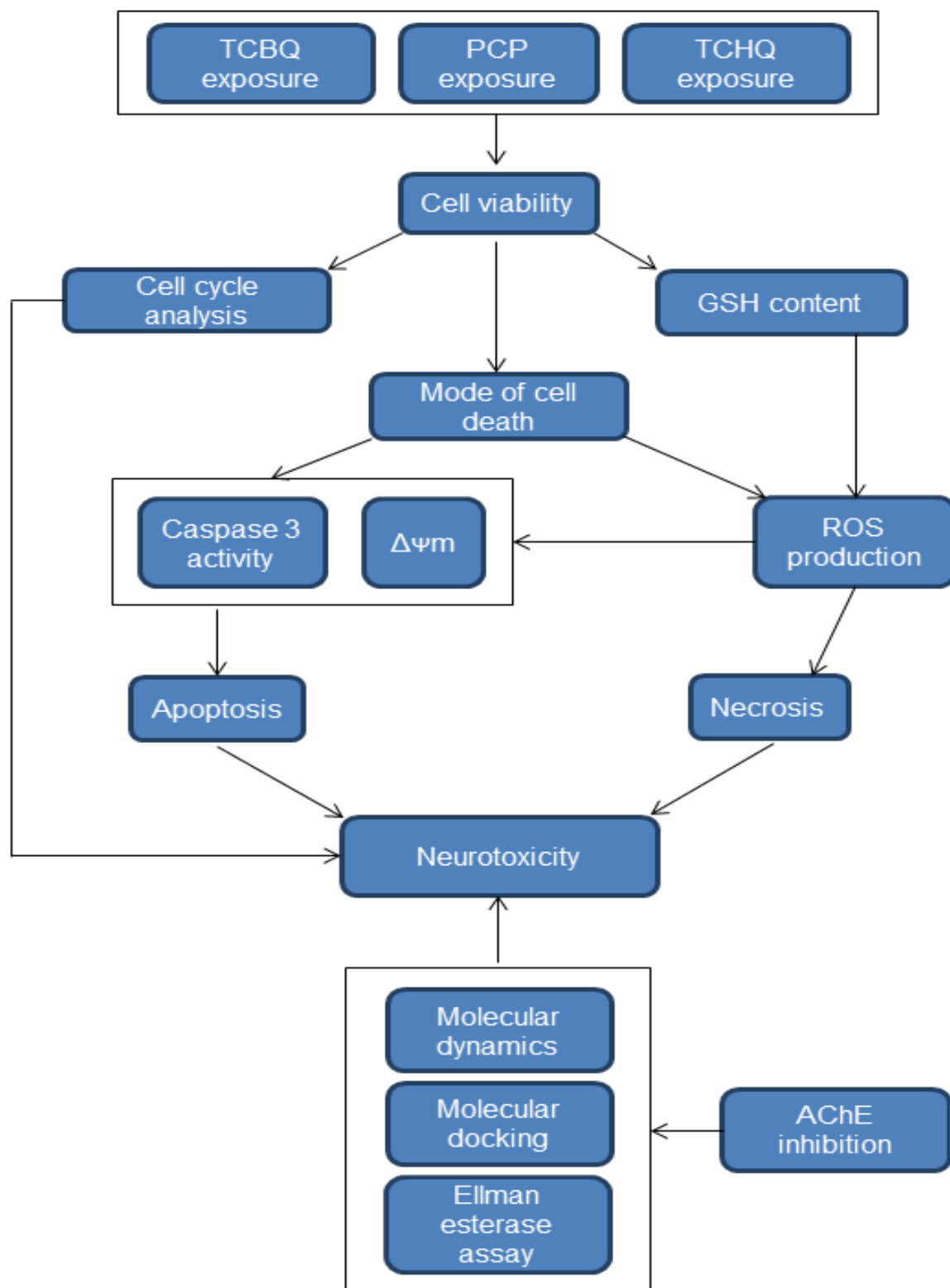


Figure 5: Schematic summary of project.

PCP - pentachlorophenol, TCBQ - tetrachloro-1,4-benzoquinone, TCHQ - tetrachlorohydroquinone, ROS - reactive oxygen species, $\Delta\psi_m$ - mitochondrial membrane potential, GSH - glutathione.

Chapter 2: Methods and materials

Ethics approval was obtained from the Ethics Committee of the Faculty of Health Sciences, of the University of Pretoria to carry out the study (Appendix I). A list of reagents used in the methods below, as well as details of reagent preparation is provided in Appendix II.

2.1. Cell maintenance

SH-SY5Y human neuroblastoma cells were purchased from American Tissue Culture Collection (ATCC: CRL-2266). Cells were cultured in T25 cell culture flasks (Greniner Bio-one, Monroe, North Carolina, USA) with a 1:1 ratio of Dulbecco's Modified Eagle's Medium (DMEM) and Ham's F-12 nutrient mixture, containing 10% foetal calf serum (FCS). Cells were trypsinised approximately every two to three days, depending on confluence. Medium was discarded, and the flask washed with 5 mL of phosphate buffered saline (PBS). Following adequate washing, 1 mL TrypLE Express trypsin was added for a few seconds in order to break cell adhesion to the flask. Trypsin was then neutralised with 1 mL of medium. If the purpose of trypsinisation was purely for cell maintenance, the medium and accompanying loose cells were then discarded, assuming sufficient cells remained attached in the flask to regrow. If the purpose was to collect cells for seeding for an experiment, the medium with cells was retained and placed in a 15 mL tube. Five milliliters of medium was then added to the trypsinised T25 flask, and the flask was incubated at 37°C, with carbon dioxide (CO₂) controlled at 5%. If the majority of cells had detached, flask contents were collected in a 15 mL tube, centrifuged at 200 g for 5 min, the supernatant discarded, and cells resuspended in new medium. Of this, an appropriate amount of cells were pipetted into the culture flask, and topped up with adequate medium. Excess cells were either discarded, or kept for experimental purposes.

2.2. Cell seeding and exposure

The concentration of cells collected was determined using a trypan blue exclusion assay. A solution of 100 μL PBS, 80 μL trypan blue, and 20 μL cells was prepared, 10 μL of which was pipetted onto a haemocytometer, and cells counted under a light microscope. The average number of cells counted in the four quadrants gave the cell concentration at $\times 10^5$ cells/mL. Cells were then diluted to 50 000 cells/mL in a volume appropriate for the particular experiment. For spectrophotometry and spectrofluorometry based assays, cells were pipetted into sterile 96-well plates (Lasec, Cape Town, South Africa), such that each well contained approximately 5 000 cells in 100 μL . For microscopy purposes, and flow cytometry based assays, cells were seeded in 6-well plates (Lasec, Cape Town, South Africa), such that each well contained approximately 150 000 cells in 3 mL medium. Seeded plates were then incubated for 24 h at 37°C to allow for cell adherence to the plate surface. After this attachment period, exposure of reagents and subsequent testing was conducted. For assays using 96-well plates, cells were exposed to test or control conditions by adding 100 μL of medium containing the desired compound, at a concentration twice that of the desired final concentration. For assays using 6-well plates, medium was aspirated, and gently replaced with 3 mL medium containing the desired final in-well concentration of the compound. For all assays, the final in-well concentration was equivalent to the IC_{50} for each test compound, unless otherwise stated. The final concentration of DMSO in vehicle controls was equivalent to the highest DMSO concentration of the test samples, which was always lower than 0.5%. A negative control was included in all experiments to ensure that the vehicle had no significant effect on cell growth or parameters tested, and it consisted of medium only, without any DMSO or compound added. Spectrofluorometry based assays made use of white bottom 96-well plates (Lasec, Cape Town, South Africa). The outside perimeter wells of 96-well plates were not used for experimental purposes, but were filled with 100 μL PBS, so as reduce error due to evaporation.

2.3. Detection of cytotoxicity

Cytotoxicity was assessed using the SRB colorimetric assay of Vichai and Kirtikara.¹⁸⁷ This was used to determine the IC_{50} values, which served as initial

assessment of the toxicity of each compound, and to determine exposure concentrations for subsequent experiments.

The SRB assay was chosen to determine growth inhibition as it has been optimised for cytotoxicity testing in 96-well plates.¹⁸⁷ The assay is based on detection of cell density via quantification of the amount of protein within cells. This assay was also selected due to its high sensitivity¹⁸⁸ and relative affordability. The reason for this choice over the tetrazolium dye (MTT) method was due to the SRB's lower rate of interference with non-testing compounds¹⁸⁷ and it does not require metabolic activity of the cells, thus the number of steps required for its optimisation are fewer, resulting in a lower chance of any compromise.¹⁸⁹ The choice of SRB over a crystal violet assay was due to greater potential of accuracy, as the crystal violet assay requires removal of medium and transfer to a reading plate, whereas the SRB retains everything in one plate, resulting in a lower chance of content loss and pipetting inaccuracies. The SRB dye binds basic amino acids of proteins in cells that have been fixed to the 96-well plate, the amount of which is directly proportional to cell mass.¹⁸⁷ This was used to determine IC₅₀ values via spectrophotometry. By ensuring an initial equal concentration of cells in each well before exposure, effects of exposure on cell proliferation due to different concentrations of the test compounds were quantified in a controlled manner.

Procedure for determining IC₅₀ with the SRB assay was as follows:¹⁸⁷

For initial IC₅₀ screening, cells were treated with 100 µL of 20, 100, 200 and 300 µM of PCP, TCBQ, or TCHQ, with in-well concentrations amounting to 10, 50, 100, and 150 µM in 200 µL. Remaining wells were divided into control sections, consisting of a medium colour control (medium only with no cells), a cell growth control (cells with medium only), a vehicle control (cells with medium and DMSO), and a positive control (cells with medium and an optimised IC₅₀ concentration of 98 µM DDT in DMSO). The concentration of the positive control, DDT, was also determined using the SRB assay. DDT was used as a positive control as it is an organochloride pesticide similar to PCP and its toxicity has been determined extensively.¹⁹⁰ In addition, colour controls were included for TCBQ and TCHQ, as these compounds had yellow colours in DMSO solution. Although PCP was a clear solution, a colour control was included to control for any interference not visible to the human eye.

Once initial screening had yielded roughly estimated IC₅₀ values, the ranges of the concentration of each compound were narrowed towards the estimated IC₅₀, and more data points added, in order to improve accuracy of IC₅₀ prediction. An example of experimental plate layout is provided in Figure 6. Once exposed, the plates were incubated at 37°C for 48 h. This exposure time was chosen as it resembles the population doubling time of the SH-SY5Y cell line.¹⁹¹

After the 48 h incubation time, 50 µL of cold 50% trichloroacetic acid (TCA) was added to the wells and incubated at 4°C overnight for fixation. The plates were then washed with tap water, and 100 µL of 0.057% SRB stain added and incubated for 30 min. The dye was then washed three times with 1% acetic acid. A 10 mM tris-base solution (pH 10.5) was added at 200 µL per well to solubilise the dye. Spectrophotometry was subsequently performed using a Biotek EL-X 800 microplate reader, with the absorbance of the dye measured at 490 nm, with a reference of 530 nm. IC₅₀ values were determined using the following equation:

$$Survival \% = \frac{T}{C} \times 100$$

where T = optical density of test well minus background, and C = average optical density of vehicle control well minus background. Using Graphpad Prism 6, a non-linear regression curve was generated using a log[inhibitor] vs response function, from which IC₅₀ values were determined.

All subsequent experiments used exposure concentrations equivalent to that of the IC₅₀ of the compound. Varying time points were used for subsequent experiments, depending on appropriateness for the assay. These time points were determined experimentally by initial screening of a range of time points, the range of which was supported by literature. Different time points used in final analysis are indicated in the relevant sections below.

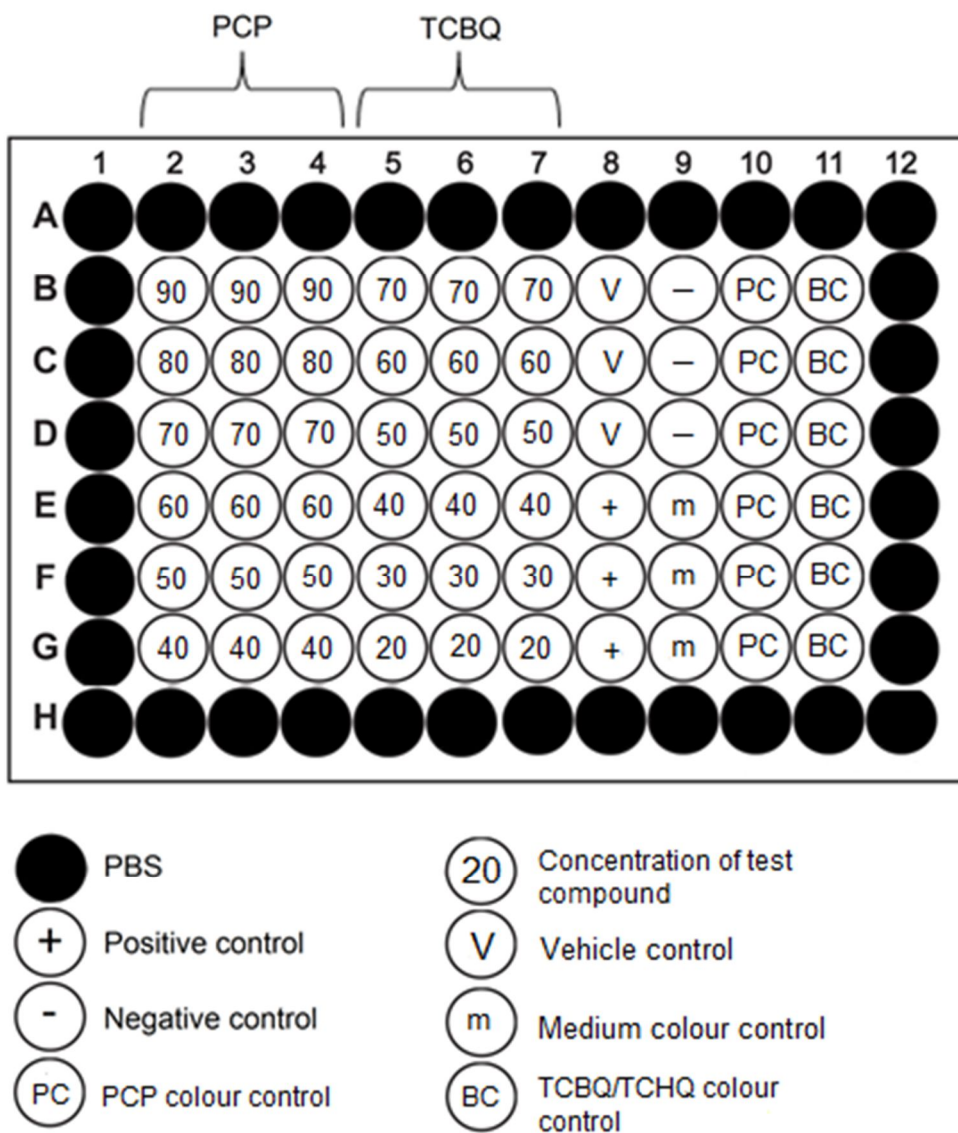


Figure 6: Experimental plate layout used for the SRB assay when conducted in a 96-well microplate.

2.4. Cell cycle analysis

Cell cycle analysis is a useful procedure to include in toxicological evaluation as it indicates which phase of the cell cycle the compounds affect, and from this, further suggestions can be made as to which specific pathways should be investigated to discover detailed mechanistic action. In this method, predominant cell cycle stages were ascertained by determining the DNA content of the cells, as the amount of DNA differs between cell cycle stages due to DNA replication and mitosis.³⁴ Flow

cytometry was used to quantify the DNA content of individual cells with PI, as this dye intercalates with nucleic acid and fluoresces.³⁴ This dye stains all types of nucleic acid,³⁴ thus the addition of ribonuclease (RNase) was a necessary step to eliminate signals coming from ribonucleic acid (RNA) components. For the purpose of this study, effects on cell cycle were assessed at 12, 24, and 48 h, in order to determine how rapidly each compound acts, as well as to observe any phenomena that may be missed once substantial cell death has occurred. Cell cycle analysis was performed using flow cytometry and PI staining as described below.³⁴

Cells were seeded into 6-well plates, at a concentration of 150 000 cells per well in 3 mL (50 000 cells/mL). After a 24 h attachment period, medium was aspirated, and wells were treated with 3 mL medium containing IC₅₀ concentrations of either PCP, TCBQ, TCHQ, positive control (DDT), cell growth control, or a vehicle control treatment. After the relevant exposure period, cells were trypsinised from wells. This was done by collecting and transferring medium from each well into 15 mL tubes, and adding 500 µL PBS to each well. The PBS was then pipetted into the same 15 mL tubes as the saved medium, and 500 µL TrypLE Express trypsin added to wells. Once cells had detached, the trypsin was neutralised by pouring the saved medium and PBS back into relevant wells. The entire content of each well was then pipetted back into corresponding 15 mL tubes. This process ensured that all cells were collected from wells, whether adherent or non-adherent at the time of trypsinisation. Collected cells were centrifuged at 300 *g* for 5 min, and the supernatant discarded. Cells were resuspended in 100 - 150 µL cold PBS, depending on pellet size. Ice cold 70% ethanol was then added drop by drop while vortex-mixing, amounting to a final volume of 1.5 – 2 mL, again depending on pellet size, and the mixture stored at 4°C until flow cytometry reading. On the day of reading, cells were centrifuged at 400 *g* for 10 min and the supernatant discarded. This elevated *g*-force and time was due to cells becoming more buoyant when suspended in ethanol. A PI-RNase solution was prepared, consisting of 100 µg/mL PI and 40 µg/mL RNase in PBS, such that 500 µL could be added to each sample. The samples were then incubated for 45 min at 37°C, and transferred to flow cytometry tubes. The DNA content of the cells was quantified using a Beckman Coulter FC500 series flow cytometer, under the FL3 channel (excitation 535 nm, emission 617 nm). Data analysis was conducted using the Weasel flow cytometry analysis programme. Forward and side scatter plots were

generated, and debris gated out according to the vehicle control, as determined by identification of small, ungranulated events occurring below the dominant cell population. Doublets were gated out in a similar manner using DNA (PI) and DNA peak scatter plots. Histograms showing DNA (PI) content of cells were generated, and a cell cycle curve fit algorithm used to identify sub-G1, G1, S, G2/M and super G2 areas within the histogram. This algorithm functions by fitting Gaussian curves to each phase, and proved more accurate and less subjective than manual determination of cell cycle regions. For each sample, the percent of events in each cell cycle phase compared to the total cell cycle of the sample was extracted from the histogram, and values for each phase was compared to the vehicle control of the same time point to determine differences in cell cycle progression.

2.5. Mode of cell death

The differentiation between modes of cell death such as apoptosis or necrosis is essential in any toxicity evaluation as increased induction of different modes of cell death is indicative of pathways upon which compounds act. They may cause up- or downregulation of key components within a pathway, and the resultant type of cell death can indicate which should be further examined. The Annexin V-FITC/PI assay is a test that is highly advantageous in such evaluation, in that it allows for the simultaneous quantitative measurement of apoptosis and necrosis.¹⁹² Annexin V of the Annexin V-FITC conjugate binds PS, which occurs on the inner cytoplasmic membrane of a healthy cell. Under early apoptotic conditions, this phospholipid is translocated to the outer membrane, allowing Annexin V to bind, and the green fluorescence of the FITC can be used to quantify the amount of cells undergoing apoptosis under an FL1 channel.¹⁹³ Propidium iodide cannot pass through the intact membrane of a healthy cell, but may only enter the cell under necrotic conditions, where the cell membrane is damaged. Propidium iodide fluoresces under the red FL3 channel, thus by measuring the amount of cells fluorescing red, necrosis can be quantified.¹⁹³ This dual-fluorescence assay is possible due to the two dyes fluorescing under two different channels, allowing for apoptosis and necrosis detection in the same sample. Exposure time for this assay was 48 h, as mode of cell death is an end-point directed objective.

Cells were seeded into 6-well plates, and exposed to test or control conditions as described in section 2.4. After the 48 h exposure period, cells were trypsinised, again as described in section 2.4. Samples were centrifuged at 200 g for 5 min, the supernatant discarded, and resuspended in 1 mL of binding buffer. The cells were again centrifuged (300 g ,10 min), supernatant discarded, and cells resuspended in 100 µL binding buffer, as well as 2.5 µL Annexin V-FITC. Samples were then incubated at 25°C in the dark for 15 min, followed by centrifuging at 300 g for 10 min. Cells were resuspended in 500 µL binding buffer, and immediately prior to flow cytometry analysis, 10 µL of 30 µg/mL PI was added, while making sure to shield it from light. Flow cytometry was performed using the Beckman Coulter FC500 series flow cytometer, and a scatterplot was produced, from which apoptosis and/or necrosis could be deduced. The scatterplot was divided into four quadrants. An accumulation of points in each quadrant indicated modes of cell death,¹⁹² as portrayed in Figure 7.

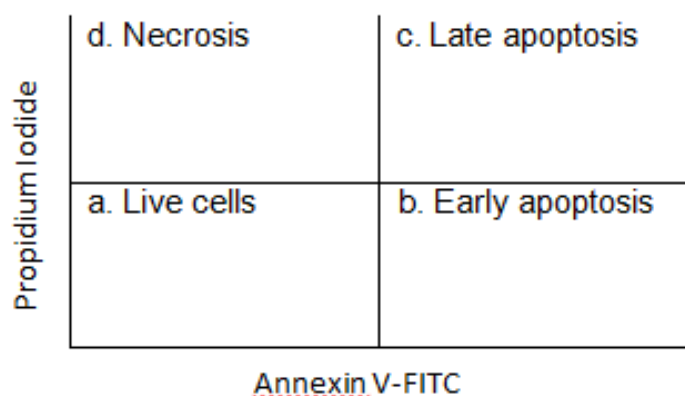


Figure 7: Quadrant compartmentalisation found in a scatter plot of Annexin V-FITC and PI fluorescence, indicating mode of cell death.

2.6. Caspase activity

Caspases are a group of proteolytic enzymes that play a role in the induction of apoptosis in the cell.¹⁹⁴ Assessing their activity is a useful way to determine pathways of apoptosis. Caspase-3 is an executioner caspase common to both the intrinsic and extrinsic apoptosis pathways. The activation of this caspase activates cysteine protease abilities, allowing it to degrade cellular components as a primary

means of apoptosis.¹⁹⁵ The tetrapeptide Asp-Glu-Val-Asp (DEVD) is cleaved specifically by caspase-3/7, the basis of which is utilised in the assessment of the protease's activity. When the tetrapeptide is complexed with the fluorophore 7-amino-4-methylcoumarin (AMC), a non-fluorescent caspase-3/7 specific substrate (Ac-DEVD-AMC) is formed. Upon cleavage of said substrate, the freed AMC molecule emits fluorescence (excitation 380 nm, emission 430-460 nm), which can be quantified in order to ascertain relative activity of caspase-3/7 in a sample.¹⁹⁶ Although the Ac-DEVD-AMC substrate confers nearly identical specificity towards both caspase-3 and -7, the hydrolysis rate of this substrate by caspase-7 is approximately ten-fold lower than its counterpart, thus changes in activity levels measured by this assay are frequently attributed to that of caspase-3 effects.¹⁹⁷ For the purpose of this study, it is sufficient to consider activity changes as that of caspase-3, however the potential small role of caspase-7 is noted.

Cells were seeded into a 96-well white bottom plate at 5 000 cells per well in 100 μ L (50 000 cell/mL). After a 24 h attachment period, cells were exposed to 100 μ L of two-fold IC_{50} concentrations of PCP, TCBQ or TCHQ for 48 h. Staurosporine (20 μ M) served as a positive control as it is known to induce caspase-3 activation,¹⁹⁸ while DMSO served as a vehicle control. Thirty minutes prior to starting the assay, 0.5 mM phenylmethylsulfonyl fluoride (PMSF) and 4.3 mM β -mercaptoethanol were added to the incomplete lysis buffer, and 0.5 mM PMSF, 4.3 mM β -mercaptoethanol, and 5 μ M Ac-DEVD-AMC were added to the incomplete caspase-3 substrate buffer. After the 48 h exposure period was complete, medium was replaced with 25 μ L cold lysis buffer and incubated on ice for 15 min. Caspase-3 substrate buffer (100 μ L) was then added, and samples incubated at 37°C for 4 h. Thereafter, the plate was further incubated in the fridge at 4°C for 16 h. The plate was then read using a BioTek Synergy 2 plate reader, with excitation and emission wavelengths of 380 nm and 460 nm respectively. Cell density was controlled for with an SRB assay in an adjacent plate – a direct SRB counterstain could not be used as the caspase assay lyses the cells, which would then not be able to be fixed by the TCA of the SRB. For this reason, six rather than three experimental repeats were performed for each biological repeat to ensure greater confidence and reproducibility in results. Once fluorescence values were normalised according to cell density, the fold change of

caspase-3 relative to vehicle control was obtained by dividing normalised test sample fluorescence by normalised vehicle control fluorescence.

2.7. Cell morphology

Cell morphology tests are useful in toxicity testing as it allows for the visualisation of effects compounds have on cells. In particular, hallmarks of apoptosis can be seen by membrane blebbing and the formation of apoptotic bodies.⁷⁶ In addition, visualisation of cell changes allows for the detection of large scale abnormalities that might not have been anticipated, and therefore not specifically tested for. Hoechst 33342 is a fluorescent dye which stains DNA blue (emission 461 nm, excitation 510-540 nm), allowing for visualisation of the nucleus.¹⁹⁹ Acridine orange is a fluorescent dye that stains acidic bodies green, the upregulation of which indicates cell death,²⁰⁰ and PI stains cells with compromised cell membranes, which is also indicative of cell death.²⁰¹

Cells were seeded into 6-well plates at a concentration of 150 000 cells per well, with 3 mL per well (50 000 cells/mL). After a 24 h attachment period, cells were exposed to test or control conditions as described in section 2.4. After a 48 h exposure period, 500 μ L of 3.5 μ g/mL Hoechst 33342 was added to each well (final concentration 0.9 μ g/mL), and incubated at 37°C for 25 min. Following this, 500 μ L of 4 μ g/mL acridine orange and 500 μ L of 40 μ g/mL PI was added (in well concentration 1 μ g/mL and 12 μ M, respectively), and the plates incubated for a further 5 min. Medium was then removed and cells washed once with 500 μ L PBS. Cells were then immersed with 1 mL PBS, and photographs taken using a Zeiss Axiovert CFL40 microscope with a Zeiss AxiovertMRm monochrome camera. Zeiss Filter 2 was used for Hoechst 33342, Filter 9 for acridine orange, and Filter 15 for PI imaging. Filters were removed for non-fluorescent light microscopy photographs. Images captured were processed using ImageJ image processing software.

2.8. Reactive oxygen species production

Reactive oxygen species are well known to cause DNA damage and oxidative stress to cells, which can largely impair their functioning, and even lead to cell death.²⁰² Oxidative stress has been noted for non-neuronal cells exposed to PCP and its metabolites,²⁰³ thus it is possible that cell damage may occur in this manner in neuronal cells as well. It is therefore important to include an assay that will ascertain the level of ROS production. In this study, ROS was determined using 2,7-dichlorofluorescein diacetate (DCFDA). This is a non-fluorescent probe, which becomes fluorescent upon oxidation into DCF by hydrogen peroxide (H₂O₂), which is a form of ROS.²⁰⁴ Changes in ROS production have been documented to have a rapid onset in some toxicity studies, while in other studies, changes have been observed after extended exposure periods, thus the time points chosen for this assay, after experimental determination were 4, 24, and 48 h.

Cells were seeded into 6-well plates at a concentration of 150 000 cells per well, with a volume of 3 mL per well (50 000 cells/mL). Cells were exposed to test and control conditions as described in section 2.4, with the exception of the positive control. For this assay, a final concentration of 500 µM 2,2'-azobis(2-amidinopropane) dihydrochloride (AAPH) was used as it is a well-established model for ROS production. After the relevant incubation period, cells were trypsinised, centrifuged at 400 g for 10 min, and resuspended in 1 mL of 10 µM DCFDA in PBS. Samples were incubated at 37°C for 15 min. Cells were then washed twice with PBS by centrifuging at 400 g for 10 min and resuspending in 1 mL PBS. After washing, cells were resuspended in 500 µL PBS, and transferred to flow cytometry tubes for reading. The amount of green fluorescent DCF in each cell was read and quantified using the Beckman Coulter FC500 series flow cytometer under an FL1. Data obtained was analysed using Weasel flow cytometry software, where histograms were generated for each sample. From this, mean values were obtained for each sample, and fold change in ROS obtained by the following equation:

$$ROS \text{ fold change} = \frac{TFL1}{CFL1}$$

where TFL1 is the mean fluorescent value obtained from the FL1 channel for the test compound, and CFL1 is that of the DMSO vehicle control

2.9. Mitochondrial membrane potential

Mitochondrial membrane permeabilization is a critical step in the intrinsic pathway of apoptosis as it allows for the efflux of apoptosis activator and effector molecules, as well as the influx of triggers that may lead to further compromise of the membrane and apoptotic signalling.⁷⁵ The permeabilization of the mitochondrial membrane can be indicated by the measurement of $\Delta\Psi_m$. 5,5',6,6'-tetrachloro-1,1,3,3'-tetraethylbenzimidazolylcarbocyanine iodide (JC-1) is a dye that fluoresces orange in healthy cells, as the dye accumulates as aggregates in the mitochondria, and green in apoptotic cells with lowered $\Delta\Psi_m$ as the dye exists as monomers throughout the cell, unable to accumulate in the mitochondria due to compromised membrane integrity. By quantifying the ratio of orange to green signals detected flow cytometrically, the level of membrane integrity loss, and thus the degree of permeabilization can be determined.⁹ Mitochondrial membrane potential is often closely linked to ROS levels, as increased ROS can damage the mitochondrial membrane, as well as be a product of declining mitochondrial membrane potential. This combination may induce a cascade of events leading to apoptosis, among other ROS- $\Delta\Psi_m$ relationships.²⁰⁵ For this reason, $\Delta\Psi_m$ assays were run concurrently with ROS assays at 4, 24, and 48 h exposure times for greater comparability.

Cells were seeded into 6-well plates, at a concentration of 150 000 cells per well in 3 mL (50 000 cells/mL). After a 24 h attachment period, cells were exposed for either 4, 24, or 48 h to test compounds and controls as described in section 2.4, with the exception of the positive control, which for this assay was 100 nM rotenone. After the relevant exposure period, cells were trypsinised, centrifuged at 400 g for 10 min, the supernatant discarded, and cells resuspended in 500 μ L of 5 μ g/mL JC-1 dye in PBS. After a 15 min incubation period at 37°C, cells were again centrifuged and washed twice with 1 mL PBS. Thereafter, cells were resuspended in 500 μ L PBS and transferred to flow cytometry tubes for reading. Fluorescence was measured using a Beckman Coulter FC500 series flow cytometer, under FL1 and FL2 channels (emission: 520 nm and excitation: 485 nm for monomers, and emission: 590 nm, excitation: 492 nm for aggregates). Mean fluorescence values were obtained from resulting histograms for both channels, the ratio of which was used to determine $\Delta\Psi_m$ fold change:

$$MMP \text{ fold change} = \frac{(TFL2/TFL1)}{(CFL2/CFL1)}$$

where TFL1/2 is the mean fluorescent value obtained from the FL1 or FL2 channels for the test compound, and CFL1/2 is that of the DMSO vehicle control.

2.10. Intracellular reduced glutathione content

Glutathione can occur in an oxidised state (GSSG) and in a reduced state (GSH). Reduced glutathione is an antioxidant which protects the cell against oxidative stress by allowing ROS to oxidise it to GSSG. The intracellular levels of GSSG and GSH can influence cell death, where increased GSSG-GSH ratio is indicative of oxidative stress, and lowered levels of GSH content may leave the cell vulnerable to ROS.³² A method to gain insight into effects on glutathione is to measure GSH content using a monochlorobimane (MCB) assay. In this assay, the MCB dye binds GSH in the cell and fluoresces, allowing for GSH quantification.²⁰⁶

Cells were seeded into a 96-well white bottom plate at 5 000 cells per well in 100 μ L (50 000 cell/mL). After a 24 h attachment period, cells were exposed to 100 μ L of two-fold IC_{50} concentrations of PCP, TCBQ or TCHQ for 48 h, while 10 μ M n-ethylmaleimide (NEM) served as positive control, and DMSO as vehicle control. Following a 48 h period of exposure, medium was replaced with 100 μ L of 16 μ M MCB in PBS and incubated at 37°C for 2 h. Fluorescence of each well was then quantified spectrofluorometrically using a BioTek Synergy 2 plate reader read at excitation and emission wavelengths of 360 and 460 nm respectively. Fluorescence values were normalised according to cell density obtained from an SRB counterstain. GSH levels relative to vehicle control were then determined using the following equation:

$$GSH \% = \frac{\text{fluorescence of sample}}{\text{average fluorescence of vehicle control}} \times 100$$

2.11. Acetylcholinesterase inhibitory activity

2.11.1. Ellman esterase assay

It is important to evaluate the presence of AChE inhibitory activity of PCP, as this is a common mechanism of many neurotoxic pesticides.¹⁵⁶ A commonly used method for AChE inhibitory activity detection is the Ellman esterase assay, the concept of which is depicted in Figure 8. This assay makes use of acetylthiocholine iodide (ATChI) due to the necessity of the thiol group. The iodide serves solubility purposes, and in solution, acetylthiocholine (ATCh) is acted upon in the same manner as ACh by AChE. In the normal reaction, ATCh is cleaved into acetate and thiocholine by AChE. The choline then reacts with 5,5'-dithiobis(2-nitrobenzoic acid) (DTNB) to form 5-thio-2-nitrobenzoate (TNB), which is a yellow compound, and is monitored at an absorbance of 412 nm. By quantifying the absorbance, the amount of ATCh cleaved can be inferred, and thus the relative activity of AChE.²⁰⁷

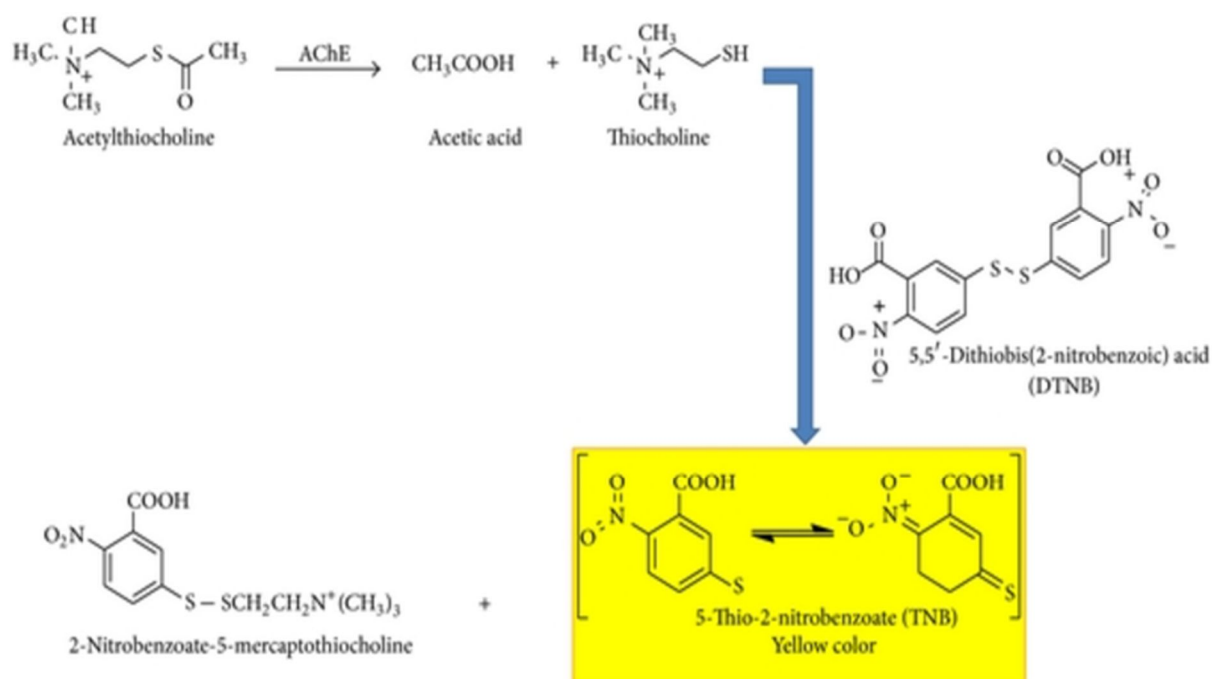


Figure 8: Depiction of Ellman esterase assay reaction.²⁰⁸

For the purpose of this study, an acellular method was used. Three buffers, namely A, B and C, were prepared prior to the start of the assay. Buffer A consisted of Tris-HCl adjusted to pH 8, buffer B consisted of buffer A containing 0.1 % bovine serum

albumine (BSA), and buffer C consisted of buffer A containing 0.1 M sodium chloride (NaCl) and 0.02 M magnesium chloride hexahydrate (MgCl₂·6H₂O). In a 96-well plate, 25 µL of 15 mM ATChI (in water), 125 µL of 3 mM DTNB (in buffer C), and 50 µL of buffer B was added to each well. Cytotoxic IC₅₀ concentrations of PCP, TCBQ, or TCHQ in buffer A were then added (initially, concentrations of compounds tested were the same as those used in cellular assays – here termed the ‘cytotoxic IC₅₀’). Water in buffer A served as a negative control, DMSO in buffer A as a vehicle control, and 20 µM galanthamine in buffer A as positive control. Galanthamine is a well characterised drug used for the treatment of Alzheimer’s disease, and is a known inhibitor of AChE.²⁰⁹ Baseline absorbance was then measured in a plate reader at 405 nm at 45 s intervals for three intervals (read 1), in order to control for spontaneous ACh cleavage. Following this, 25 µL of 0.2 U/mL AChE was added, and fluorescence measure again every 45 s, eight times consecutively (read 2). This initial rate kinetic run provided V_{max} values for both reads, from which AChE activity was inferred. Background activity was corrected for by subtracting V_{max} values for read 1 from read 2, and the following equation was used to determine AChE activity relative to the negative control:

$$AChE \text{ activity } \% = \frac{V_{max}(T)}{V_{max}(C)} \times 100$$

where V_{max}(T) is background adjusted V_{max} of the test, and V_{max}(C) is the background adjusted V_{max} of the negative control.

Following determination of effects of cytotoxic IC₅₀ concentrations on AChE activity, the concentration at which each compound inhibited AChE activity by half, here termed AChE IC₅₀, was determined. This was performed using the same protocol as above, but with varying exposure concentration ranges between 10 – 150 µM, based on preliminary screening. Dose-response curves were generated on Graphpad prism 6 with the use of a log[inhibitor] vs response function, which plotted the percent of enzyme activity against the log of the concentration of the suspected AChE inhibitor.²¹⁰

2.11.2. Molecular docking

In order to assess the plausibility of theorised molecular mechanisms of AChE inhibition, computational molecular docking was performed. Structural analogues of PCP and TCHQ stemming from the addition of cleaved ACh constituents, acetate or choline, were postulated to competitively inhibit AChE. This hypothesis is further detailed in results and discussion, as well as reasons for the exclusion of TCBQ from this section. Ligands of predicted competitive AChE inhibitors were drawn from PCP and TCHQ structures in ChemsSketch (Advanced Chemistry Development, Inc. 2016.2.2),²¹¹ from which ligand names and simplified molecular-input line-entry system (SMILES) notations were generated. Ligand SMILES notations were then converted to Protein Data Bank (PDB) files using the National Cancer Institute's online SMILES translator and structure file generator.²¹² These files were subsequently converted to PDBQT files containing partial charges and AutoDock 4 (AD4) atom types. Eel origin AChE receptor molecules were identified from the RCSB.org database, the structures (and bound ligands where applicable) of which have been previously determined by X-ray crystallography and published to the database. The PDB codes of proteins (receptors) used were 1acj, 1acl, 1amn, 1ax9, 1cfj, 1e3q, 1e66, 1eve, 1fss, 1gpk, 1gpn, 1gqr, 1gqs, 1h22, 1h23, 1hbj, 1odc, 1qti, 1u65, 1ut6, 1vot, 1w4l, 1w6r, 1w67, 1zgb, 1zgc, 2cek, 2ckm, 2cmf, 2j3q, 2v96, 2v97, 2v98, 2xi4, 3i6z, 4tvk, 4w63, 4x3c, 5bwb, 5bwc, 5dpl, 5e2i, 5e4j, 5e4t, 5ehx, 5ei5, and 5ih7. Identified receptors' PDB files were downloaded, and prepped for docking by removing the solvent, optimising amino acid rotamers, adding hydrogens, removing bound ligands, and resolving amino acids using UCFS Chimera 1.11.2.²¹³ PCP and TCHQ metabolite ligands were then docked to prepped receptors using two different docking software tools: Autodock Vina²¹⁴ and QuickVina2.²¹⁵ Each software tool utilises different parameters to determine binding energies for docked ligands, and the use of multiple software tools confers greater confidence to accurate *in vivo* prediction. Binding energies were captured and used to infer binding affinity of the ligand to receptor, and a binding energy of less than -9 was assumed to constitute a strong binding affinity. Binding energies were sorted in a hierarchy of lowest (strongest) to highest (weakest) in order to determine patterns with regard to ligand and/or receptor classes.

2.11.3. Molecular dynamics simulation

Docked ligands of interest were identified for further investigation for an *in silico* molecular dynamics simulation in order to assess binding stability. The MD simulations were performed using GROMACS 4.6.5,²¹⁶ and the AMBER99sb force field for proteins.²¹⁷ The non-bonded force calculations were accelerated through graphics processing unit (GPU) acceleration using CUDA 5.0.²¹⁸ Ligands from the original X-ray structure or the docked poses were used in the simulations. The ligand topologies were prepared with ACPYPE²¹⁹ using *antechamber* from the AMBER 12 suite.²²⁰ The system was prepared by heating it to 310 K ($\tau_t=0.2$) during a 500 ps constant volume simulation with 2 fs time step using the modified Berendsen thermostat (V-rescale) using velocity rescaling.^{221,222} The pressure was equilibrated to 1 atm during a 1000 ps constant pressure simulation with a 2 fs time step using the Parrinello-Rahman parameters for pressure coupling.²²³ In both simulations, all heavy atoms were position restrained with the force constant of 1000 kJ/(mol.nm²). For the molecular dynamics run, the temperature and pressure were maintained at 310 K and 1 atm using the Berendsen thermostat (V-rescale) and Parrinello–Rahman pressure coupling method. The short-range non-bonded interactions were computed for the atom pairs within the cut-off of 1 nm, and the long-range electrostatic interactions were calculated using particle-mesh-Ewald summation method with fourth-order cubic interpolation and 0.12 nm grid spacing.²²⁴ The parallel Linear Constraint Solver (LINCS) method was used to constrain bonds.²²⁵ The *g_mmpbsa* package with the molecular mechanics Poisson–Boltzmann surface area (MM-PBSA) software from the Gromacs and APBS packages was used to calculate the binding energy.^{226,227} The average binding energy of docked ligands was compared to that of ligands from the original x-ray structure for indication of relative binding affinity and stability.

2.12. Statistical analysis

All experiments for which 96-well plates were used were performed in at least triplicate, with a minimum of three biological repeats. Flow cytometry experiments using 6-well plates were also performed on at least three separate occasions, and a statistical power was ensured as each cell counted as an event, and a minimum of

10 000 events was obtained for each sample. Descriptive statistics were expressed as mean \pm standard deviation. Data analysis was performed on Microsoft Excel 2010, Graphpad Prism 6 and Weasel flow cytometry software. Nonlinear regression was used to determine IC₅₀ values. Significance of differences between two groups (vehicle control and test) was performed using a two tailed Student t-test in Microsoft Excel 2010. Alpha (α) was set at 0.05, and a p value below 0.05 was considered significant.

Chapter 3: Results

3.1. Cell proliferation

Initial broad range IC_{50} screening revealed PCP, TCBQ, and TCHQ IC_{50} concentrations to be between 50-100, 10-50, and 50-100 μM , respectively. Concentration ranges were then narrowed around suspected IC_{50} values, and the number of data points increased. Dose-response curves were then generated from which IC_{50} values were determined (Figure 9). All three compounds exhibited dose-dependent induction of SH-SY5Y cytotoxicity after 48 h exposure, with the least potent being the parent compound PCP (Figure 9C), and the most potent TCBQ (Figure 9B).

All experiments were accompanied by a cell growth control and a vehicle control containing the same v/v % DMSO as the compound with highest v/v % in assay solution. Stock solutions were prepared such that less than 0.5 v/v % DMSO occurred in final concentrations of an assay. No significant difference ($p > 0.05$) was observed between vehicle and growth control, indicating that the vehicle had no effect on cell proliferation. The positive control used in the SRB assay was DDT, as it a pesticide known to exhibit neurotoxicity. Optimisation of this control was performed by ascertaining the IC_{50} concentration for the SH-SY5Y cell line, which was revealed to be 98.1 μM (Figure 10), and was used to ensure that the SRB assay was performed to satisfaction.

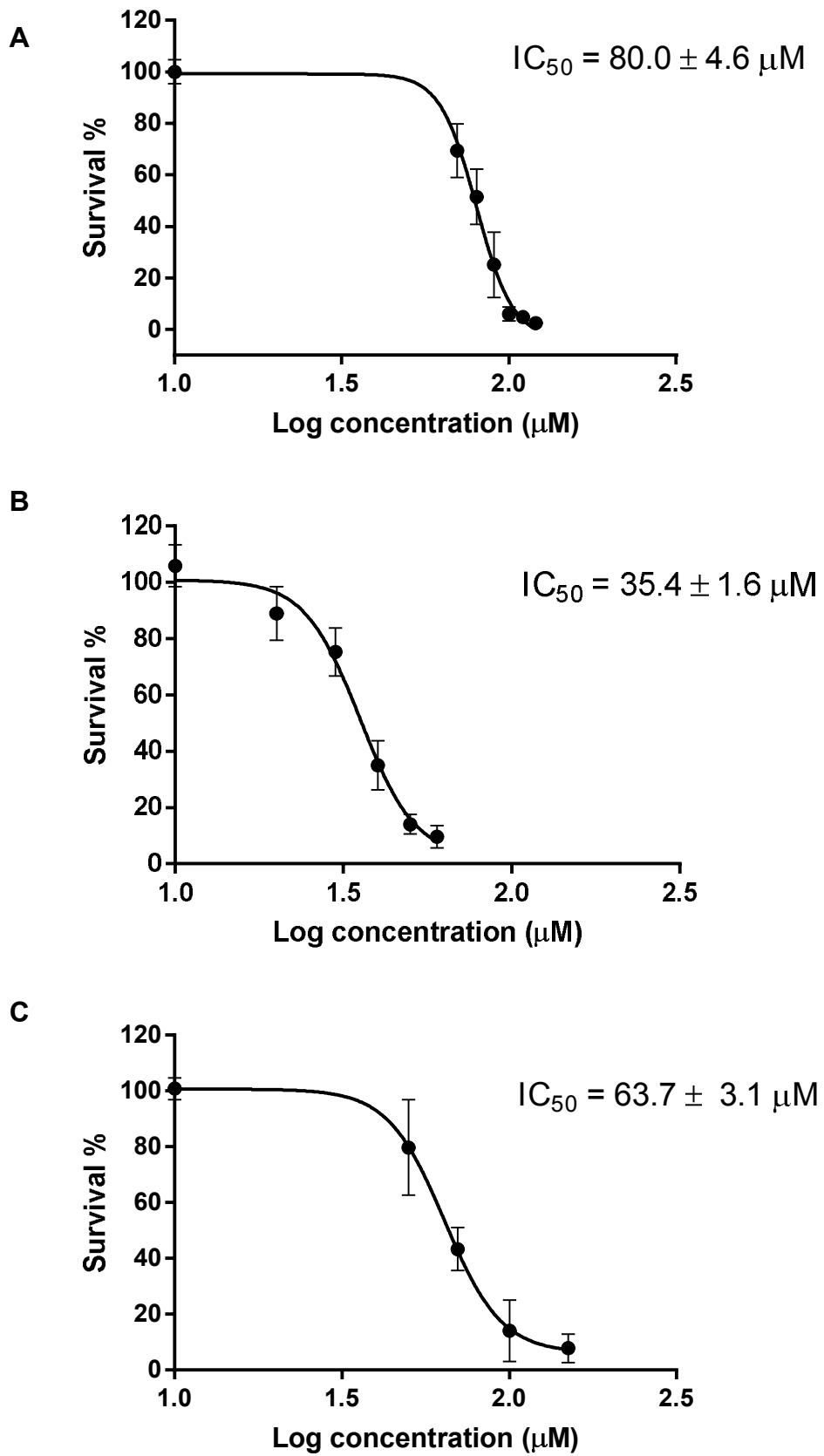


Figure 9: Dose-response curves of cells treated with A) PCP, B) TCBQ, and C) TCHQ.

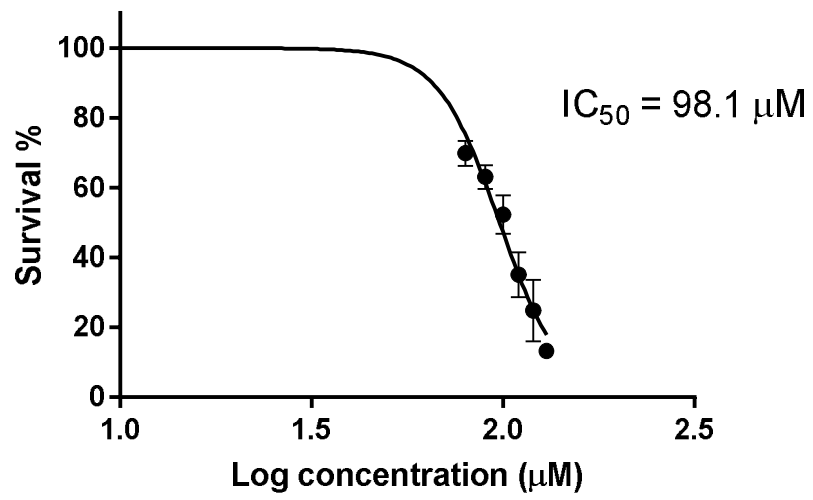


Figure 10: Dose-response curve in cells treated with DDT.

3.2. Cell cycle analysis

Cell cycle progression was assessed flow cytometrically using PI after 12, 24, and 48 h of treatment. Cell cycle histograms were generated after different exposure protocols. The cell cycle histograms for 12, 24, 48 h and various PCP concentrations are depicted in Figures 11, 13, 15 and 17, respectively.

Cell cycle phases sub-G1, G1, S and G2/M were defined using a Cell Cycle Curve Fit algorithm, and the phases colour coded in the following manner: red = sub-G1, first blue peak = G1, turquoise = S, and second blue peak = G2/M. This definition of phases produced the percent of events occurring in each phase, which was utilised for quantitative and statistical analysis. The results for 12, 24, 48 h and various PCP concentrations are provided in Figures 12, 14, 16 and 18, respectively.

At all time points the DMSO vehicle control yielded a highly characteristic cell cycle histogram against which compound exposure could be compared. The vehicle control did not depart significantly from the cell growth control. For the SH-SY5Y cell line, the vehicle control resulted in a negligible sub-G1 population, and an average of 54, 28, and 13 % events in the G1, S and G2/M phases respectively. Appropriate gating ensured the exclusion of doublet cells, resulting in a negligible super G2 population. This characteristic histogram indicated the assay to be successful.

3.2.1. 12 h exposure

After 12 h exposure to the compounds (Figures 11 and 12), no significant difference was seen between the vehicle control (Figure 11A) and PCP (Figure 11B), while TCBQ exposure resulted in a 20% average increase in the S phase ($p < 0.001$), along with a 28% decrease in G1, indicating an S phase block (Figure 11C). This was accompanied by a significant ($p < 0.01$) increase of 13% in the sub-G1 population, representing a relatively early onset of cell death. At this time point, TCHQ also began to display effects on the cell cycle in an apparent G2/M phase block, as indicated by a significant ($p < 0.001$) increase of 8% in the G2/M population, accompanied by a 18% decrease in G1 (Figures 11D and 12).

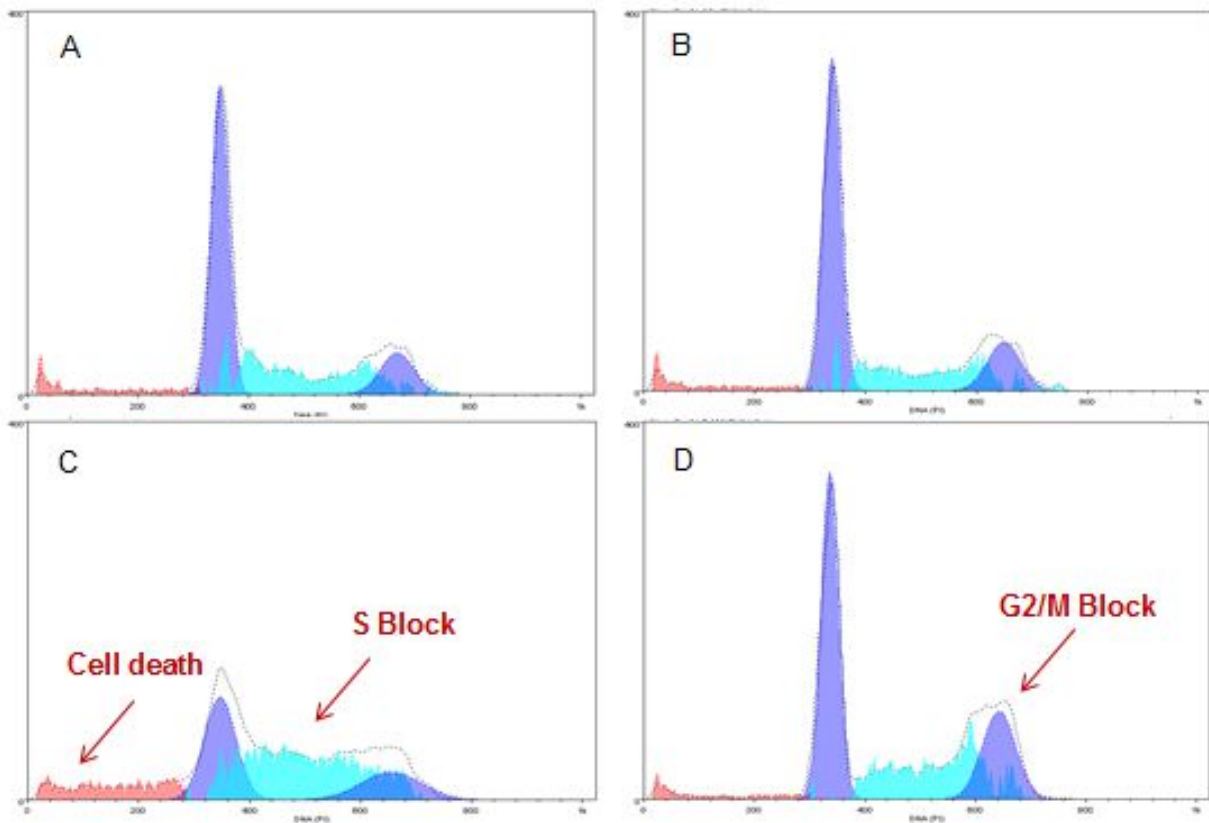


Figure 11: Histograms depicting stages in the cell cycle after 12 h exposure to A) DMSO (vehicle control), B) PCP, C) TCBQ, and D) TCHQ.

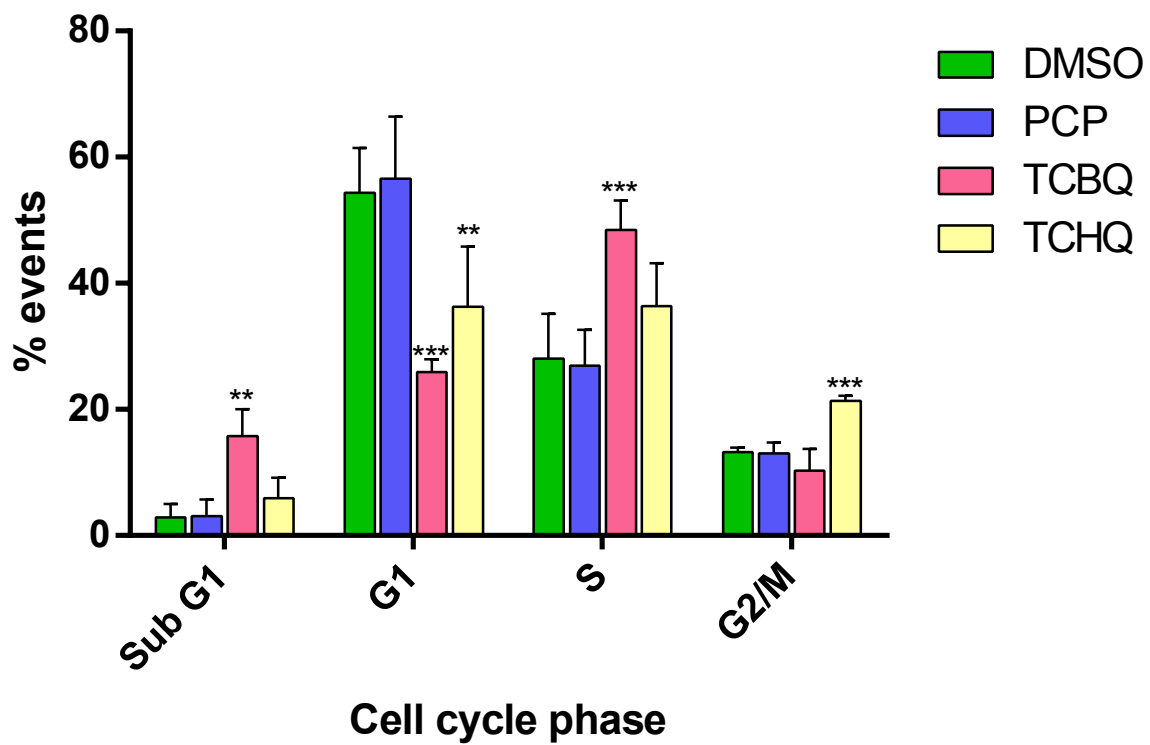


Figure 12: Average percent events for each cell cycle phase after 12 h exposure to PCP, TCBQ, or TCHQ. Significance of changes relative to vehicle control of the same cell cycle phase are indicated as ** = $p < 0.01$, *** = $p < 0.001$.

3.2.2. 24 h exposure

After 24 h exposure to PCP, a small, but consistent and significant ($p < 0.01$) increase of 11% and 6% occurred in G1 and sub-G1 populations, respectively, and a 15% decrease in S populations was noted (Figures 13B and 14). Pronounced cell death was already evident at this time point after TCBQ and TCHQ exposure with 20 and 35% increases in sub-G1 populations, respectively, while indicators for cell cycle blocks observed at 12 h had disappeared for both compounds at this point (Figures 13C, 13D and 14).

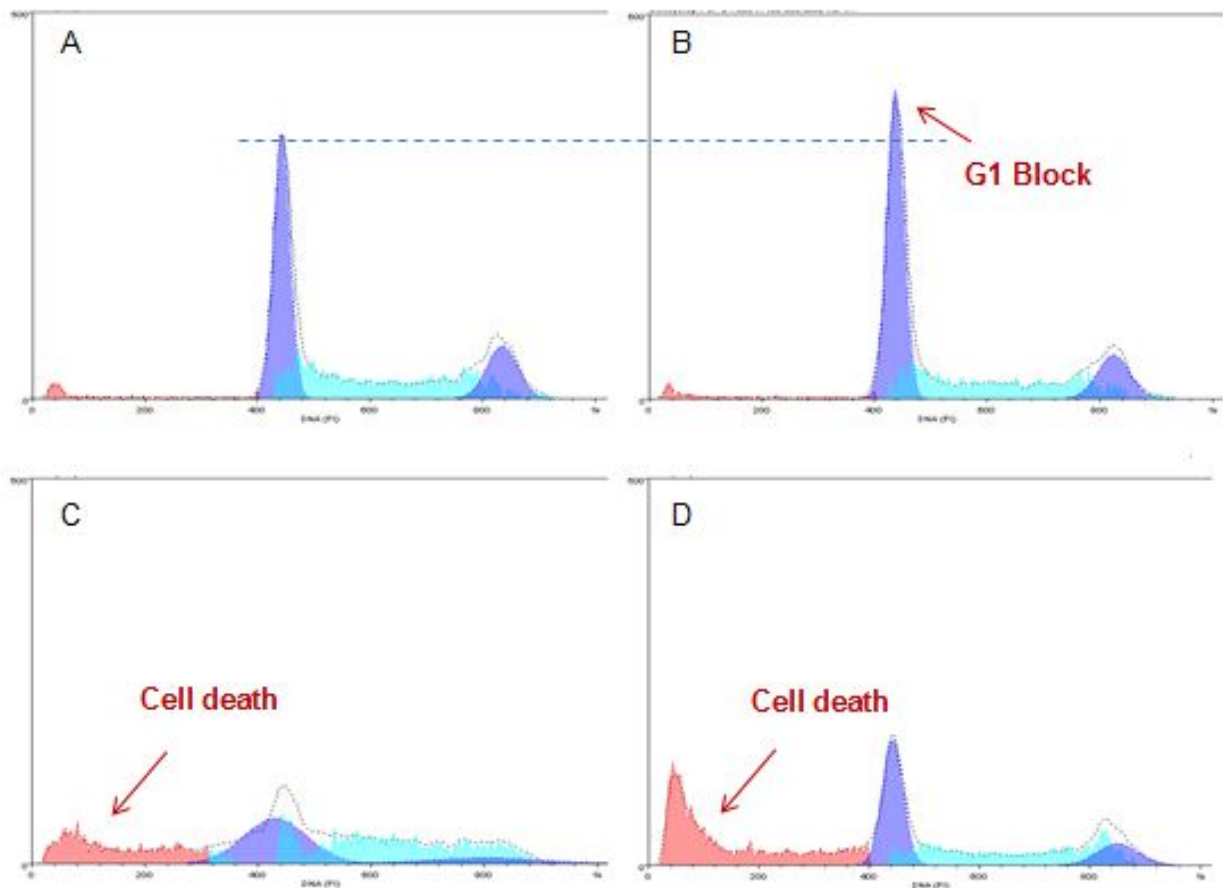


Figure 13: Histograms depicting stages in the cell cycle after 24 h exposure to A) DMSO (vehicle control), B) PCP, C) TCBQ, and D) TCHQ.

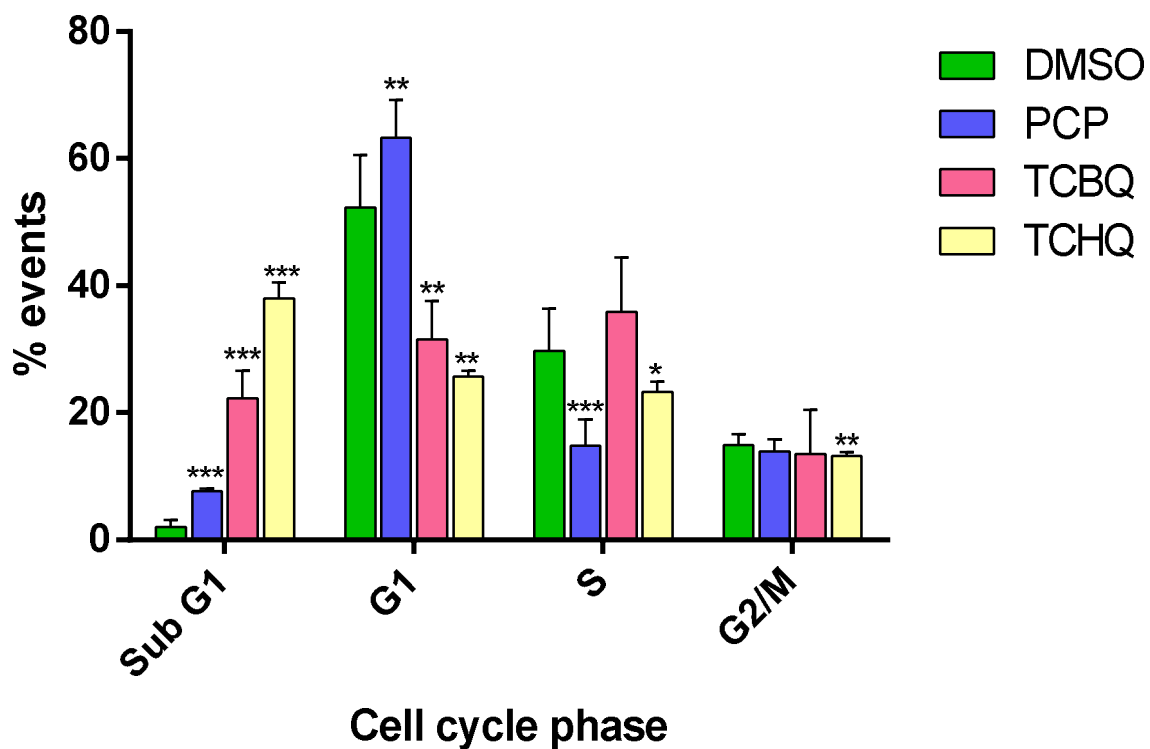


Figure 14: Average percent events for each cell cycle phase after 24 h exposure to PCP, TCBQ, or TCHQ. Significance of changes relative to vehicle control of the same cell cycle phase are indicated as * = $p < 0.05$, ** = $p < 0.01$, *** = $p < 0.001$.

3.2.3. 48 h exposure:

After 48 h exposure, sub-G1 populations had increased vastly for all compounds: 57, 61, and 36% increases due to PCP (Figures 15B and 16), TCBQ (Figure 15C) and TCHQ (Figure 15D) respectively. This was accompanied by G1 and S decreases for all compounds as the cell evidently fell out of the cell cycle into cell death, as well as decreases in G2/M due to PCP and TCBQ exposure (Figure 16). No significant change was observed in this phase as a result of TCHQ exposure. Cell cycle blocks revealed at previous time points were no longer evident after 48 h as the majority of affected cells appeared in the sub-G1 population.

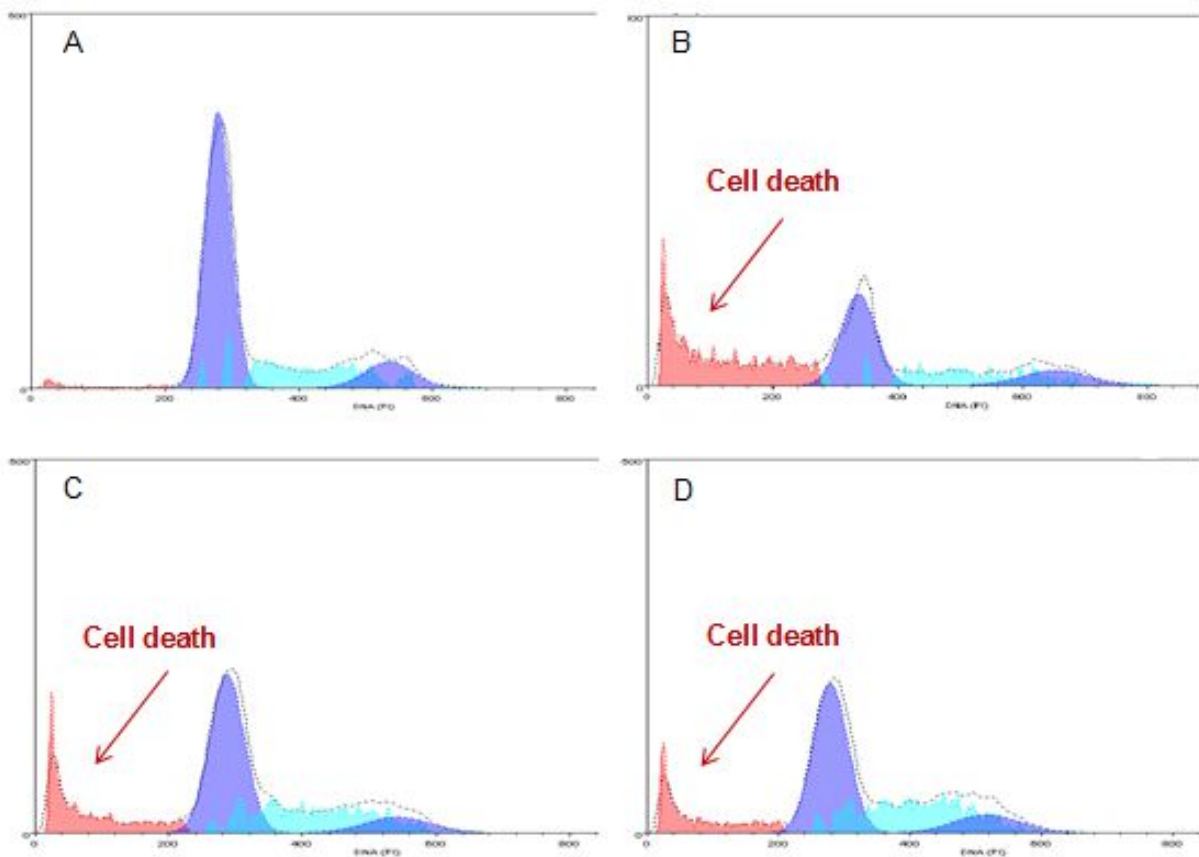


Figure 15: Histograms depicting stages in the cell cycle after 48 h exposure to A) DMSO (vehicle control), B) PCP, C) TCBQ, and D) TCHQ.

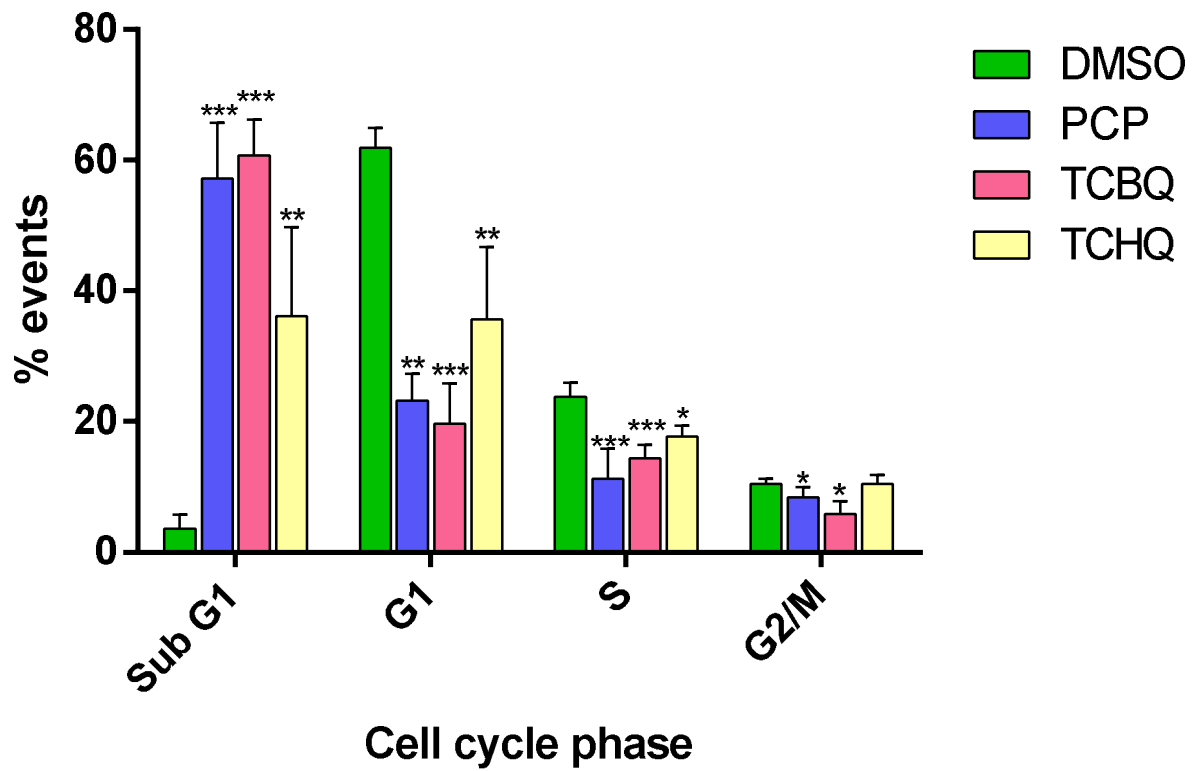


Figure 16: Average percent events for each cell cycle phase after 48 h exposure to PCP, TCBQ, or TCHQ. Significance of changes relative to vehicle control of the same cell cycle phase are indicated as * = $p < 0.05$, ** = $p < 0.01$, *** = $p < 0.001$.

3.2.4. Varying concentrations of PCP

Effects following 48 h exposure to various concentrations of PCP were assessed. Concentrations ranged between 60 and 90 μM in 10 μM intervals, one of which was the IC_{50} concentration (Figure 15B and 18), and the remainder (Figures 17B, 17C, 17D and 18) served to further investigate dose-response effects observed in the SRB assay. Dose-response increases in sub-G1 cells were noted. The highest concentration of PCP (90 μM) resulted in the largest sub-G1 population, which accounted for 73%. Although the lowest concentration of 60 μM appeared to mimic 24 h of 80 μM PCP exposure by an increase in G1 phase, this change was insignificant when compared to the vehicle control. All concentrations resulted in S phase decreases ranging from 14 to 21%, while only 80 and 90 μM exposure resulted in significant ($p < 0.001$) G1 and G2/M decreases.

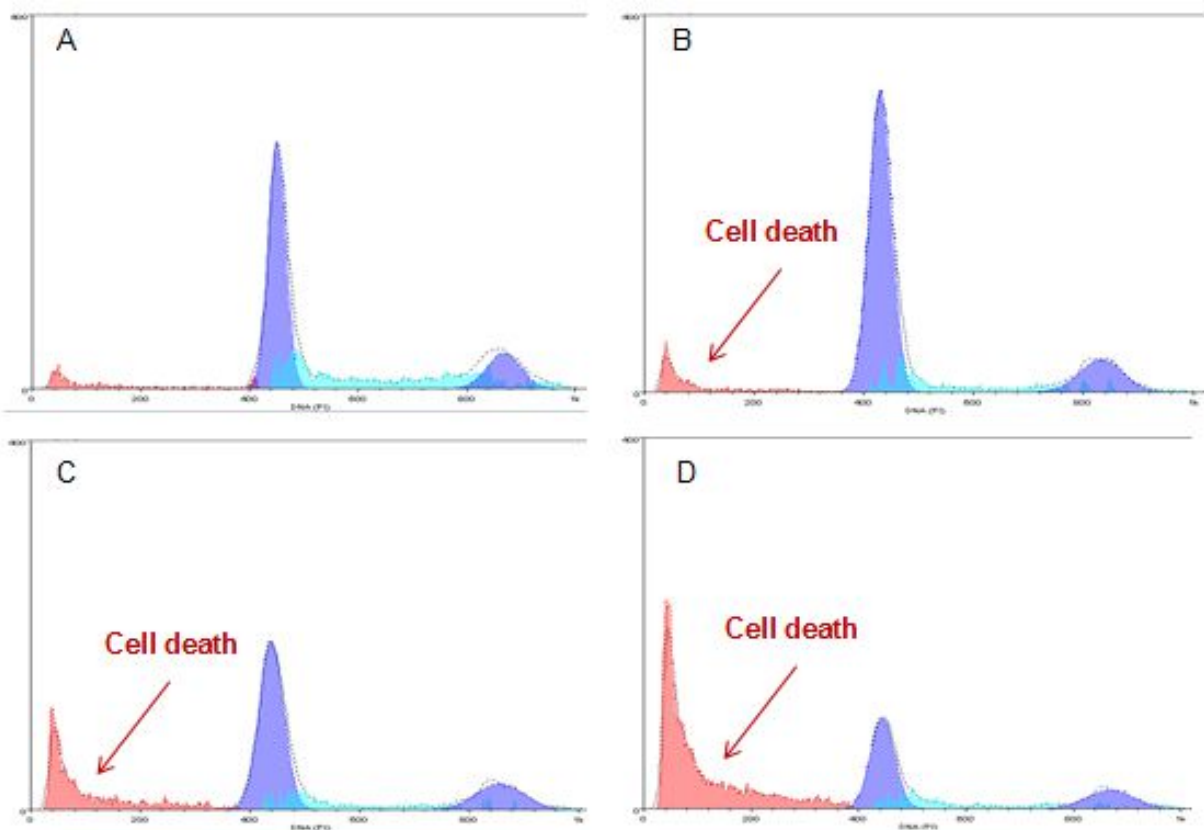


Figure 17: Histograms depicting stages in the cell cycle after 48 h exposure to A) DMSO (vehicle control), B) 60 μM , C) 70 μM , and D) 90 μM PCP.

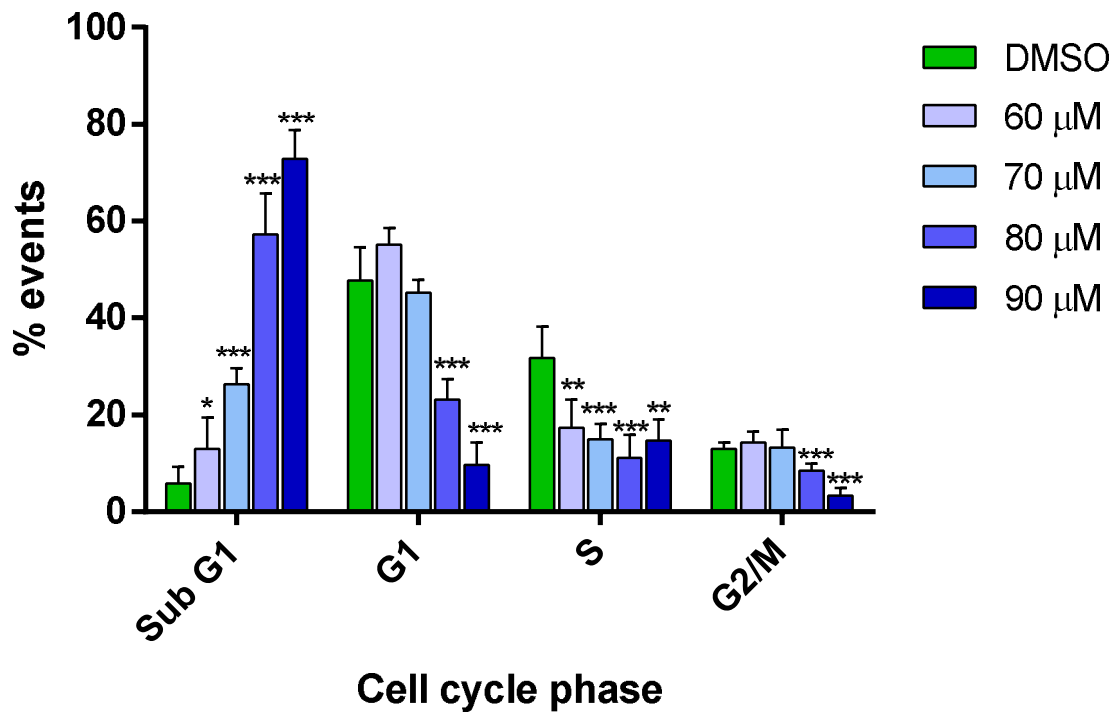


Figure 18: Average percent events for each cell cycle phase after 48 h exposure to 60, 70, 80, or 90 μ M PCP. Significance of changes are relative to the vehicle control. ** = $p < 0.01$ and *** = $p < 0.001$.

3.3. Mode of cell death

Scatter plots of FL1 log/FL3 log for each sample are depicted in Figure 19, and are divided into 4 quadrants according to the vehicle control. The lower left quadrant indicates live cells (Annexin V-FITC⁻/PI⁻), upper left early apoptotic cells (Annexin V-FITC⁺/PI⁻), upper right late apoptotic cells (Annexin V-FITC⁺/PI⁺), and lower right necrotic cells (Annexin V-FITC⁻/PI⁺). The upper right quadrant (putatively denoted late apoptosis) contains cells fluorescing both Annexin V-FITC and PI and thus apoptosis or necrosis cannot be confidently distinguished. Percentages of cells in each quadrant were extracted and compared to DMSO values for significant changes (Figure 20), and differences examined to aid mode of cell death determination (Table 1).

The vehicle control yielded scatter plots with the bulk of cells residing in the live quadrant, and did not depart significantly from a medium only control. Cells residing outside the live quadrant may be attributed to normal cell attrition and processing during the assay. All test exposure conditions resulted in significant ($p < 0.001$) decreases in live cell populations. Exposure to PCP resulted in increases in necrotic and late apoptotic cells, the most significant ($p < 0.001$) of which was a 25% increase in necrosis, while no significant increases in apoptosis occurred. Cells exposed to TCBQ behaved differently, and displayed 28 and 21% increases in early and late apoptosis, respectively, without any change in necrosis. Interestingly, cells exposed to TCHQ appeared to result in one of two fates. In the first instance (indicated as TCHQ 1 in Figure 20), there were 19% ($p < 0.01$) and 7% ($p < 0.05$) increases in early apoptotic and late apoptotic cells, respectively, with negligible change in the amount of necrotic cells compared to baseline. The second TCHQ induced fate (indicated as TCHQ 2) resulted in 34 and 16% increases ($p < 0.01$) in late apoptosis and necrosis respectively. The increase observed in apoptotic cells was not significant when compared to DMSO. Thus, the first fate yielded cells predominantly expressing Annexin V-FITC, and the second fate predominantly expressing PI. A further difference observed between the two fates was the effect on live cells, wherein in the first fate live cells were decreased by 26%, whereas the second fate decreased this population by a much larger percentage (59%) (Figure 20). These

results were concluded from 9 assay repeats, where 5 of the 9 repeats yielded fate 1, while 4 repeats yielded fate 2.

The positive control for cell death induction, DDT, resulted in a 19% increase in apoptotic cells ($p < 0.01$), with no significant changes in late apoptosis or necrosis, indicating that the assay was performed satisfactorily.

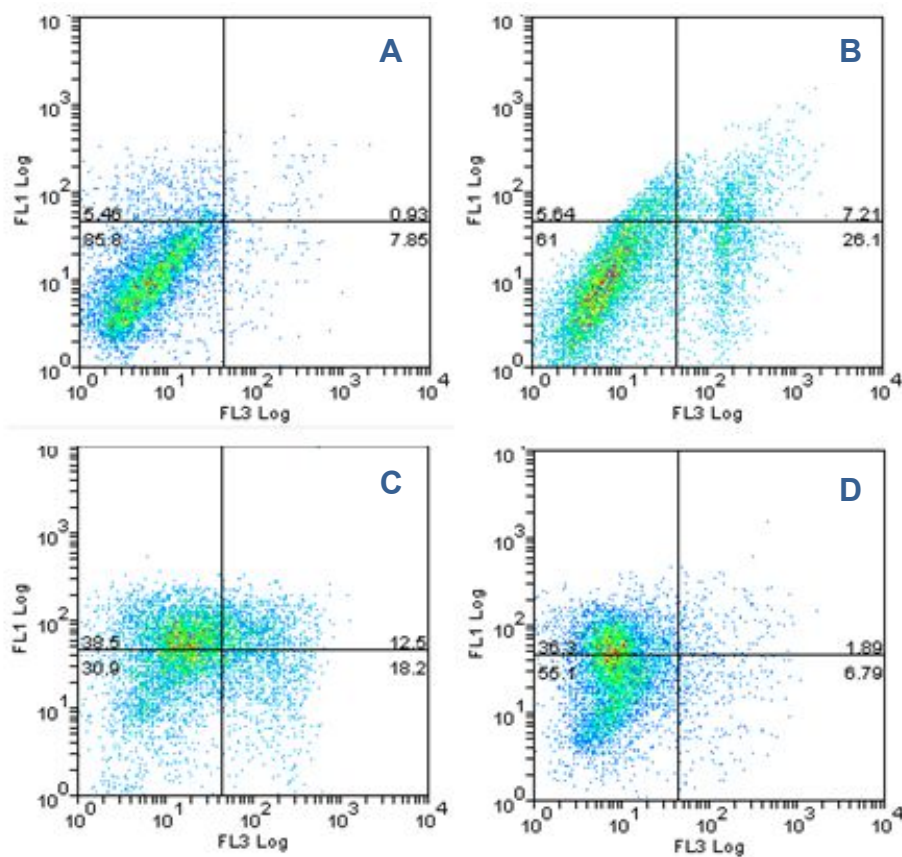


Figure 19: Annexin V-FITC/PI staining scatter plots after 48 h exposure to A) DMSO (vehicle control), B) PCP, C) TCBQ, and D) TCHQ. FL3 log indicates PI fluorescence, and FL1 log indicates Annexin V-FITC fluorescence.

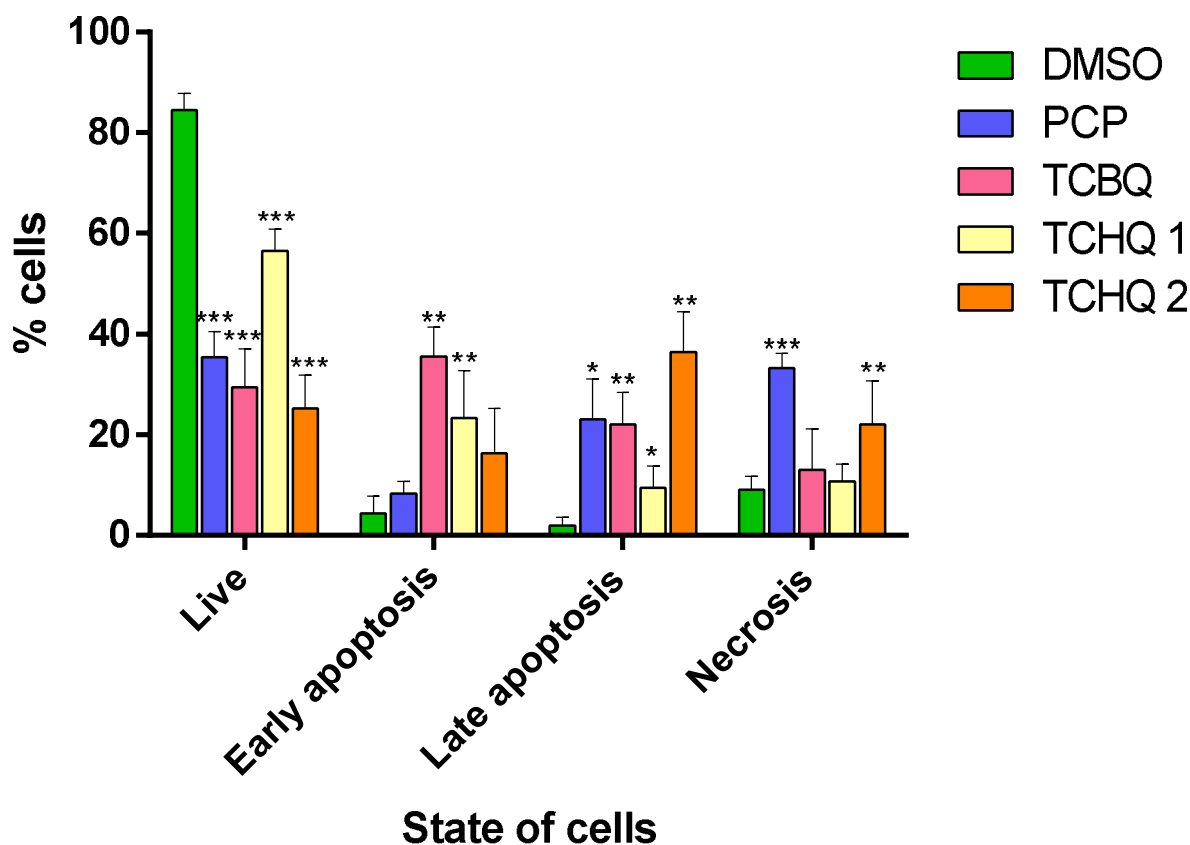


Figure 20: Percent of various states following 48 h exposure to vehicle control (DMSO), PCP, TCBQ and TCHQ (1 and 2 indicate different fates). Significance is indicated by * = $p < 0.05$, ** = $p < 0.01$, and *** = $p < 0.001$.

Table 1: Percent changes between cell states compared to DMSO following 48 h exposure to PCP, TCBQ, TCHQ (1 and 2 indicate different fates), and the positive control (DDT).

State	PCP	BQ	TCHQ 1	TCHQ 2	DDT
Live	-46.8	-55.2	-26.3	-59.1	-19.8
Early apoptosis	2.3	28.3	18.1	9.0	19.3
Late apoptosis	19.9	20.6	6.3	34.0	3.1
Necrosis	24.8	6.4	1.9	16.2	-2.5

3.4. Caspase activity

Caspase-3 activation was measured by assessing fluorescence levels arising from Ac-DEVD-AMC cleavage. When compared to the vehicle control, significant ($p < 0.001$) increases in caspase-3 activity was noted after 48 h exposure. Exposure to TCBQ exposure, resulted in the largest increase (3.2 fold) in caspase-3 activity, followed by PCP (1.4 fold) and TCHQ (1.3 fold) (Figure 21).

There was no significant difference between vehicle control and untreated cells. Staurosporine, known to induce caspase-3 activity,¹⁹⁸ was used as a positive control and produced a 1.7 fold increase in activity ($p < 0.001$) (Figure 21), indicating that the assay produced satisfactory results.

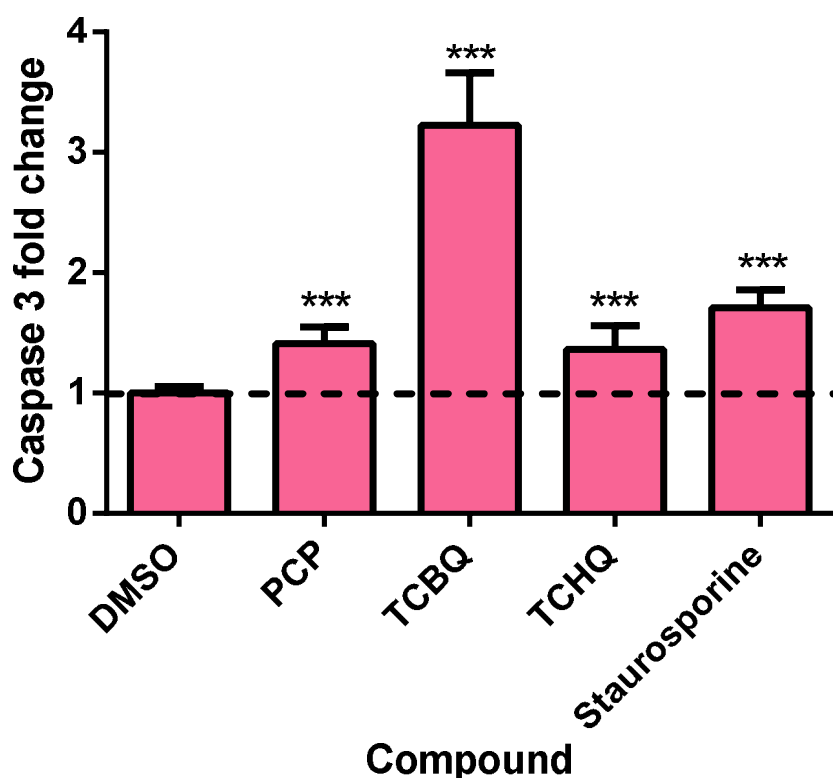


Figure 21: Fold change in caspase-3 activity relative to vehicle control (DMSO) following 48 h exposure to PCP, TCBQ, TCHQ or staurosporine (positive control). Significance of changes compared to vehicle control are indicated as *** = $p < 0.001$.

3.5. Cell morphology

Images of unfixed, unstained SH-SY5Y cells were taken after 48 h exposure to DMSO, PCP, TCBQ, TCHQ, and DDT (Figure 22). This allowed for raw visualisation of changes in cell confluence and morphology. Cells exposed to the vehicle control indicated high confluence, with characteristic dendritic-like connections between cells, and distinguishable cell bodies analogous to somas found in neurons *in vivo* (Figure 22A). Exposure to the test compounds resulted in decreases in confluence, particularly after exposure to TCBQ and TCHQ (Figures 22C and D). These two metabolites also caused breaks in the dendritic-like connections between cells, which would impair inter-cell communication and possibly contribute to cell death, as these connections are essential for SH-SY5Y cell growth. Inter-cell connection loss was also observed, but to a lesser extent after exposure to PCP (Figure 22B). Light microscopy indicated disruption of cell body morphology when exposed to all test compounds, as individual somas were not as easily distinguishable, and the cell shape was no longer consistent. In comparison, DDT did not exhibit inter-cell connection breaks, and cell bodies appeared to be more rounded and tightly condensed (Figure 22E).

Fluorescence microscopy was used to further visualise cell changes. Hoechst 33342 was used to stain nuclei blue, acridine orange to stain acidic bodies green, and PI to stain cells with compromised membrane integrity red, indicating cell death. The vehicle control (DMSO) yielded images with distinguishable, round nuclei situated within a green acridine orange area which stained cytoplasmic cell areas. Minimal PI was detected in DMSO samples, indicating that cells appeared healthy (Figure 23A). The dendritic-like connections were not visually evident under these stains. Exposure to PCP resulted in nuclei disfigurement as they were not as tightly confined to distinct round shapes, which can be visualised in the merge of Figure 23B. Acridine orange revealed a few pin point areas fluorescing more brightly than surrounding green areas outside the nuclei. Furthermore, there was an upregulation in PI fluorescence compared to DMSO, indicating greater cell death. Confluence across a well containing cells exposed to PCP was not uniform, with some areas retaining very few cells, with other areas being more confluent but with compromised cell integrity (Figure 23B). Similar results were observed after exposure to TCBQ (Figure 23C)

with regard to Hoechst 33342 and PI fluorescence, however acridine orange did not exhibit bright pin points, but merely a loss in overall morphology integrity. A further difference observed between PCP and TCBQ was that cells exposed to TCBQ displayed more uniformity in confluence, with compromised cells not congregating, but rather separated throughout the well (Figure 23C). Cells exposed to TCHQ clumped together and lifted off the surface, indicating weakened surface adhesion properties. This was not noted under light microscopy, and could be ascribed to the assay procedure. Although fluorescence microscopy images of TCHQ treated cells were optically aberrated, an extensive increase in PI fluorescence is clear, a stark indicator for the occurrence of cell death (Figure 23D).

3.5.1 Light microscopy

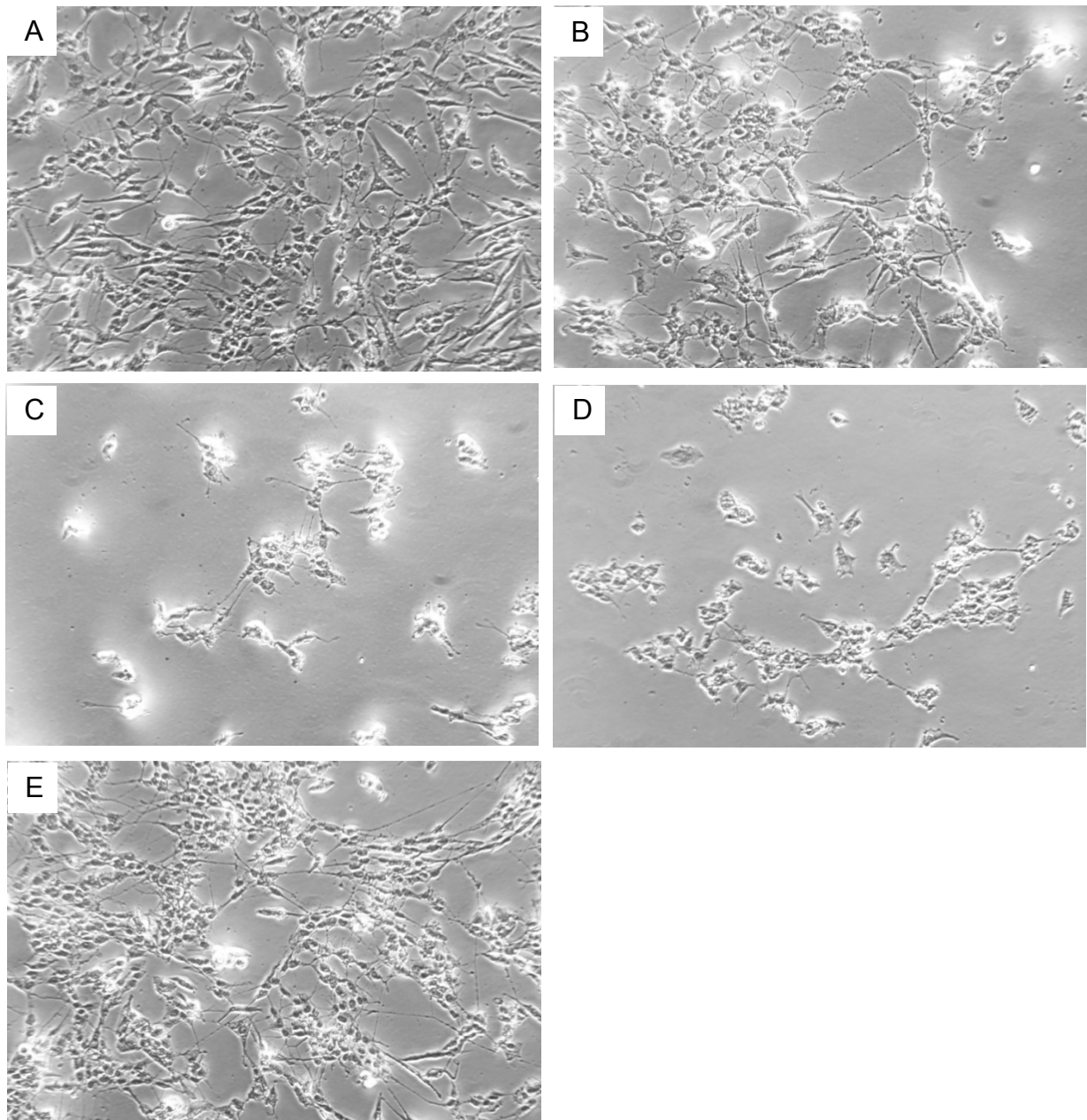


Figure 22: Light microscopy images of SH-SY5Y cells following 48 h exposure to A) DMSO (vehicle control), B) PCP, C) TCBQ, D) TCHQ, and E) DDT (100x magnification).

3.5.2 Fluorescence microscopy

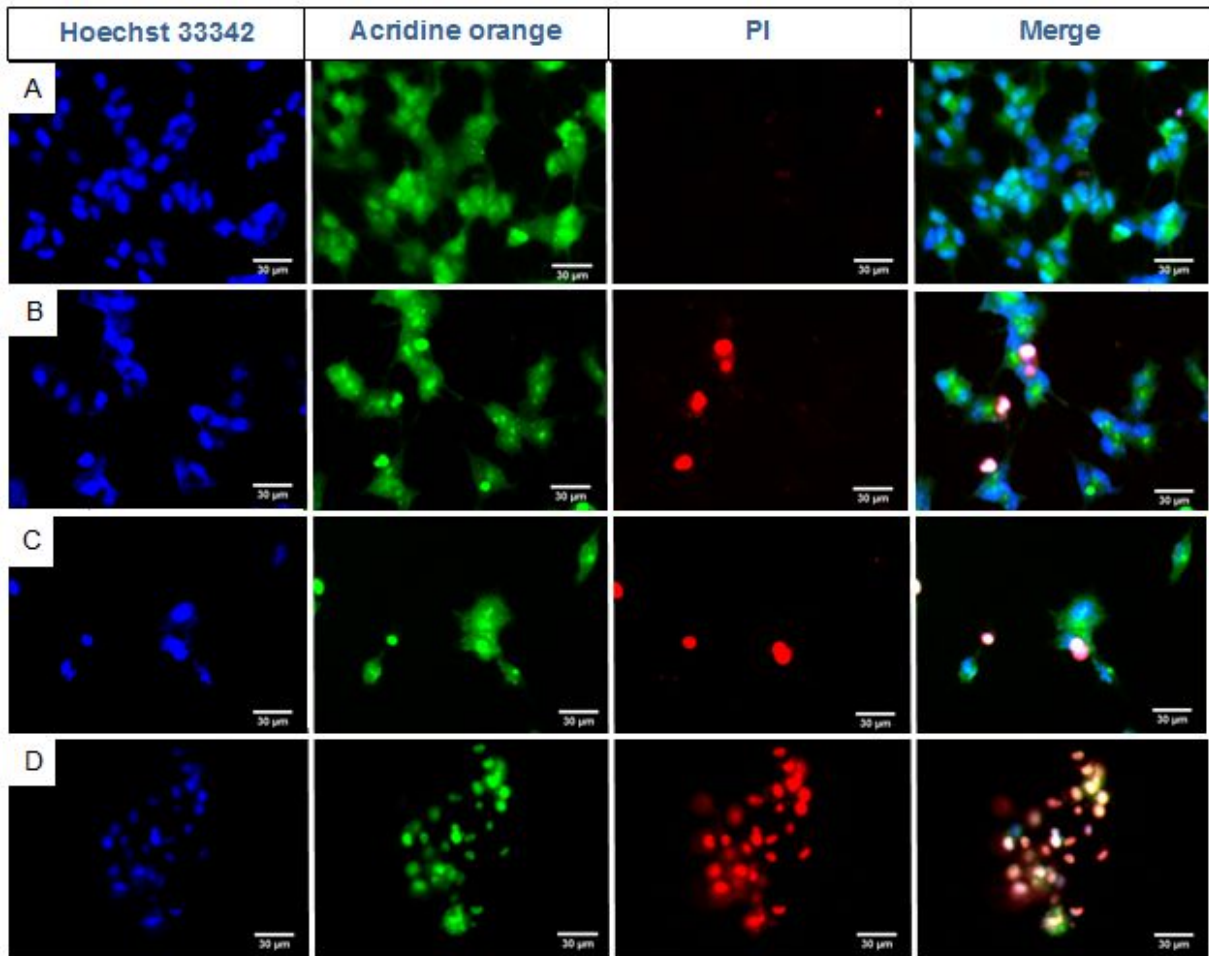


Figure 23: Fluorescence microscopy images of SH-SY5Y cells at 400x magnification following 48 h exposure to A) DMSO, B) PCP, C) TCBQ and D) TCHQ. Fluorescent dyes used were Hoechst 33342, acridine orange and PI. Merge indicates superimposed images of the three dyes.

3.6. Reactive oxygen species

Reactive oxygen species levels were assessed flow cytometrically using DCFDA, which in the presence of ROS is oxidised to form the fluorescent DCF molecule, which was used to quantify fold changes in ROS levels relative to the vehicle control (Figure 24). End point ROS was determined after exposure to the compounds for 4, 24, and 48 h exposure. The vehicle control did not depart significantly from the negative control. Pentachlorophenol resulted in a 2.2 fold increase in ROS only after 48 h, with no changes observed after 4 and 24 h exposure. Changes in ROS levels after TCBQ exposure appeared earlier. Although no activity was noted after 4 h, 1.9 and 2.0 fold increases after 24 and 48 h exposure were noted, respectively. Interestingly, there was a 0.7 fold decrease in ROS following 4 h exposure to TCHQ, which was reversed to 1.7 and 1.9 fold increases after 24 and 48 h exposure respectively. The positive control, AAPH, resulted in increased ROS levels, indicating assay efficacy. Results were confirmed via spectrofluorometry using the same dye, which also indicated increased ROS levels following 48 h exposure to test compounds.

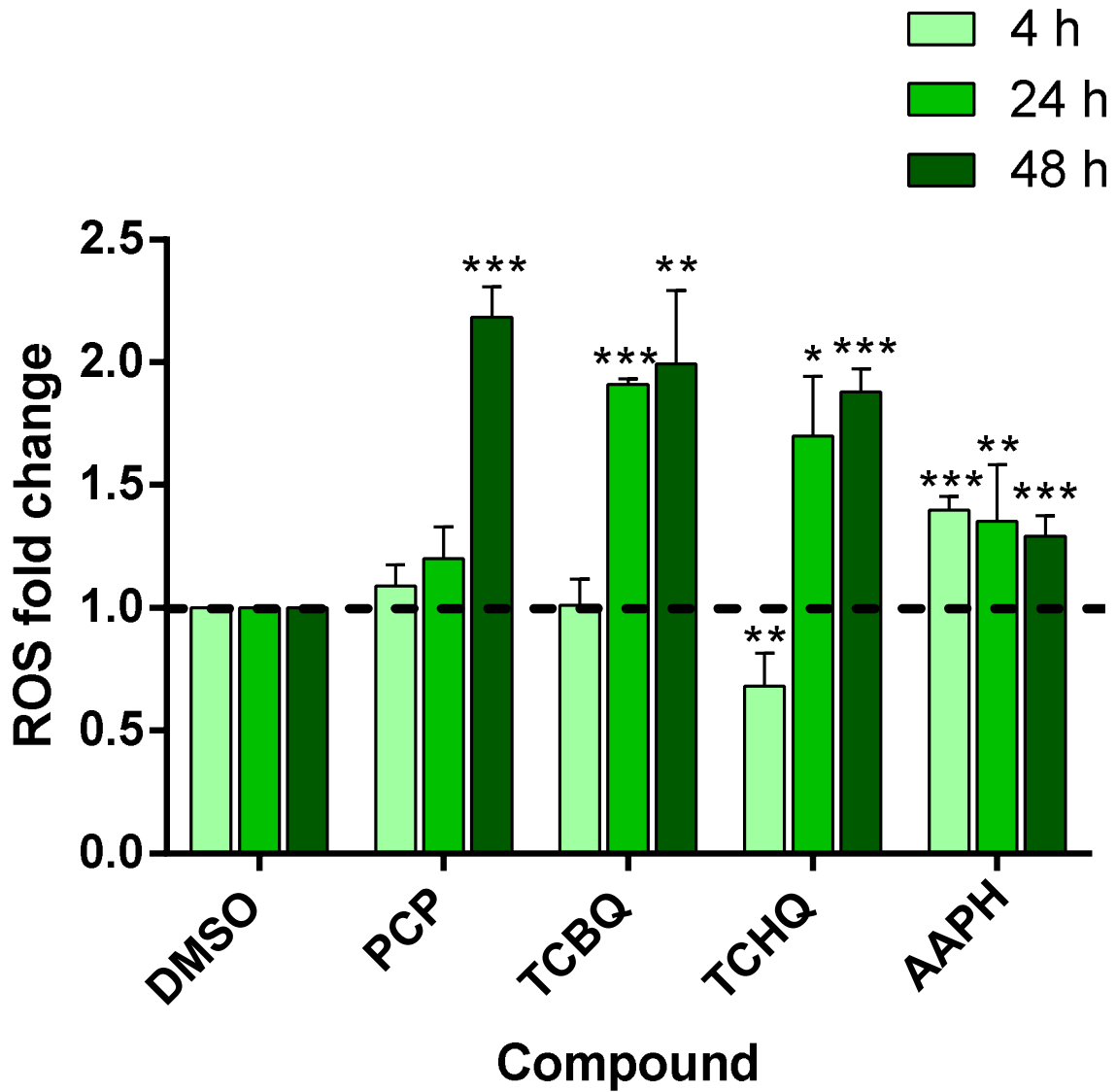


Figure 24: Fold change in reactive oxygen species (ROS) relative to vehicle control (DMSO) following 4, 24, or 48 h exposure to PCP, TCBQ, TCHQ, or AAPH (positive control). Significance of changes compared to the vehicle control of the same time point are indicated as ** = $p < 0.01$, and *** = $p < 0.001$.

3.7. Mitochondrial membrane potential

Changes in $\Delta\psi_m$ were quantified flow cytometrically using JC-1 dye. The ratio of orange to green was detected; orange indicates JC-1 aggregate formation in healthy mitochondria, whereas green indicates monomers as a result of decreased $\Delta\psi_m$. This was performed in tandem with ROS assessment at 4, 24 and 48 h time points. Fold changes in $\Delta\psi_m$ were obtained by comparison to the vehicle control, which was not significantly different to the negative control. Exposure to PCP resulted in a reduced $\Delta\psi_m$ after all exposure times, with reduction being greater following 24 and 48 h exposure ($p < 0.01$). Reduction in $\Delta\psi_m$ due to TCBQ occurred in a time-dependant manner, the greatest of which was a 0.4 fold change after 48 h. Effects on $\Delta\psi_m$ were not as pronounced following TCHQ exposure, which exhibited 0.8 fold changes after 4 and 48 h ($p < 0.05$), and no change after 24 h. Rotenone, known to decrease $\Delta\psi_m$, served as the positive control, which worked as expected (Figure 25).

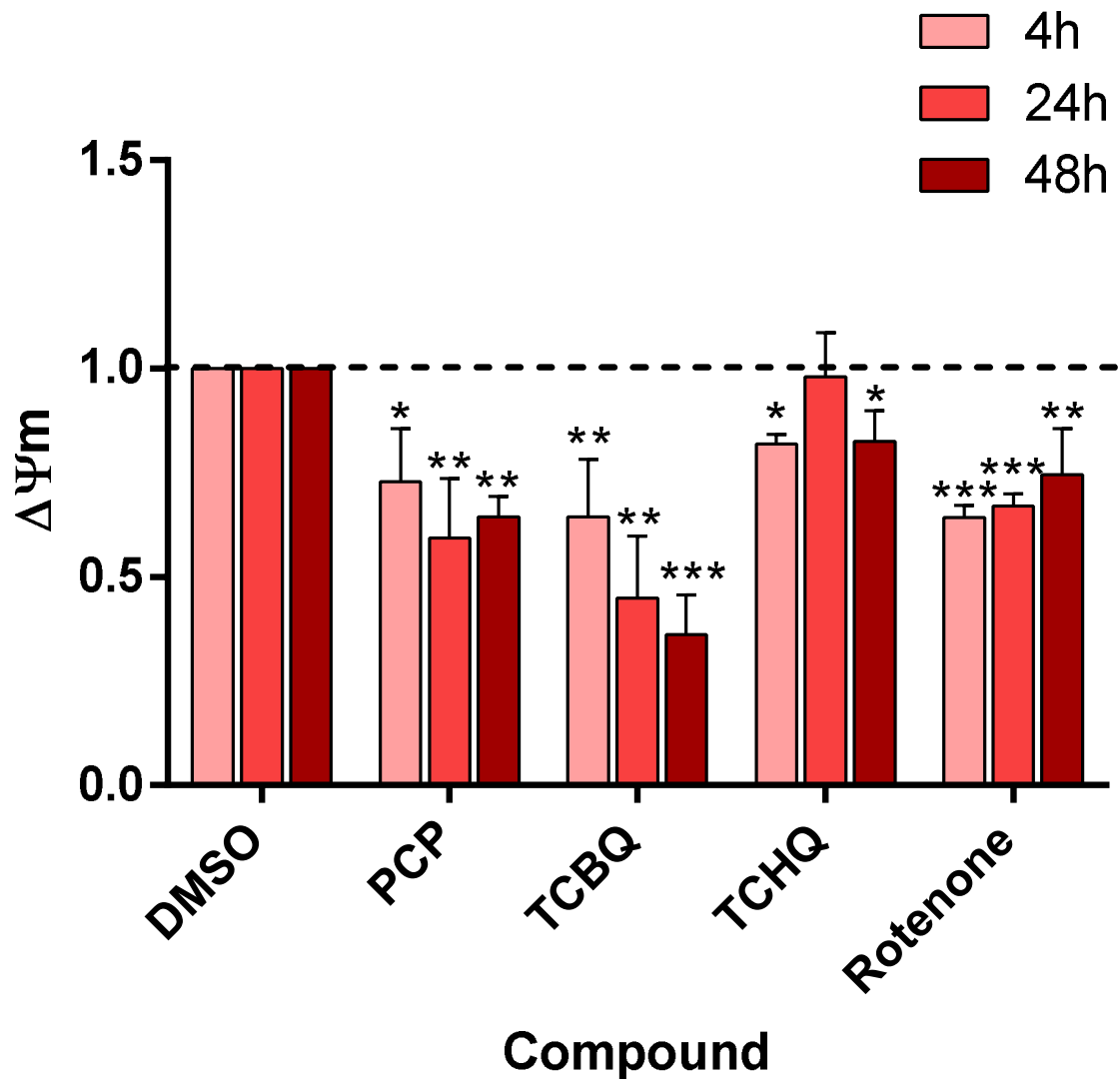


Figure 25: Fold change in mitochondrial membrane potential ($\Delta\Psi_m$) relative to DMSO (vehicle control) following 4, 24, or 48 h exposure to PCP, TCBQ, TCHQ or rotenone (positive control). Significance of changes compared to the vehicle control of the same time point are indicated as * = $p < 0.05$, ** = $p < 0.01$, and *** = $p < 0.001$.

3.8. Reduced glutathione content

Reduced glutathione was assessed spectrofluorometrically by quantifying the fluorescence of MCB caused by binding GSH. Fold changes in GSH levels were obtained when compared to DMSO, which was not significantly different to the negative control. Exposure to PCP and TCBQ for 48 h resulted in 0.8 and 0.7 fold decreases in GSH respectively ($p < 0.01$). In contrast, exposure to TCHQ yielded a 1.4 fold increase in GSH. n-Ethylmaleimide served as positive control and resulted in an expected GSH decrease, indicating satisfactory performance of the assay (Figure 26).

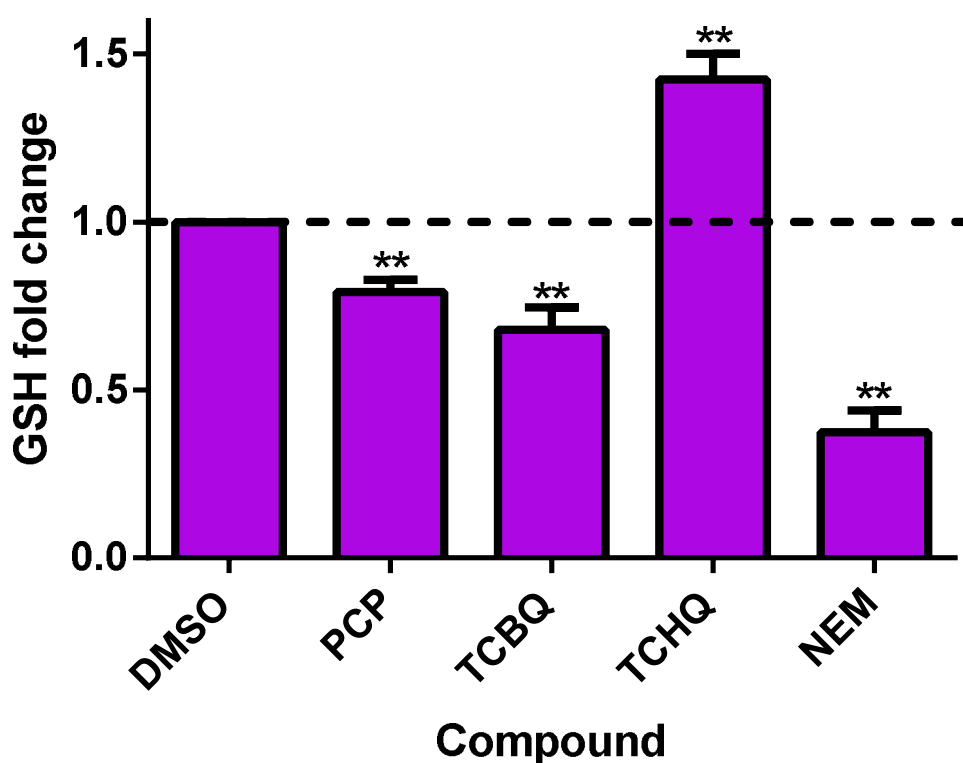


Figure 26: Change in GSH levels relative to DMSO (vehicle control) following 48 h exposure to PCP, TCBQ, TCHQ, or NEM (positive control). Significance of changes compared to the vehicle control are indicated as ** = $p < 0.01$.

3.9. Acetylcholinesterase activity

3.9.1. Ellman esterase assay

Effects of cytotoxic IC_{50} concentrations of PCP, TCBQ and TCHQ (concentrations obtained from the SRB assay) on AChE activity was assessed using the Ellman esterase assay. A small, but significant ($p < 0.01$) decrease in activity was observed between the negative and vehicle control. Vehicle control values were used for comparison purposes in this assay. Although PCP and TCBQ had no effect on AChE activity, 63.7 μ M TCHQ reduced AChE activity to 82% (Figure 27). Galanthamine, which served as positive control, reduced AChE activity to 11% functionality, indicating satisfactory assay performance.

The same assay was used to determine concentrations at which AChE activity is inhibited by 50%, termed the Ellman IC_{50} . Concentrations assessed ranged from 20 μ M below each compound's cytotoxic IC_{50} concentration, and ascended to 150 μ M in 20 μ M increments. No effect was observed under 150 μ M PCP or TCBQ, indicating negligible effects on AChE activity. Higher concentrations were not tested as these are not deemed physiological. In contrast, a dose-response effect was observed for TCHQ, producing an Ellman IC_{50} of 79.7 ± 7.7 μ M (Figure 28). It should be noted that after 24 h, wells containing TCHQ were visually much lighter, while wells containing galanthamine had returned to the dark yellow akin to the negative control, possibly indicating that TCHQ may be an irreversible inhibitor. This observation is however anecdotal as the assay is not designed for long term assessment.

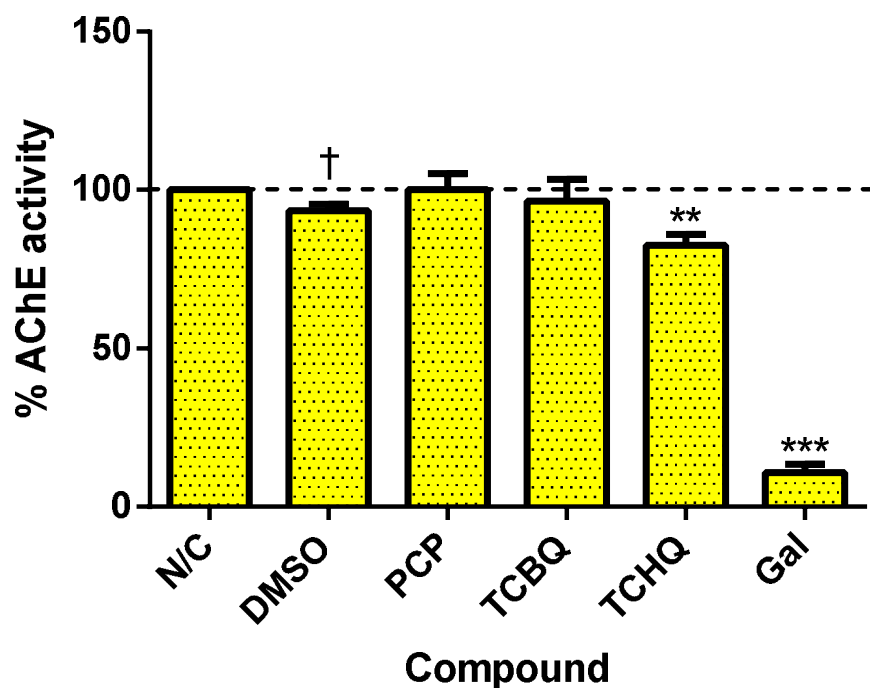


Figure 27: Effect of cytotoxic IC_{50} concentrations of PCP, TCBQ, and TCHQ, (concentrations determined from the SRB assay), on AChE activity. Significance is indicated by † = $p < 0.01$ when compared to negative control (N/C), and ** = $p < 0.01$ and *** = $p < 0.001$ when compared to DMSO (vehicle control).

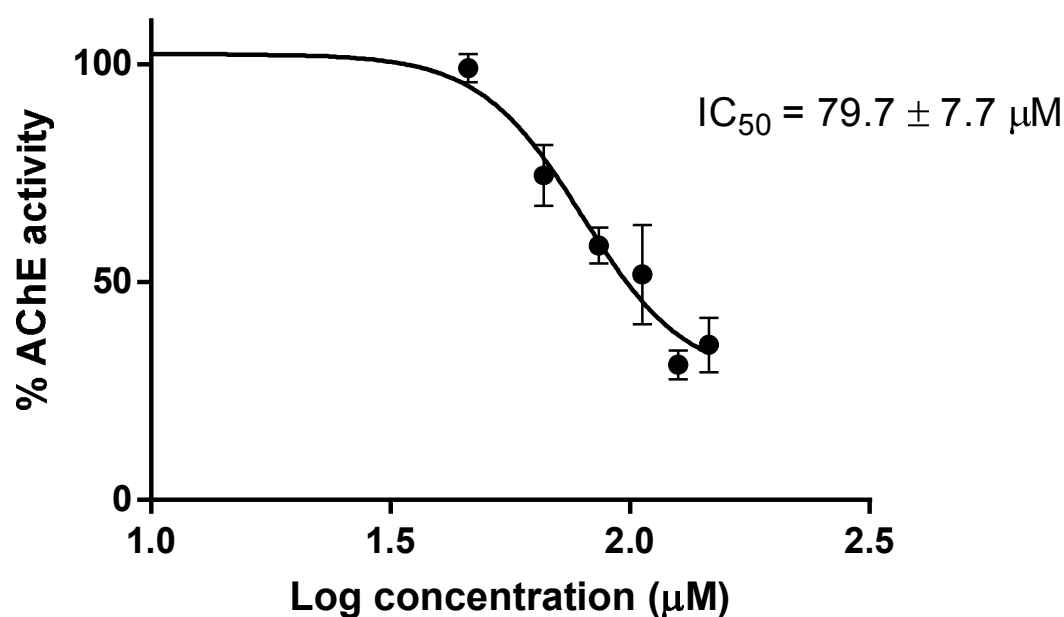


Figure 28: Inhibitory activity of TCHQ on AChE. The Ellman IC_{50} was determined as $79.7 \pm 7.7 \mu\text{M}$.

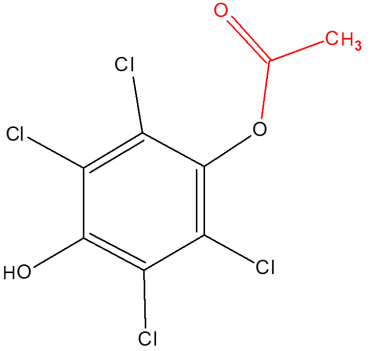
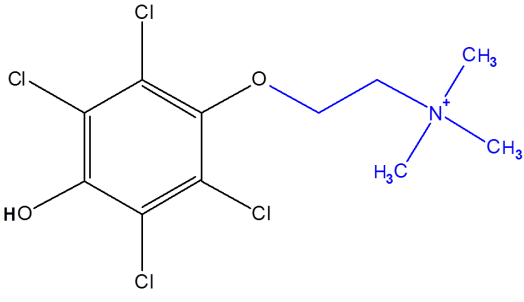
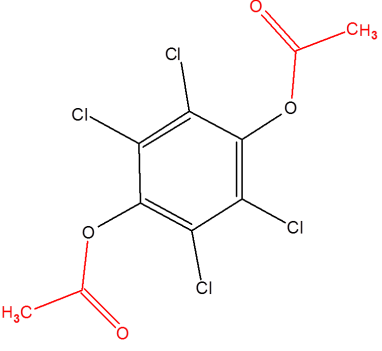
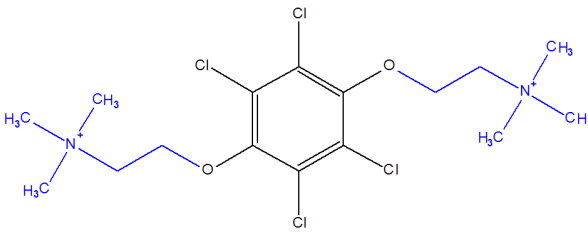
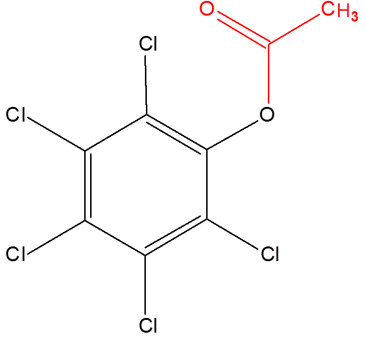
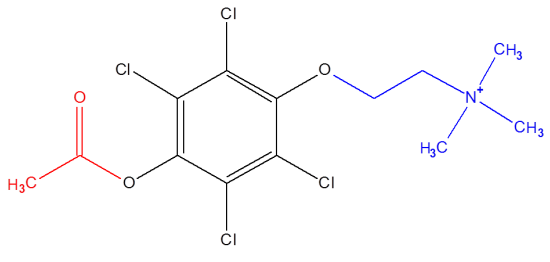
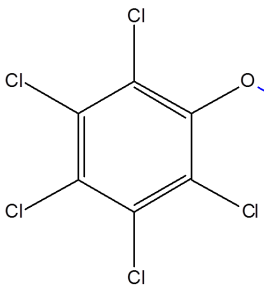
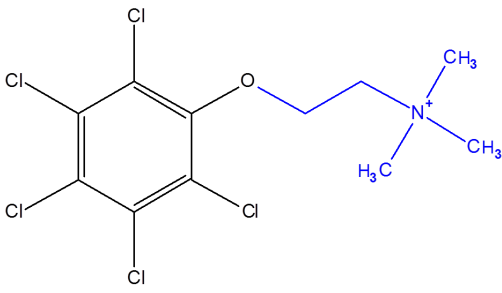
3.9.2. Molecular docking

It was hypothesised that TCHQ (and PCP at high concentrations) may competitively inhibit AChE activity by the binding of structural analogues within the active site gorge of AChE, thus barring normal catalytic action on ACh, a concept which is detailed in the discussion. The structural analogues were thought to stem from the binding of PCP or TCHQ to acetate or choline. This hypothesis was tested by docking the suspected inhibitors (ligands) to the active site of AChE (receptor) in order to obtain realistic plausibility of the working theory, where a good fit and binding affinity would further support the hypothesis, while a poor fit or binding affinity would refute it. Seven structural analogues of PCP and TCHQ were determined as possible ligands. These were generated in ChemsSketch, where acetate (Ac) or choline (Ch) was bound to either one or both oxygen atoms of the test compounds. Each structural analogue was allocated a simplified name, and IUPAC names were generated (Table 2). The molecular structures of these ligands are depicted in Table 3. The hypothesised mechanism was considered improbable for TCBQ, as, unlike PCP and TCHQ, it confers a very low probability of binding acetate or choline, and cannot form structural analogues as possible AChE inhibitors. For this reason, TCBQ was not included in *in silico* assessment.

Table 2: Simplified and IUPAC names of ligands suspected to be implicated in AChE inhibition.

Simplified name	IUPAC name
TCHQ-Ac	2,3,5,6-tetrachloro-4-hydroxyphenyl acetate
TCHQ-choline	N,N,N-trimethyl-2-(2,3,5,6-tetrachloro-4-hydroxyphenoxy)ethan-1-aminium
Ac-TCHQ-Ac	2,3,5,6-tetrachloro-1,4-phenylene diacetate
Choline-TCHQ-choline	2,2'-[(2,3,5,6-tetrachloro-1,4-phenylene)bis(oxy)]bis(N,N,N-trimethylethan-1-aminium)
Ac-TCHQ-choline	2-[4-(acetyloxy)-2,3,5,6-tetrachlorophenoxy]-N,N,N-trimethylethan-1-aminium
PCP-Ac	Pentachlorophenyl acetate
PCP-choline	N,N,N-trimethyl-2-(pentachlorophenoxy)ethan-1-aminium

Table 3: Chemical structures and simplified names of PCP and TCHQ structural analogues hypothesised to be involved in AChE inhibition. Red = acetate addition, blue = choline addition.

	
TCHQ-Ac	TCHQ-choline
	
Ac-TCHQ-Ac	Choline-TCHQ-choline
	
PCP-Ac	Ac-TCHQ-choline
	
	PCP-choline

Numerical output of molecular docking:

Forty-seven electric eel AChE PDB files were identified on the RCSB protein bank database as receptors to be used in the docking process.²²⁸⁻²⁵⁸ Each receptor carries an identifiable name, such as 1acj. Electric eel AChE receptors were used as this was the origin of AChE used in the Ellman esterase assay. These are files of AChE structures solved by x-ray crystallography, most of which harboured bound ligands in the active site. These ligands were predominantly Alzheimer's drugs such as tacrine or galanthamine, or derivatives thereof, which are reversible inhibitors of AChE. For docking purposes, these original ligands were removed from PDB files and the PCP- and TCHQ-analogous ligands docked in their place in the active site. This docking process yielded predicted binding energies for each ligand docked to each receptor, and the averages obtained from the two docking software packages used were assessed. Binding energies hardly deviated from one software package to another, indicating high agreement.

None of the binding energies reached below -9 kJ/mol, and ranged between -8.1 and -5.3 kJ/mol. Box plots of binding energies were generated for each ligand, which indicated minimum, maximum, first and third quartile, and median values (Figure 29). Surprisingly, PCP-Ac displayed the best binding energies, such as -8.1 and -8.0 kJ/mol when docked to 1e66²³³ and 1ut6.²⁴⁰ The ligand with the next best binding energy was Ac-TCHQ-Ac at -7.9 when bound to 1fss. This ligand displayed the lowest maximum binding energy of -7 kJ/mol, as well as a narrower range compared to the other ligands. Ac-TCHQ-Ac also displayed the lowest binding energy of ligands bound to 1qti,²⁴¹ a receptor whose original ligand was galanthamine, the same inhibitor used as positive control in the Ellman esterase assay.

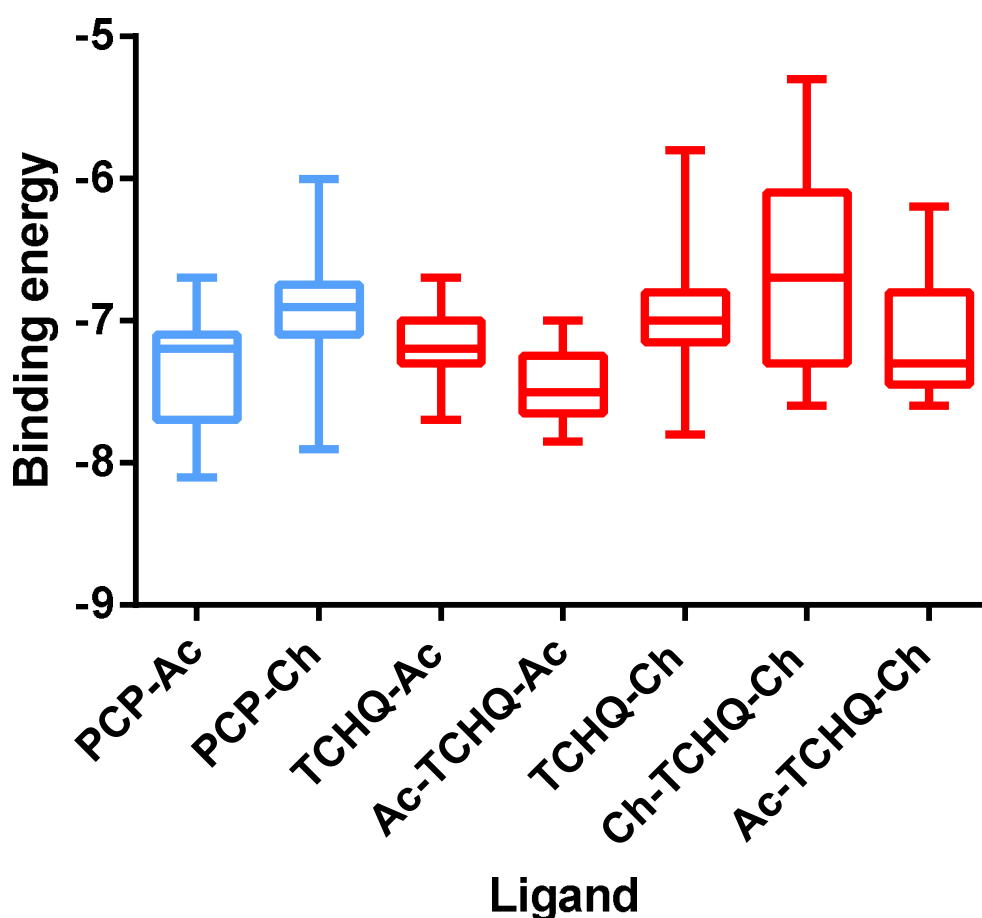


Figure 29: Box plots showing binding energies of ligands docked to 47 AChE receptor molecules. Whiskers indicate maximum and minimum, box edges indicate first and third quartiles and horizontal lines inside boxes indicate medians of binding energy.

Visual output of molecular docking:

Ligands docked to receptors were viewed in a 3D rotational capacity in Chimera, which revealed spatial orientation of the ligand with regard to placement in the receptor and surrounding amino acids (Figures 30 and 31). Superimposition of ACh (Figure 32), or the receptor's original ligand (Figure 33) allowed for the assessment of any ligand overlap, which would indicate incompatibility for mutually inclusive occurrence. Four receptor docked ligands were chosen for presentation purposes: A) PCP-Ac in 1ut6, which displayed one of the lowest binding energies, B) Ac-TCHQ-Ac in 1qti, which was the ligand with the lowest binding energy in the original

galanthamine containing receptor, C) TCHQ-Ac in 1zgc,²⁴⁵ which was the lowest binding energy of the TCHQ-Ac ligands, and D) Ch-TCHQ-Ch in 1acj,²²⁸ which was the docked ligand displaying the highest binding energy, and was chosen for comparison purposes.

In the evaluation of spatial positioning of docked ligands with regard to binding site amino acids, the PCP-Ac and TCHQ-Ac ligands appeared sandwiched in parallel with the aromatic moieties of TRP 84 and PHE 330, as well as perpendicularly covered by TYR 334 (Figures 30A and C) These ligands also appeared to be in relatively close proximity to TYR 121, GLU 199, and HIS 440. Positioning of Ac-TCHQ-Ac was perpendicular to TRP 84, and proximal, but not perpendicular or parallel to PHE 330, PHE 331 and TYR 334. Other proximal amino acids included TRP 279, TYR 121, and PHE 290 (Figure 30B). Docked Ch-TCHQ-Ch was relatively far removed from TRP 84, and its aromatic moiety was most closely perpendicular to TRP 279 (Figure 30D).

Visualisation of docked ligands with receptor surfaces shown displayed the general ligand position within the binding site. PCP-Ac and TCHQ-Ac sit deep within the active site gorge (Figures 31A and C), while Ac-TCHQ-Ac spans this gorge lengthwise (Figure 31B). Ch-TCHQ-Ch poses at the entry of the gorge and does not penetrate far inside (Figure 31D). Docked ligands were superimposed with ACh in order to assess ligand-substrate overlap. The three ligands with relatively low binding energies displayed a small amount of overlap (Figures 32 A-C), the most pronounced of which was Ac-TCHQ-Ac (Figure 32B). In contrast, Ch-TCHQ-Ch exhibited no overlap with ACh (Figure 32D). In a similar fashion, docked ligands were superimposed with original receptor ligands. This revealed aromatic moieties of docked ligands to be positioned in a similar orientation of original ligands, which were the AChE inhibitors: tacrine, galanthamine and (RS)-tacrine(10)-hupyridone for the three ligands with low binding energies (Figures 33A-C), while Ch-TCHQ-Ch was far removed from its corresponding original (Figure 33D). Figures 34 and 35 represent examples of ligand spatial relation to ACh within AChE.

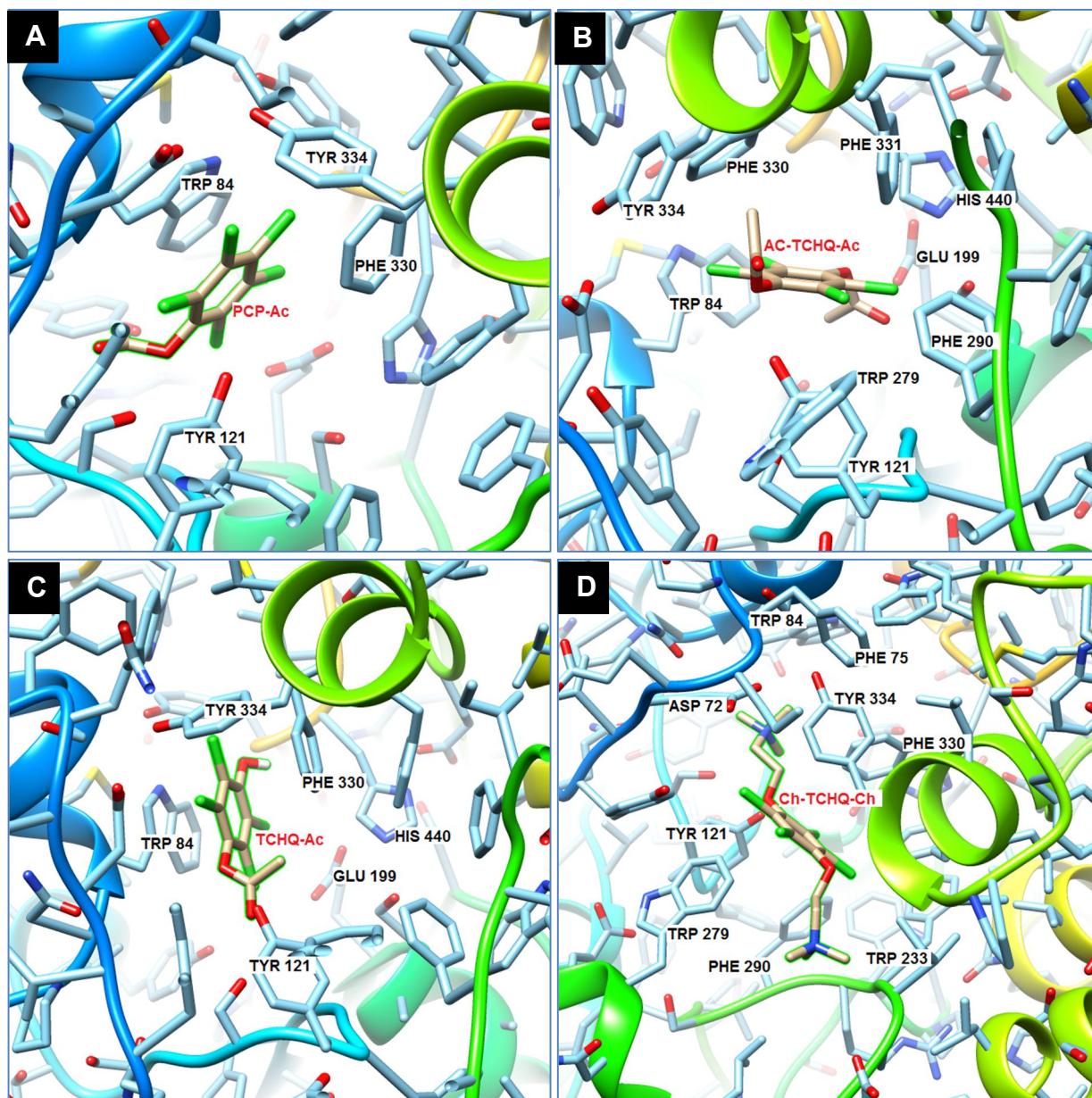


Figure 30: Docked ligands in AChE receptors with surrounding amino acid and ribbon structures. Ligands in receptors are: A) PCP-Ac in 1ut6, B) Ac-TCHQ-Ac in 1qti, C) TCHQ-Ac in 1zgc and D) Ch-TCHQ-Ch in 1acj.

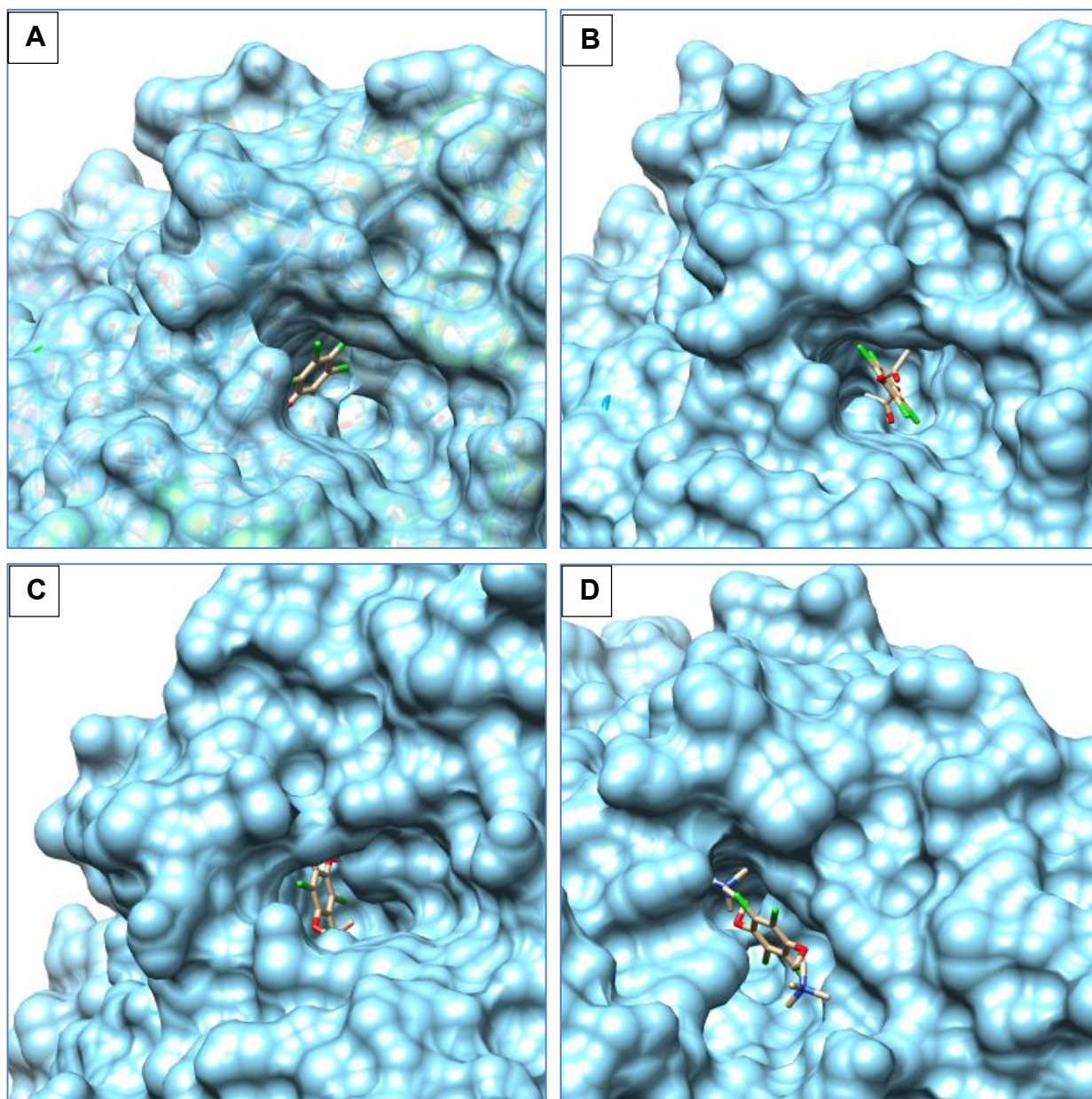


Figure 31: Docked ligands in AChE receptors. Receptor surfaces are shown for visualisation of ligand positioning within the active site gorge. Ligands in receptors are: A) PCP-Ac in 1ut6, B) Ac-TCHQ-Ac in 1qti, C) TCHQ-Ac in 1zgc and D) Ch-TCHQ-Ch in 1acj.

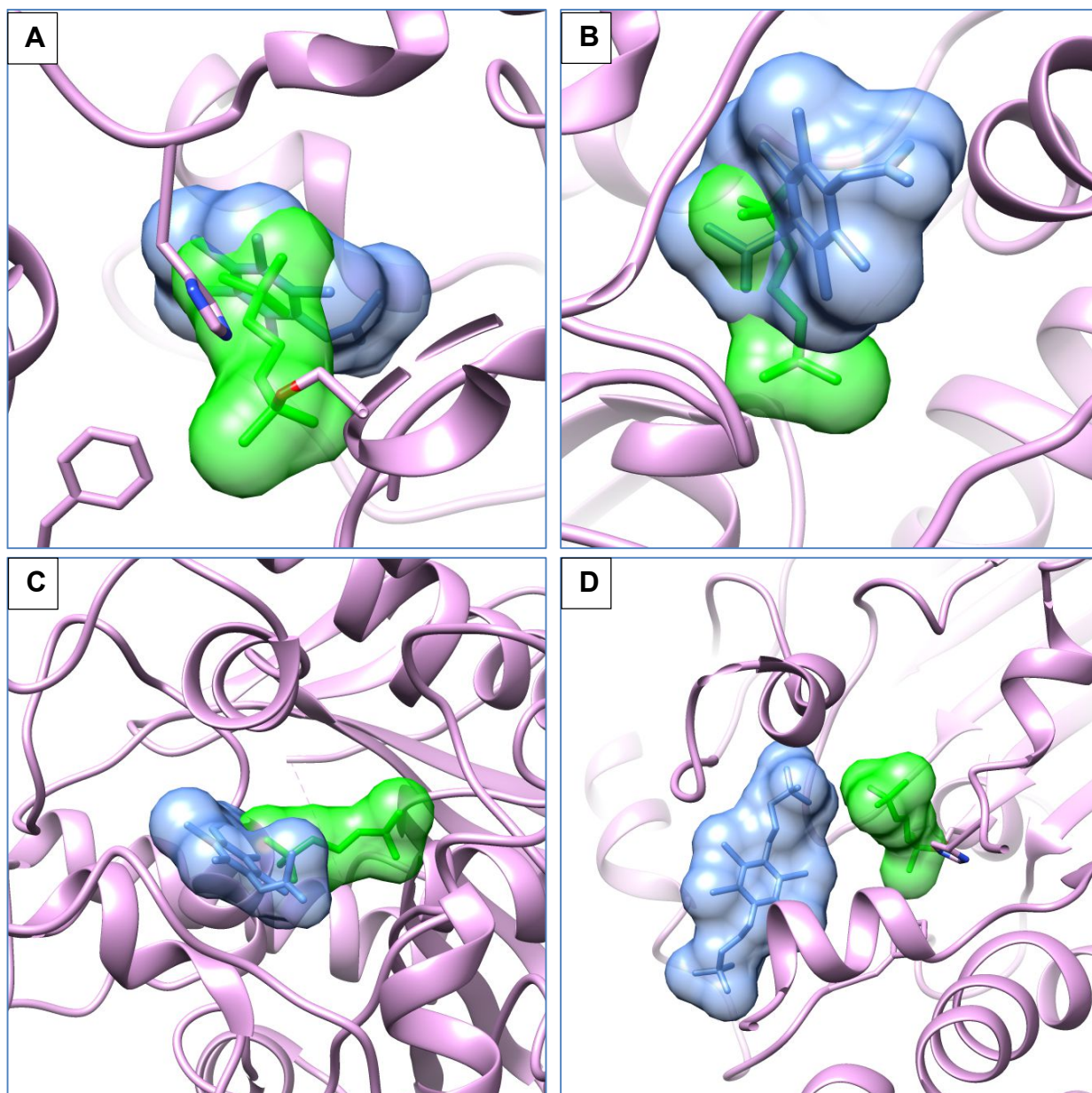


Figure 32: Docked ligands (blue) superimposed with ACh (green). Ligand and ACh surfaces are shown for overlap visualisation. Ligands in receptors are: A) PCP-Ac in 1ut6, B) Ac-TCHQ-Ac in 1qti, C) TCHQ-Ac in 1zgc and D) Ch-TCHQ-Ch in 1acj.

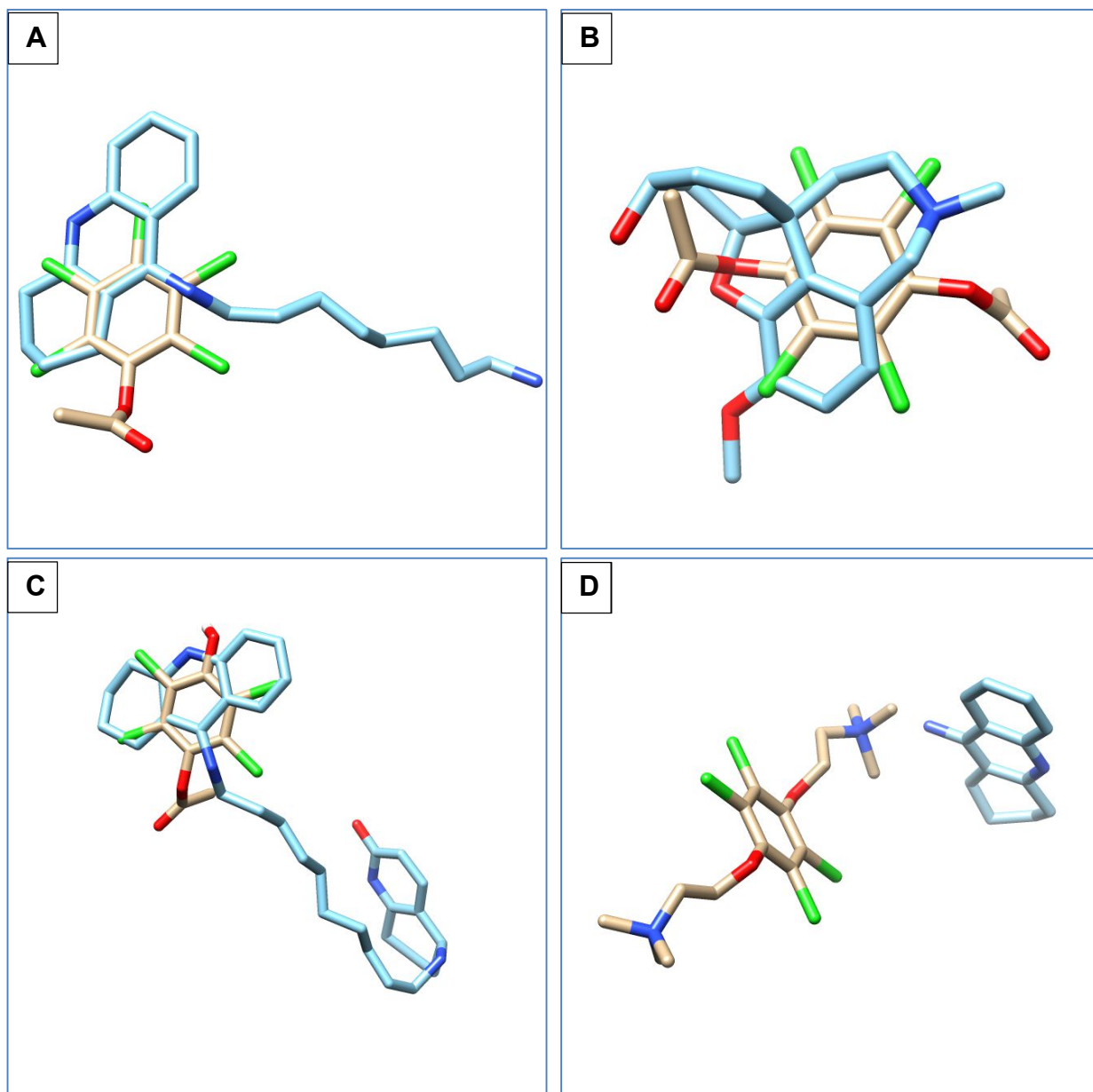


Figure 33: Docked ligands (beige) superimposed with receptor's original ligand (blue). Docked ligands superimposed with original ligands are: A) PCP-Ac with tacrine derivative, B) Ac-TCHQ-Ac with galanthamine, C) TCHQ-Ac with (RS)-tacrine(10)-hupyrindone and D) Ch-TCHQ-Ch with tacrine.

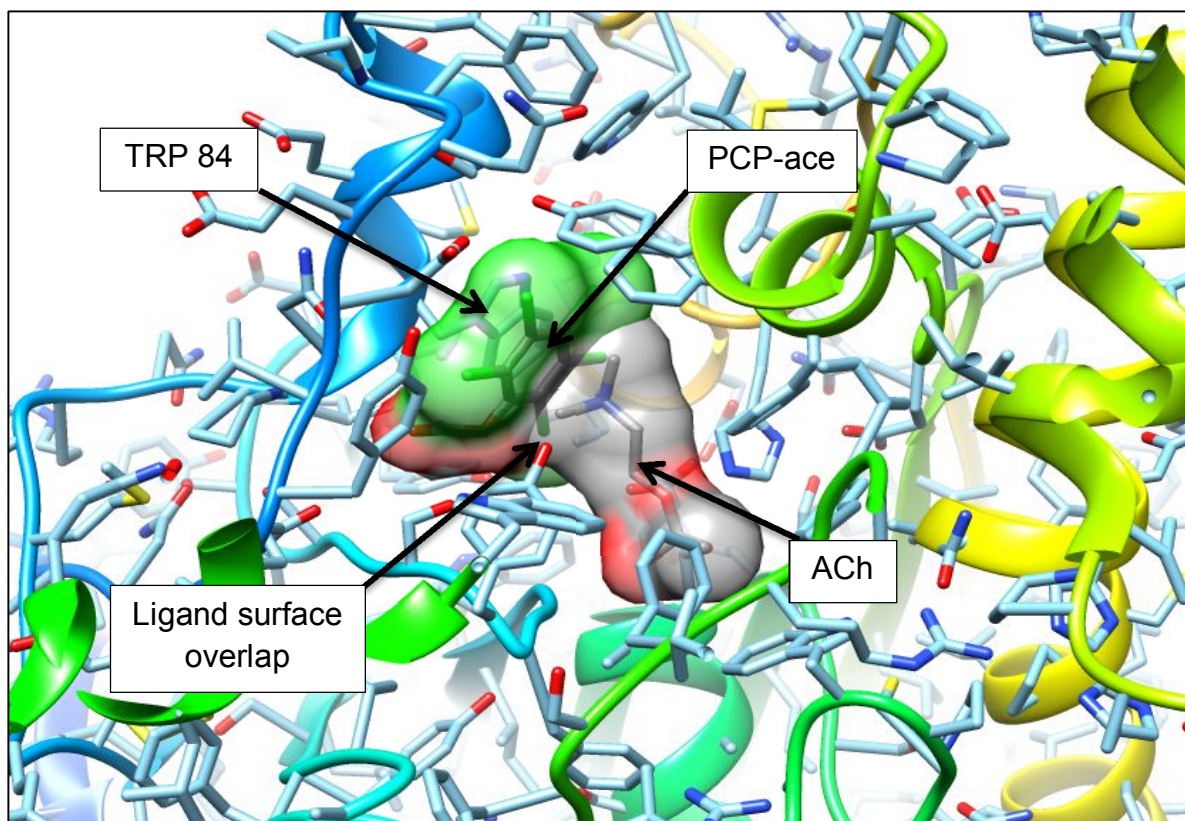


Figure 34: Visualisation of ligand PCP-Ac docked to receptor 1ut6, superimposed with ACh. Atoms of AChE are shown, with focus on the ligands.

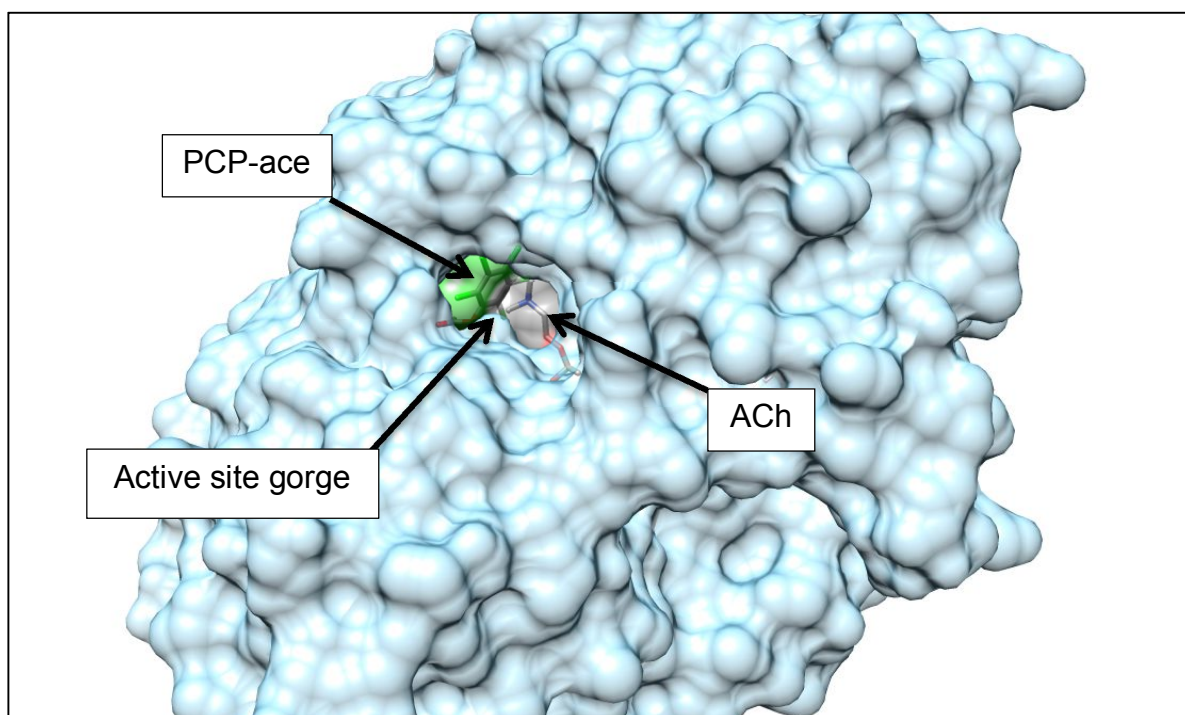


Figure 35: Visualisation of ligand PCP-Ac docked to receptor 1ut6, superimposed with ACh. Surface of AChE is shown to visualise ligand atoms within the active site gorge.

3.9.3. Molecular dynamics simulation

Molecular dynamics simulations were performed in order to assess ligand binding stability and behaviour within a simulated environment. This process requires a large amount of processing power and time, thus two ligands were chosen upon which to run the simulation: PCP-Ac in 1ut6, which had one of the lowest binding energies in molecular docking, and Ac-TCHQ-Ac in 1qti, which had the lowest binding energy for the receptor whose original ligand was galanthamine. Upon visualisation in virtual molecular dynamics software, the position of both ligands remained fairly stable within the active site gorge, and did not fall out of the binding site. Average binding energies of both test ligands were relatively high when compared to the original ligands simulated in the same manner (Table 4).

Table 4: Summary of average binding energies from two molecular dynamics simulations.

Ligand	Receptor	Binding energy (kJ/mol)	Original ligand	Original ligand binding energy (kJ/mol)
Ac-TCHQ-Ac	1qti	-223.376 +/- 47.453	Galanthamine	-999.803 +/- 57.560
PCP-Ac	1ut6	-222.497 +/- 12.116	Tacrine derivative	-1174.465 +/- 100.129

Chapter 4: Discussion

4.1. Detection of cytotoxicity

All three compounds exhibited cytotoxic effects on SH-SY5Y cells in a dose-dependent manner. Of the three compounds tested, the most potent was the metabolite TCBQ, and the least potent was the parent compound PCP. This was unsurprising, as the occurrence of metabolites harbouring greater toxicity than their parent compound is a common phenomenon in drug and xenobiotic metabolism.²⁵⁹ The IC₅₀ concentrations were found to be in a fairly high micromolar range, however remained below 100 µM, suggesting that adverse neurotoxic effects would be more likely observed in chronic rather than acute exposure circumstances *in vivo*, especially given the bioaccumulation discussed in the introduction.

A few studies have been conducted to assess PCP toxicity on neuronal cell lines, but neglected to include evaluation of its metabolites. Folch *et al.* conducted a study on the pathway of apoptosis induced by PCP in rat cerebellar granule neurons (CGNs).⁵⁰ This study found PCP to decrease cell viability in a dose-dependent manner at concentrations ranging from 10-100 µM, a similar effect as seen in the SH-SY5Y cell line in the present study. Tang *et al.* evaluated the toxicity of a number of polycyclic aromatic hydrocarbons, one of which was PCP, in SH-SY5Y cells and C6 rat glioma cells.²⁶⁰ Concentrations of PCP used in this study were between 0.03 and 30 µM. At these concentrations, no significant differences were found in cell viability without metabolic activation of the cells. Higher concentrations, however induced some reduction in cell viability when cells were metabolically activated. This is in agreement with the cytotoxic results obtained in the present study, which also suggest PCP inactivity against neuronal cells at concentrations lower than 30 µM.

Cytotoxicity studies have also been conducted focusing on adherent, non-neuronal mammalian cell lines to varying capacities. Schroeder *et al.* demonstrated IC₅₀ values of 68, 129 and 144 µM for PCP, TCBQ and TCHQ, respectively in the hepatocyte HepG2 cell line.²⁸ This study indicated greater potency of the parent than the metabolites, which is in contrast to results obtained in the present study as well as others,^{203,261,262} and may be cell line specific. Tanaka *et al.* reported PCP IC₅₀ values in mammalian cell lines at 193 µM in HeLa cells (human cervical cancer), 298

μM in NRK-52E rat kidney cells, and $93 \mu\text{M}$ in NB-1 human neuroblast cells.²⁶³ The IC_{50} found for PCP in this study corresponds with that of the human neuroblast cell line. Lower IC_{50} values in neuronal cell lines indicate neurons to be more sensitive to PCP toxicity than some other cell lines, excluding the case of HepG2 cells.

Concentrations at which TCBQ has been demonstrated to induce similar cytotoxic effects as observed in the present study in different cell lines include $25 \mu\text{M}$ in PC12 cells (neural crest pheochromocytoma),²⁶⁴ and $50 \mu\text{M}$ in mouse embryonic cells.²⁶⁵ In Jurkat T (lymphocyte) cells, TCHQ was able to induce 30-40% cell death at $20 \mu\text{M}$,²⁶² while $50 \mu\text{M}$ TCHQ has been reported to reduce mouse splenocyte viability to 28%.²⁰³ This suggests that concentrations at which the two metabolites exert cytotoxicity in SH-SY5Y cells do not depart largely from that seen in other cell lines.

The use of the SRB assay provides an essential starting point for the assessment of toxicity, however does not provide specific information relating to mechanistics, as it is based on cell density as determined indirectly by total protein content relevant to the vehicle control. A loss in cell density may relate to induction of cell death, or mere anti-proliferative action (although visualisation of effects under a microscope indicated cell death), and does not indicate specific effects. As such the SRB was complimented by an array of further investigation delineated below.

4.2. Cell cycle

The use of multiple time points in cell cycle analysis allowed for the evaluation of time-dependent effects, and was appropriate as the use of a single end point would have resulted in potentially missing effects occurring early on. No change in cell cycle was observed following 12 h exposure to PCP, however effects were noted following 12 h exposure to TCBQ and TCHQ, indicating that the two metabolites act more quickly than the parent compound.

At this time point, TCBQ caused an accumulation of cells appearing in S phase, accompanied by a decrease in the G1 population, however no significant change occurred in the G2/M phase. This suggests a prolonged traverse of cells through S-phase, which ultimately fall out of cell cycling before G1 phase is reached. The prolongation of S phase has been reported to be eventuated via a ubiquitination

proteolytic pathway, whereupon the downregulation of ubiquitin-conjugating enzyme H7 (UbcH7) modulates Chk1 to delay the passage of cells to G2 phase.^{266,267} This pathway may have been activated due to DNA damage accumulated during replication as a result of TCBQ exposure in order to allow time for an attempt at DNA repair. While a number of cells will likely fall out of the cell cycle into cell death at this point, this type of prolongation of S phase may allow cells to eventually progress to G2 phase, which may explain the maintenance of events observed in the G2/M population. Failure to repair extensive DNA damage will however result in an impasse at the G2/M checkpoint, also resulting in a cascade of events causing apoptosis,²⁶⁸ which is already seen after 12 h by an increased sub-G1 population. Cells in sub-G1 are characterised by less DNA content than their G1 counterparts, a phenomenon observed in apoptotic cells due to specific DNA fragmentation laddering patterns, which result in DNA strand lengths of 180-200 base pairs.²⁶⁹ This systematic DNA fragmentation is usually a downstream result of the apoptosis process. This may be accompanied by other fragment lengths if DNA strand breaks are an upstream cause of cell death induction.²⁷⁰ In order for cells to appear in the sub-G1 peak of cell cycle analysis, cells must have lost enough DNA such that the DNA content is below that of cells in G1.²⁷¹ This concept may lead to the underestimation of apoptotic events, as G2 cells undergoing early apoptosis may not have lost enough DNA to present as sub-diploid, and their DNA content may resemble that of cells in S phase. While this may be a contributing factor to the increase observed in S phase events, it is unlikely to be the primary cause of this increase. Morphological DNA changes associated with S phase prolongation include nuclear lobulation,²⁶⁷ micronuclei, and excessive chromosome decondensation.²⁷² The inability to restore changes in chromosomal decondensation following replication may potentiate S-phase lag, as appropriate resting chromatin architecture is essential to gap phases of interphase.²⁷³ On the other hand, it has been reported that cells blockaded at early stages in S phase are due to a disabled capacity for chromosome decondensation due a reduction in minichromosome maintenance protein complex (MCM).²⁷⁴ This process bars access of replication machinery to DNA, and thus impairs DNA replication, in which case the DNA content of S phase cells would resemble that of G1, making it an unlikely scenario for TCBQ action, as DNA replication was already apparent by the increase in DNA content in S phase. As such, the first described processes of S phase prolongation are the preferred

proposition for TCBQ effects on cell cycle. Sequential increases of events in the sub-G1 population were evident after 24 and 48 h exposure to this compound, the most drastic of which was after 48 h exposure, suggesting that, while apoptosis may be as early onset as 12 h, the bulk of apoptotic eventuation occurs after more extended TCBQ exposure. The increase in S phase population observed at 12 h was no longer apparent at 24 h, however a decrease in G1, along with restoration of S phase back to similar levels as the vehicle control, indicated cells lost to apoptosis before they were able to cycle back to G1. Decreases in G1, S and G2/M populations after 48 h correspond to a large amount of apoptotic cells unable to continue the cell cycle traverse.

After 12 h TCHQ exposure to SH-SY5Y cells, there was an accumulation of cells in the G2/M phase, accompanied by a decrease of events in the G1 population, indicating a G2/M block. Two possibilities exist for the occurrence of this, the predominantly occurring one being the activation and maintenance of the G2/M checkpoint, whereupon cells are unable to proceed to mitosis due to detected DNA damage, the threshold of which is up to 20 DSB.²⁷⁵ This checkpoint may be activated via p53-dependent or independent pathways, or an overlap of both.⁹⁵ One such pathway independent of p53 involves the maintained inactivation of CDK1.²⁷⁶ This is initiated upon the recognition of DNA damage by ATM or ataxia telangiectasia and Rad3-related protein (ATR),²⁷⁷ which subsequently phosphorylate Chk1 or Chk2, which in turn phosphorylate and inhibit CDC25.²⁷⁶ This ultimately leads to inhibitory action by wee1 on CDK1, preventing it from binding cyclin B, thus preventing G2/M transition.²⁷⁸ A p53 dependent pathway also involves the inhibition of CDK1⁹⁵ by initiating transcription of CDK1 inhibitors p21, 14-3-3 σ , and Growth Arrest and DNA Damage-inducible 45 (GADD45),²⁷⁹⁻²⁸¹ as well as through the inhibition of CDK activating kinase (CAK).²⁸² This is not an exhaustive description of events involved in a G2/M checkpoint blockade, but serves to indicate possible predominant features that might be implicated by the TCHQ induced G2/M block. Cells remaining at the G2/M boundary for extended periods are reported to subsequently undergo cell death.²⁸³ Abrogation of the G2/M checkpoint and inappropriate progression to mitosis in the presence of DNA damage has also been reported to potentiate cell death,²⁸³ however this is doubtful to be the mode of action incurred by TCHQ exposure as it would not result in the observed increase in events at G2/M in cell cycle analysis.

The second possible cause of the accumulation of events in the G2/M population is an impasse reached at the spindle checkpoint, preventing cells from completing mitotic division and progressing to G1 phase. Under this assumption, improper chromosomal separation causes the maintained inactivation of microtubule action due to cadherin-1 and CDC20 via the inhibition of APC, thus preventing cells from completing mitotic division.²⁸⁴ A prolonged spindle checkpoint arrest has been demonstrated to cause DNA degradation due to caspase-activated DNase (CAD), which then promotes p53 dependent cell death.²⁸⁵ The DNA content of cells is the same for those in G2 phase as M phase,³⁴ and as such cells in these two phases are indistinguishable from one another in the PI cell cycle method used in the present study, thus it cannot be explicitly determined whether cells treated with TCHQ are arrested at the G2/M boundary or in the mitotic phase due to spindle checkpoint activation. Further investigation such as PCR would need to be conducted in order to determine which cell cycle factors are implicated in order to infer the particular cause of the G2/M block. Nonetheless, the impaired progression of cells to G1 phase can be a potent initiator or contributing factor to cytotoxicity and cell death. No increase in cell death was observed in the sub-G1 phase following 12 h exposure to TCHQ, indicating that there is a more rapid onset of cell death by TCBQ than TCHQ. After 24 h exposure however, there was an increase in the sub-G1 population, which was larger than the corresponding TCBQ sub-G1 population, signifying a more sudden onset of cell death occurring after at least a 12 h delay. This sub-G1 increase was further augmented after 48 h, indicating cell death to occur in a time dependent manner, with DNA fragmentation processes being present. This time-dependent increase in sub-G1 cells was likely observable due to the cells not being synchronised in cell cycle prior to TCHQ exposure, as cells already in or near G2 would undergo cell death earlier than those in prior cell cycle phases as they required time allowed to traverse to the G2/M blockade. After both 24 and 48 h TCHQ exposure, the cell cycle block seen at 12 h was no longer apparent due to decreases in G1, S and G2/M phases as the cells had evidently fallen out of the cell cycle into cell death. One exception was that no significant change was observed in the G2/M fraction when compared to the vehicle control at 48 h, which might indicate either a latent re-emergence of the G2/M block in the remaining live cell population, or an attempt at cell growth recovery by cells for which death did not ensue.

After 24 h, PCP exerted a G1 block as seen by a relatively small increase in the G1 population, which was consistent throughout all runs and statistically significant ($p < 0.01$). This was accompanied by a decrease in S phase, as well as an increase in sub-G1, indicating cell cycle exit before entry into S phase. The most likely cause of this is arrest at the G1/S checkpoint, which can result in one of two fates: inhibition of proliferation, or cell death. It is evident that the latter was the fate of PCP treated cells due to the increase in the sub-G1 population. Cell death arising from this may be as a direct result of the G1 block, or the G1 arrest may cause cells to be sensitised to DNA damage. The onset of continued G1 arrest or cell death at this point is often dependent on p53, which may be activated either by detection of DNA damage or by direct stimuli of cytotoxic compounds.²⁸⁶ This activation causes p21 to inhibit CDK-cyclin D complexes and RB phosphorylation, which inhibits progression to S phase.^{113,287} In cases where damage is insurmountable, subsequent cell death has been reported to be ensued by p53 activation of pro-apoptotic factors such as Bcl-2-associated X protein (Bax), Insulin-like growth factor-binding protein 3 (IgF-Bp3), and TNF receptor genes such as Fas and death receptor 5 (DR5),^{113,288,289} which results in a cascade of events leading to cell death. It has also been reported that G1 arrest due to p21 activation and eventual cell death can occur due to metabolic stress in the absence of DNA damage.²⁹⁰ Considering the ability of PCP to uncouple oxidative phosphorylation and the elevated ROS production observed in the present study, it is probable that a combination of DNA damage and metabolic stress stimuli contributed to the G1 arrest. After 48 h PCP exposure, the evidence of a G1 block had subsided as the majority of events occurred in the sub-G1 fraction. The assessment of a range of concentrations of PCP revealed a dose-dependent increase in the sub-G1 population, which supports the dose-dependent effect on cell growth observed in the SRB assay. This is corroborated by Yang *et al.*, who also found time- and dose-dependent cell death as a result of PCP exposure.²⁹¹ The two lower concentrations yielded a decrease in S phase events only, while the two higher concentrations resulted in a decrease in all non-sub-G1 phases, indicating that S-phase is the first phase from which cells dissipate, further supporting the induction of cell death at the G1/S boundary.

A moderate amount of literature exists regarding the effects of PCP and its metabolites on ROS and GSH in different cell lines, however very few studies have

evaluated effects on cell cycle, which is surprising given the profound impact ROS and GSH can have on the cell cycle.²⁹²⁻²⁹⁴ In lieu of this, a few studies have used cell cycle analysis for the evaluation of DNA fragmentation in apoptosis determination. These studies tended to focus on sub-G1 changes, with no discussion pertaining to the other cell cycle phases. DNA fragmentation is most frequently associated with apoptosis, however is known to occur in necrotic cell death as well. This is particularly so for ROS-mediated necrosis, where oxidative damage to DNA includes single and double strand breaks.²⁷⁰ Apoptotic DNA fragmentation presents with characteristic DNA laddering as DNA is cleaved into short 180 base pairs oligonucleotides by CAD.²⁹⁵ The presence of apoptosis or necrosis cannot be explicitly determined by the sub-G1 population of cell cycle analysis alone, and requires confirmation with further assays, such as the TUNEL assay, gel electrophoresis, or Annexin V/PI staining among others. A number of studies on PCP and its metabolites have used the sub-G1 population of cell cycle analysis to determine the occurrence of DNA fragmentation. Wispriyono *et al.*, Schaefer *et al.* and Chen *et al.* found apoptotic DNA fragmentation by increased sub-G1 due to PCP, which was confirmed by other techniques.^{262,296,297} Chen *et al.*, however, noted that PCP was able to induce both apoptosis and necrosis in a similar concentration range, while Schaefer *et al.* did not rule out the possibility of necrosis. Dong *et al.* did not conduct cell cycle analysis, but did find that PCP induced DNA laddering.²⁹⁸ In contrast, Michałowicz *et al.* and Wang *et al.* found necrotic-like DNA strand breaks in their assessment of PCP, indicating that resultant DNA damage may be dependent on cell type, as each of these studies focused on different mammalian cell lines.^{299,300} Apoptotic DNA fragmentation has also been described for TCHQ at slightly lower concentrations by sub-G1 increases and confirmed by DNA laddering.^{262,300} Interestingly, Chen *et al.* found an increase in sub-G1 and DNA laddering for lower doses of TCHQ (12.5 μ M), however this was not the case for higher doses (50 μ M), where necrosis occurred, and no fragmentation presented in the sub-G1 population.²⁰³

These results empirically demonstrate that cell cycle is affected in neuronal cells *in vitro*, which suggest the possibility that proliferative neurons *in vivo* may also be affected in a similar manner. Alternatively, or additionally, the ability to affect cell cycle may be manifested by either a disruption of neural plasticity, which relies on a

differential role of cell cycle proteins,¹²⁷ or the onset of abortive cell cycle re-entry, particularly in the case of elicited DNA damage.³⁰¹ Indeed, Folch *et al.* found aberrant expression of proteins implicated in cell cycle re-entry in rat CGNs following PCP exposure, but did not consider effects of its metabolites.⁵⁰ Cell cycle dysregulation such as aberrant cell cycle re-entry, along with ROS have been implicated in the onset of Alzheimer's disease (AD), however the exact mechanisms of this involvement is poorly understood and somewhat disputed in literature, and may only be applicable to genetically susceptible individuals.^{149,302,303} Chronic low-dose pesticide exposure has been associated with the development of AD as well as other neurodegenerative diseases, and is quickly becoming recognised as a risk factor.^{304,305} Thus, further investigation into the cell cycle effects of PCP and its metabolites on post-mitotic and *in vivo* neurons is warranted, as accurate extrapolation from a proliferative cell line is limited, however these results certainly highlight an avenue for exploration of poorly understood risk factors in neurodegenerative diseases. Even in the absence of AD onset, the loss of neurons to cell death or changes in plasticity have the potential to induce aberrant brain functioning.

4.3. Mode of cell death

The ultimate consequence of PCP, TCBQ or TCHQ exposure varied in terms of mode of cell death, indicating different pathways leading to demise. It should be noted that the Nomenclature Committee on Cell Death has proposed recommendations⁷⁴ that the usage of terms classifying cell death should be explicitly clarified in light of the emergence of blurred distinction between modes of cell death, due to continuous discovery of atypical cell death process.¹⁴⁷ In this study, apoptosis was determined by the presence of presented PS without compromised cell membrane (Annexin V⁺/PI⁻), and necrosis as cells with compromised membrane integrity (Annexin V⁻/PI⁺). The presence of both factors on its own is ambiguous, thus the relative contribution of the first two instances served in combination with Annexin V⁺/PI⁺ to determine predominant type of cell death. Terms such as apopnecrosis, pyronecrosis and necroptosis are deemed tentative and are thus avoided, however

the overlap of apoptotic and necrotic processes are discussed, as it becomes ever clearer that the two are not necessarily mutually exclusive.³⁰⁶

Necrosis appeared to be the predominant mode of death of PCP in SH-SY5Y cells, indicated by the cellular perfusion of PI, which implicates compromised cell membrane integrity, a hallmark of necrosis.⁷⁴ Apoptotic cell death was not evident as an ultimate mode of cell death, as there was negligible exposure of membranous PS upon Annexin V-FITC staining in the absence of a permeated cell membrane. There was however a slight increase in caspase-3 activation, as well as DNA fragmentation in the sub-G1 fraction of cell cycle analysis. Caspases are usually associated with apoptosis,⁸² and although their involvement in non-apoptotic processes have been discovered,³⁰⁷⁻³⁰⁹ it is more likely that caspase dependent apoptosis was initiated, and subsequently diverted to necrosis due to disrupted cellular bioenergetics,³¹⁰ since increased ROS and $\Delta\psi_m$ collapse was observed. Apoptosis is an energy dependent process and requires adenosine triphosphate (ATP) to be carried out to completion.³¹¹ While apoptosis is frequently onset by mitochondrial membrane permeabilization, extensive $\Delta\psi_m$ collapse may also result in disrupted cellular metabolism and depleted ATP production, as the mitochondria is the main source of cellular ATP.³¹⁰ Depleted ATP levels lasting for a short period of time initiate apoptotic signalling, and the recovery of ATP allows for apoptosome formation and subsequent apoptosis, while extended absence of sufficient ATP results in necrotic cell death due to the inability of cyt c to bind pro-caspases.³¹² This process, while resulting in initial caspase activation, contributes to the inhibition of continued intrinsic apoptosis pathway activity. It is unknown whether a threshold of caspase activation is required for ultimate apoptotic death, however Racke *et al.* noted that for apoptosis morphology to occur, activation of caspase-3 alone did not suffice.³¹³ Somewhat paradoxically, the activation of caspases can in fact potentiate the onset of necrotic death by cleaving mitochondrial complexes I and II in the presence of $\Delta\psi_m$ collapse, thus further hindering ATP production.^{314,315}

Independent of caspase activity, an energy dependent switch between apoptosis and necrosis involving the TNF death receptor pathway has been described by Los *et al.*³¹⁶ Here, it was discovered that the cleavage and activation of poly (ADP-ribose) polymerase 1 (PARP-1) caused ATP depletion, which potentiated the diversion of necrosis from apoptosis. The activation of PARP-1 was augmented by oxidative

stress, which indicates that this process may be present in PCP induced necrosis as increased ROS was also observed in the present study. Los *et al.* also found that PARP-1-mediated energy disruption occurred in the glycolytic pathway of cellular metabolism, however it was noted that $\Delta\psi_m$ permeabilization may occur as a secondary result.³¹⁶ There is therefore a possibility of co-operation between PARP-1 and mitochondrial dependent ATP depletion involved in the apoptosis-necrosis switch postulated in the present study. The switch from apoptosis to necrosis in PCP cell death would explain not only the small increase observed in caspase-3, but also the presence of DNA fragmentation in cell cycle analysis. It is possible however that the sub-G1 population may have contained cleaved DNA strands from upstream DNA damage elicited by ROS in addition to apoptotic oligonucleotides.

The presiding mode of cell death induced by PCP is disputed in literature, with a number of studies finding either apoptotic or necrotic cell death in different cell lines (Table 5). There appears to be no pattern evident in the type of cells suffering apoptosis or necrosis, however it is possible that the mode of death induced may be highly cell line specific, with those more susceptible to ATP depletion presenting with necrosis. The precise reason for this discrepancy would require further investigation.

Table 5: Summary of literature for PCP induced mode of cell death in different cell lines.

Mode of cell death	Cell line	Factors implicated/Additional comments	Reference
Apoptosis	Rat CGNs (neurons)	Caspase-3 and-8 and Bad, glutathione and cell cycle factors, p53	Folch <i>et al.</i> ⁵⁰
	Vero cells (monkey kidney epithelial cells)	Lysosome destabilisation, mitochondrial dysfunction, condensed and fragmented nuclei	Fernandez Freire <i>et al.</i> ³¹⁷
	Jurkat T cells (human lymphocyte)	Apoptosis was suppressed by p38 and MAPK/ERK kinase inhibitors	Wispriyono <i>et al.</i> ²⁶²
	Primary fish hepatocytes	DNA laddering, caspase activation, Ca ²⁺ , Mg ²⁺ -ATPase, ROS, Δψ _m , ATP depletion, and GSH	Dong <i>et al.</i> ²⁹⁸
	Primary mouse splenocytes	ERK activation, ROS, Δψ _m , DNA fragmentation, caspase-3, PARP-1	Chen <i>et al.</i> ²⁰³
	Panc-1 and MIA PaCa-2 (human pancreatic cancer)	Caspase, cathepsin B, Δψ _m , NF-B/p65, JNK, AKT	Schaefer <i>et al.</i> ²⁹⁶
Necrosis	Rat neurons, kidney and liver	Morphological changes	Villena <i>et al.</i> ³¹⁸
	L929 cells (mouse fibroblast)	Non-apoptotic DNA fragments	Chen <i>et al.</i> ²⁹⁷
	Chang liver (human liver) and T 24 (human bladder carcinoma)	CAS gene (downregulated). No changes in other molecules examined	Wang <i>et al.</i> ³⁰⁰
	Mouse livers (<i>in vivo</i>)	Liver specific parameters	Umemura <i>et al.</i> ³¹⁹
	Rat sertoli cells (testes cells)	Morphological changes	Yang <i>et al.</i> ²⁹¹

Exposure of cells to TCBQ resulted in classical apoptosis manifestations, namely PS presentation in the absence of membrane compromise (Annexin V⁺/PI⁻), pronounced caspase-3 activation, and DNA fragmentation. The occurrence of membrane permeation in Annexin V⁺/PI⁺ cells were likely cells in a late stage of apoptosis, as, in the absence of phagocytes, the membrane of apoptotic cells becomes porous and allows for PI penetration, whilst still expressing PS. Apoptotic cell death due to TCBQ is consistent with literature, which, unlike for PCP, is in relatively high agreement of apoptosis across different cell lines.^{264,265,320-322} The large increase in caspase-3 activation observed in the present study indicates a caspase dependent onset of apoptosis via either intrinsic or extrinsic pathways. Hu *et al.* found that both pathways contributed to TCBQ induced apoptosis in PC 12 cells. Similar to the present study, they found an increase in caspase-3, $\Delta\psi_m$ reduction, and reported apoptosis to be ROS dependent.³²⁰ Intrinsic-extrinsic crosstalk was found to be a result of BH3 interacting-domain death agonist (Bid). Here, Fas caused Fas-associated protein with death domain (FADD) to activate caspase-8. This in turn either directly activated caspase-3, or cleaved Bid, which caused reduced $\Delta\psi_m$ and subsequent cyt c release and intrinsic activation of caspase-3. Since this process was found to be ROS dependent, it is possible that a similar cascade may have occurred in the present study. Liu *et al.* further supported ROS-mediated extrinsic apoptosis as a result of FADD and subsequent caspase-3 and -8 activation.³²¹ This particular study implicated ER stress, DR5, and PARP-1 cleavage in TCBQ induced apoptosis. In their 2017 study, they further identified roles of protein disulfide isomerase (PDI) and Bcl-2 homologous antagonist/killer (Bak) in mitochondrial membrane permeabilization leading to apoptosis.³²² Fu *et al.* found the upregulation of inflammatory cytokines (including TNF) in TCBQ-induced apoptotic PC12 cells as a result of nuclear factor kappa-light-chain-enhancer of activated B cells (NF- κ B) signalling, which indicates inflammatory response and extrinsic apoptosis signalling.³²³ Roles of TNF and NF- κ B have also been implicated in neuronal synaptic plasticity,³²⁴ thus the possibility exists that the dysregulation of these factors may contribute to cell cycle disruption and apoptosis caused by TCBQ, however this would require further investigation. A moderate amount of evidence is therefore in support of extrinsic apoptotic mechanisms of TCBQ, particularly in PC12 cells, however this may not necessarily translate to mature human neurons or similar such cell lines. An exception to the generally consistent mode of cell death across cell

lines was found by Ling *et al.*, who noted apoptosis and caspase-3 activation in one breast cancer cell line (MCF-7), and in contrast, necrotic like cell death in another of breast cancer origin (SK-Br-3).³²⁵ This difference was ascribed to cell line specific ROS tolerability, where the more sensitive cell line underwent necrosis due to a reduced capability of coping with ROS insults.

Exposure of cells to TCHQ presented with an interesting case, as it was able to induce either predominantly apoptotic (fate 1) or necrotic like cell death (fate 2). It was noted that populations predominantly undergoing apoptosis resulted in a lower decrease in viable cells, indicating it to be the less potent outcome. Death by apoptosis is considered a more contained form of demise,⁷⁸ and while cells in culture will tend to send apoptotic signalling to neighbouring cells, this signalling is often not as detrimental to surrounding cells as that of spilt content originating from necrotic cells.³²⁶ This may have accounted for the greater magnitude of cell death observed in fate 2. *In vivo*, apoptotic cells are engulfed by phagocytes before their membrane becomes porous,³²⁷ however late stage apoptotic cells *in vitro* become pervious to PI in the absence of phagocytes.¹⁹² The large increase in Annexin V⁺/PI⁺ cells in fate 2 may consist partially of late apoptotic cells (concomitant with the process proposed below), especially if a large number of cells were in G2/M cell cycle phase near the start of TCHQ exposure, as cell death would occur more rapidly in such cells considering the G2/M block observed.

Bearing in mind the increase in caspase-3 activity and DNA fragmentation, Annexin V/PI⁺ cells, as well as oxidative stress factors, it is likely that the bulk of the Annexin V⁺/PI⁺ population comprised of cells for which apoptosis was initiated, and subsequently switched to necrosis. This process may have occurred in a similar fashion to PCP, with the exception that apoptosis was not avoided in TCHQ fate 1. The occurrence of two different fates between biological repeats indicates that exposure to TCHQ brought cells to the cusp of the apoptosis/necrosis line. The fact that cell cycle was not synchronised may have somewhat contributed to the difference between the two fates. Fate 2 may have occurred in cells starting closer to the G2/M phase, as the longer cells remain blockaded at this phase, the more susceptible they are to undergo necrosis than other cell cycle blocks.²⁸³ Cell cycle data for TCHQ could not be divided into distinct apoptosis and necrosis data sets, as mode of cell death and cell cycle analysis cannot be run simultaneously, thus

apoptotic and necrotic populations could not be distinguished within cell cycle analysis. In lieu of this, larger error was noted for the TCHQ sub-G1 fraction after 48 h than other test compounds, which may correspond to different survival rates related to the different fates of TCHQ exposed cells. Error for other cell cycle phases of TCHQ exposed cells was however similar to other compounds, indicating that the defining factor for apoptosis-necrosis switch would be downstream of observed cell cycle effects. An additional contributing factor, is the possibility of dual cytotoxic and antiproliferative activity, (which may apply to PCP and TCBQ as well), which is indicated as not all treatments incurred a 50% reduction in cell viability. The precise underlying cause for these differences would however require further investigation. The presence of PI permeated cells with the absence of Annexin V-FITC indicates that necrotic-like effects were not only the result of advanced apoptosis, but definite occurrence of primary necrosis. The propensity for cells to differentially undergo apoptosis or necrosis as a result of TCHQ exposure has been previously described in splenocytes.²⁰³ This switch implicated similar characteristics as found in the present study, including caspase-3, ROS and $\Delta\psi_m$ factors. The study ascribed the switch to ROS effects arising due to prolonged extracellular signal-regulated kinase (ERK) activation, as well as PARP-1 signalling, indicating similar mechanisms to those proposed for PCP induced necrosis. Implications of both ERK and PARP-1 in cell cycle have been reported in literature.^{328,329} Wispriyono *et al.* further implicated the role of mitogen-activated protein kinase (MAPK) signalling, including that of ERK in TCHQ induced cell death in Jurkat T cells, however this mode of cell death was constrained to apoptosis.²⁶² Here, ERK, p38 and c-Jun N-terminal kinase (JNK) were phosphorylated, leading to cell death. The same study however found no such phosphorylation upon PCP treatment, thus the MAPK pathway may contribute to the difference in necrosis susceptibility. The MAPK pathway is regulated by PARP-1,³²⁹ and PARP-1 may also inhibit caspase mediated apoptosis and induce necrosis upon severe ATP depletion.³³⁰ Differential effects of PCP and TCHQ on PARP-1 activity may therefore determine cell fates, however the precise effects and cross-talk between these factors would require further investigation. Wang *et al.* also noted similar differences between TCHQ and PCP as in the present study, wherein partial apoptosis was observed following TCHQ exposure, while PCP yielded cell death more characteristic of necrosis.³⁰⁰ This, however, was not observed in the evaluation of a second cell line, indicating effects to be cell line specific.

The results of the present study indicate that cells exposed to TCHQ are more resistant to ROS, and exposure to the different compounds yield complex molecular interactions, creating different environments which confer differential likelihoods of cells succumbing to apoptosis or necrosis under ATP depletion insults. The higher IC_{50} of PCP suggest the possibility of resistance to cell death completion, until eventually the extent of cellular damage initiates necrosis, while cells exposed to TCHQ may be capable of dying by apoptosis until a threshold (presumably cell cycle dependent ROS or ATP levels) is reached.

4.4. Reactive oxygen species, mitochondrial membrane potential, and reduced glutathione content

The crosstalk between ROS, $\Delta\psi_m$, and GSH is essential for cellular defence against toxic exogenous compounds, and is frequently implicated in the initiation and orchestration of cell death.¹³⁵ Exposure to PCP resulted in increased ROS after 48 h, while $\Delta\psi_m$ was reduced after 4 h, indicating that effects occurred first in the mitochondria. This timing indicates that the initial cause of ROS increase was due to the leakage of electrons from a compromised mitochondrial membrane, which subsequently reacted with oxygen to form ROS. This, as opposed to the inverse: $\Delta\psi_m$ reduction as a result of ROS-induced mitochondrial damage. Although the initiation of ROS- $\Delta\psi_m$ events occurred in the mitochondria, the resultant increased production of ROS would create a vicious cycle of further $\Delta\psi_m$ reduction and ROS production.³³¹ Pentachlorophenol is known to uncouple oxidative phosphorylation, a process which may recruit uncoupling proteins or adenine nucleotide translocase.³³² This process may allow for inappropriate passage of protons to the mitochondrial matrix, thus impairing ATP production, as well as electron leakage through a permeabilized mitochondrial membrane,³³³ which would cause the observed reduction in $\Delta\psi_m$. A permeated mitochondrial membrane would result in the release of apoptosis signalling factors such as cyt c, SMAC, and apoptosis inducing factor among others, which further induce a cascade leading to cell death, often including caspase activation.¹⁴⁴

Fernandez Fiere *et al.* attributed lysosome destabilisation to PCP-induced disruption of mitochondrial function,³¹⁷ which may explain the observed necrotic cell death, as

this mechanism is commonly associated with necrosis.³³⁴ The uncoupling of oxidative phosphorylation and mitochondrial dysfunction arising from PCP exposure may result in an impaired ability for ATP production, favouring necrosis to apoptosis, as postulated earlier in mode of cell death. The ability of PCP to bind mitochondrial respiratory complex II (succinate dehydrogenase) has been demonstrated,^{335,336} and the inhibition of this complex may contribute to diminished ATP production. Nnodu *et al.* found depleted ATP upon PCP exposure to natural killer cells,³³⁷ however this occurrence, and its link to mitochondrial events, would require confirmation in neuronal cells. Nonetheless, the role of mitochondrial disruption in cytotoxic effects of PCP has been described in a number of instances,^{50,298,338,339} and is confirmed for SH-SY5Y cells in the present study.

Electrons leaked from the compromised mitochondrial membrane would have the ability react with oxygen to form superoxide anions, which would subsequently be catalysed to H₂O₂ by superoxide dismutase (SOD).³⁴⁰ Hydrogen peroxide would constitute the observed increase in ROS, as this is the species primarily measured by DCFDA, however other species may have been concurrently present, as DCFDA is not necessarily exclusively oxidised by the presence of H₂O₂.²⁰⁴ Upregulation of SOD has been reported in PCP exposed cells,⁵⁰ which provides support for this particular ROS conversion pathway. The arise of ROS would not only augment $\Delta\psi_m$ reduction by exerting various forces of mitochondrial damage, but also inflict damage in other cell areas. Hydrogen peroxide is not as reactive as other ROS (e.g. hydroxyl radicals), which allows it to be preserved by the time it reaches the DNA, upon which it is able to exert a plethora of mutations and strand breaks.³⁴¹ The infliction of DNA damage is a strong potentiator for cell death and cell cycle disruption, and insurmountable damage, coupled with further cellular damage and mitochondria-derived cell death signalling, may result in cell death through a multitude of mechanistic pathways. Reactive oxygen species have been implicated in PCP-induced cell death for a number cell lines,^{28,261,298,338,342,343} the attenuation of which may serve as a possible therapeutic target for PCP exposure. The application of antioxidants such as NAC has been reported to ameliorate cell death *in vitro*,^{28,203} however antioxidant treatment or prevention strategies would require refinement and evaluation *in vivo*.

A further factor to be considered in mitochondrial and ROS related cell death cross-talk is GSH, which is a key modulator of cellular redox homeostasis,³⁴⁴ and the depletion of which was observed for PCP. This molecule serves to regulate ROS levels through the donation of an electron from a thiol group, which is accepted by ROS, rendering it neutralised and unable to exert oxidative stress.³⁴⁵ Excess ROS causes GSH depletion, as cellular GSH pools are reduced by ROS to GSSG, leaving the cell vulnerable to unchecked ROS effects. Alternatively or additionally, GSH may be depleted by direct reduction by exogenous compounds, or through impaired GSH production, allowing ROS to accumulate and initiate cell death signalling.¹⁵¹ Although such signalling is putatively derived from ROS and mitochondrial membrane permeation, initiation of apoptosis signalling due to a more direct result of GSH depletion has been reported.¹³⁶ In the absence of sufficient GSH, other antioxidant mechanisms may be recruited in an attempt at ROS management. Upregulation of catalase, which is an enzyme that protects against ROS, has been described for PCP,^{343,346} suggesting ROS to overwhelm GSH regulatory abilities. Similar to the present study, decreased GSH has been reported as a result of PCP exposure in hepatocytes,^{298,343} however GSH levels had not previously been directly examined in neuronal cells. Folch *et al.* did not directly assess GSH levels, but investigated the effect of PCP on antioxidant related genes in rat neurons.⁵⁰ They found an upregulation of the gene responsible for glutathione S-transferase, an enzyme which aids GSH-mediated detoxification, as well as cell death signalling via MAPK pathway. The possibility of MAPK signalling is however somewhat refuted by Chen *et al.*, who found no change in ERK activation upon PCP exposure.²⁰³ In addition to enabling ROS accumulation and possible cell death signalling, GSH disruption also has implications for cell cycle. The presence of GSH is involved in the regulation of DNA synthesis, and is essential for progression to S phase,³⁴⁷ thus the decrease in GSH observed in the present study may contribute to the accumulation of cells in G1 phase.

Exposure of cells to TCBQ resulted in fairly similar effects on ROS, $\Delta\psi_m$ and GSH as PCP, with the exception that ROS increased earlier, at 24 h as opposed to 48 h. This indicates faster acting mechanisms for TCBQ in terms of ROS production. The earlier increase in ROS for TCBQ (and TCHQ) may be linked to cell cycle, as effects on cell cycle also appeared earlier for metabolite exposure, however it is unknown

whether different effects on cell cycle caused different timing in ROS increases or visa versa. It is unlikely that ROS and cell cycle changes were merely coincidental, as ROS is closely associated with cell cycle. Under normal circumstances, ROS increases gradually throughout cell cycle progression,³⁴⁸ and the dysregulation of either system may in turn disrupt the other, and when the impact is severe enough, lead to cell death.¹⁴⁹ In the present study, apoptotic mechanisms of cells exposed to TCBQ were evidently more capable of coping with resultant ROS insults, despite the earlier appearance thereof. Unlike for PCP, ROS-related MAPK signalling has been described for TCBQ,^{323,349} the downstream events of which, while not capable of preventing ultimate cell demise, may contribute to preservation of apoptotic machinery functioning. Specifically, Su *et al.* noted the involvement of JNK signalling in the activation of nuclear factor (erythroid-derived 2)-like 2 (Nrf2) in TCBQ exposed cells.³⁴⁹ This is a protein involved in the regulation of antioxidant enzyme expression, and is active upon accumulation within the nucleus.³⁵⁰ Su *et al.* found nuclei levels of Nrf2 to be increased due to JNK signalling upon TCHQ exposure. In addition, nuclear Nrf2 was increased due to Kelch-like ECH-associated protein 1 (Keap1) ubiquitination, and BTB and CNC homolog 1 (Bach1) inactivation, which allows for Nrf2 entry into the nucleus.³⁴⁹ It is therefore possible that enhanced antioxidant enzyme transcription by Nrf2 may promote more competent ROS regulation attempts, however extended $\Delta\psi_m$ decrease, coupled with continued ROS production lead to eventual cell death in the form of apoptosis.

An early event in TCHQ exposure was decreased $\Delta\psi_m$, which was recovered after 24 h, and again diminished after 48 h. This transient $\Delta\psi_m$ recovery may be a further contributor to ultimate cell fate, where, if mitochondrial functioning is recovered for long enough, sufficient ATP may be produced to see apoptosis through to completion, while a shorter recovery period may eventuate necrosis due to insufficient ATP production. Recovery of $\Delta\psi_m$ has been reported to protect cells against necrosis,³⁵¹ however this particular concept has not been previously explored in TCHQ toxicity. Endpoint $\Delta\psi_m$ decreases have however been reported for TCHQ, and similar to the present study, has also been linked to increased ROS production.^{28,203,338,352} The relatively low levels of $\Delta\psi_m$ reduction compared to other compounds may suggest additional mitochondria-independent pathways affecting ROS production, such a through peroxisomes, ER stress, or activation of death

receptor pathways.¹⁴² The production of ROS as a by-product of spontaneous conversion of TCHQ may be considered, although this has not been described in literature. An unexpected result of TCHQ was the increase in GSH. Increased GSH is usually associated with increased cell proliferation,³⁵³ however its role in toxicity has been discovered in the form of reductive stress.³⁵⁴ Less common than oxidative stress, this process has the potential to exert pathological effects by inappropriately reducing cellular components due to the altered redox status of elevated GSH levels.³⁵⁵ Increased GSH may have arisen due to either an overreaction to ROS production, dysregulated GSH synthesis, or a combination thereof. Two key modulators of GSH synthesis are glutamate cysteine ligase, and GSH synthetase, and are regulated by Nrf2, NF- κ B, as well as antioxidant response element, and the upregulation of which may result in increased GSH and subsequent reductive stress.³⁵⁶ In addition, glutathione reductase, which catalyses the conversion of GSSG to GSH may have been recruited to a similar effect. Although increased GSH would confer enhanced antioxidant activity against ROS, a paradoxical effect of further increased ROS production has been recently discovered. Korge *et al.* demonstrated that ROS is produced in an environment of reductive stress due to leaked electrons from glutathione reductase and thioredoxin reductase, which are subsequently accepted by oxygen to form ROS in the absence of appropriate electron acceptors such as GSSG.³⁵⁷ This ROS increase, accompanied by ROS derived from other processes such as mitochondrial damage, results in a net increase in ROS despite greater antioxidant activity, thereby switching toxic actions from reductive to oxidative stress.³⁵⁸ The period whereupon this switch occurred may have constituted the $\Delta\psi_m$ recovery observed in the present study if redox status was transiently neutralised. The length of this period may have been the determining factor for the amount of ATP produced and subsequent cell fate. An alternative hypothesis for increased GSH may be that there was an impaired ability of GSH to reduce ROS, or an adaptive response to protect against insults. Levels of GSH are not uniform with different cellular compartments, but are differentially distributed, with unique synthesis and transport processes.³⁵⁹ Mitochondrial GSH pools, for example, arise from cytosolic GSH import, as *de novo* synthesis does not occur within this compartment.³⁶⁰ Localisation of ROS and GSH in different compartments may have presented as overall increases, as the assays used cannot discriminate locations of increase. Their separation would render increased GSH ineffective if residing in a

different compartment, particularly if mitochondrial transport is impaired. Although this possibility should be considered, the first explanation seems the more likely scenario. The concept of reductive stress complicates the possibility of antioxidant treatment options, as such treatment, while protecting against PCP and TCBQ, may potentiate effects of TCHQ. This further highlights the differences in mode of action between the three compounds.

4.5. Acetylcholinesterase activity

4.5.1. Ellman esterase assay

The decrease in AChE activity between DMSO and the negative control was expected, as DMSO is known to inhibit AChE.³⁶¹ This phenomenon was negated from test compound assessment however as they were compared against DMSO values and not the negative control. The only test compound to exert activity against AChE was TCHQ, of which the Ellman IC_{50} was higher than the corresponding cytotoxic IC_{50} . This suggests that cytotoxic effects would occur at lower concentrations before neurotransmitter irregularities would arise, however this would require further validation *in vivo*. Although the Ellman IC_{50} was higher, it was not vastly departed from the corresponding cytotoxic IC_{50} , thus at chronic concentrations, cytotoxic and neurotransmitter effects may quickly overlap and compound one another to produce greater overall neurotoxicity. Inhibition of AChE would result in an accumulation of ACh as the enzyme is rendered unable to hydrolyse it into acetate and choline, causing extended activation of its cognate receptors.¹⁵⁶ No previous studies have explored TCHQ inhibition of AChE, however other pesticides such as carbamates and organophosphates are known to inhibit AChE. While both pesticide classes exert similar acute AChE inhibition effects, binding carbamates reversibly may serve in a limited therapeutic capacity,³⁶² while long term organophosphate binding becomes irreversible, causing neurotoxic effects.³⁶³ The reversibility of TCHQ binding would clarify its role in ACh effects, and would require longer term enzymatic studies, however it is suspected to be irreversible. Reversible AChE inhibitors are used as AD drugs,¹⁶³ and it is somewhat paradoxical that pesticides have been linked to AD onset.³⁰⁴ It is possible that chronic persistence of concentrations high enough to inhibit AChE, yet low enough to avert poisoning

symptoms mimic therapeutic effects of reversible AChE inhibitors during the process of cell cycle disruption. This may lead to insidious AD onset, masked by AD drug mimicry, with symptoms only appearing upon advanced late stage neurological changes. This possibility is supported by AD occurring in individuals after extended chronic exposure to low doses of pesticide.³⁶⁴ The effects of PCP, and in particular its metabolite TCHQ, has previously been vastly unexplored, and the findings of the present study simultaneously sheds new light and sets a platform for further investigation of the area.

4.5.2. *In silico* assessment

Pentachlorophenol has the ability to bind acetate at the PCP hydroxyl group to form pentachlorophenol-acetate.³⁶⁵ The consideration of this ability, along with critical evaluation of the molecular reactions involved in the Ellman esterase assay (Figure 8), was initially thought to be a possible confounding factor of the assay, however led to the development of a hypothesis to explain AChE inhibition at a molecular level.

It was hypothesised that normal ACh cleavage would yield acetate, which would bind PCP, and the acetate conjugate acted upon by AChE in an attempt to cleave it into its original counterparts, thus diverting AChE activity from its normal cleaving action on ACh (Figure 36). This was predicted since AChE cleaves ACh at the connecting oxygen, and may attempt to exert similar catalytic tendencies on an analogous site.³⁶⁶ Additional support for this theory is provided in that the active site gorge of AChE is rich in amino acids containing aromatic rings, and thus would provide opportunity for binding of another aromatic ring (a property of PCP and its metabolites) via pi-pi interactions.³⁶⁷ Although PCP showed no activity at the concentrations tested in the Ellman esterase assay of this study, it has been reported to inhibit AChE at much higher concentrations,³⁶⁸ and thus it was hypothesised that a similar mechanism may be at play in TCHQ inhibition of AChE, as this molecule possesses two hydroxyl groups to which acetate may bind. Another possibility considered was that the normal ACh cleavage produces choline, the hydroxyl group of which would also have the potential to bind a TCHQ hydroxyl group, resulting in a water molecule as a by-product. All possibilities of acetate or choline binding to one

or both hydroxyl groups of TCHQ were considered, as well as the PCP hydroxyl group for completeness and comparison purposes (Table 2).

In general, ligands with acetate (PCP-Ac, TCHQ-Ac and Ac-TCHQ-Ac) seemed to exhibit better binding energies, with lower maximums than those containing choline, suggesting greater binding affinity attributed to acetate bound aromatic rings. This suggests relative incompatibility for AChE active site binding for choline bound molecules due to structural disagreement. This observation is however speculative, and requires further investigation, as binding energy differences observed between these ligands were not particularly large.

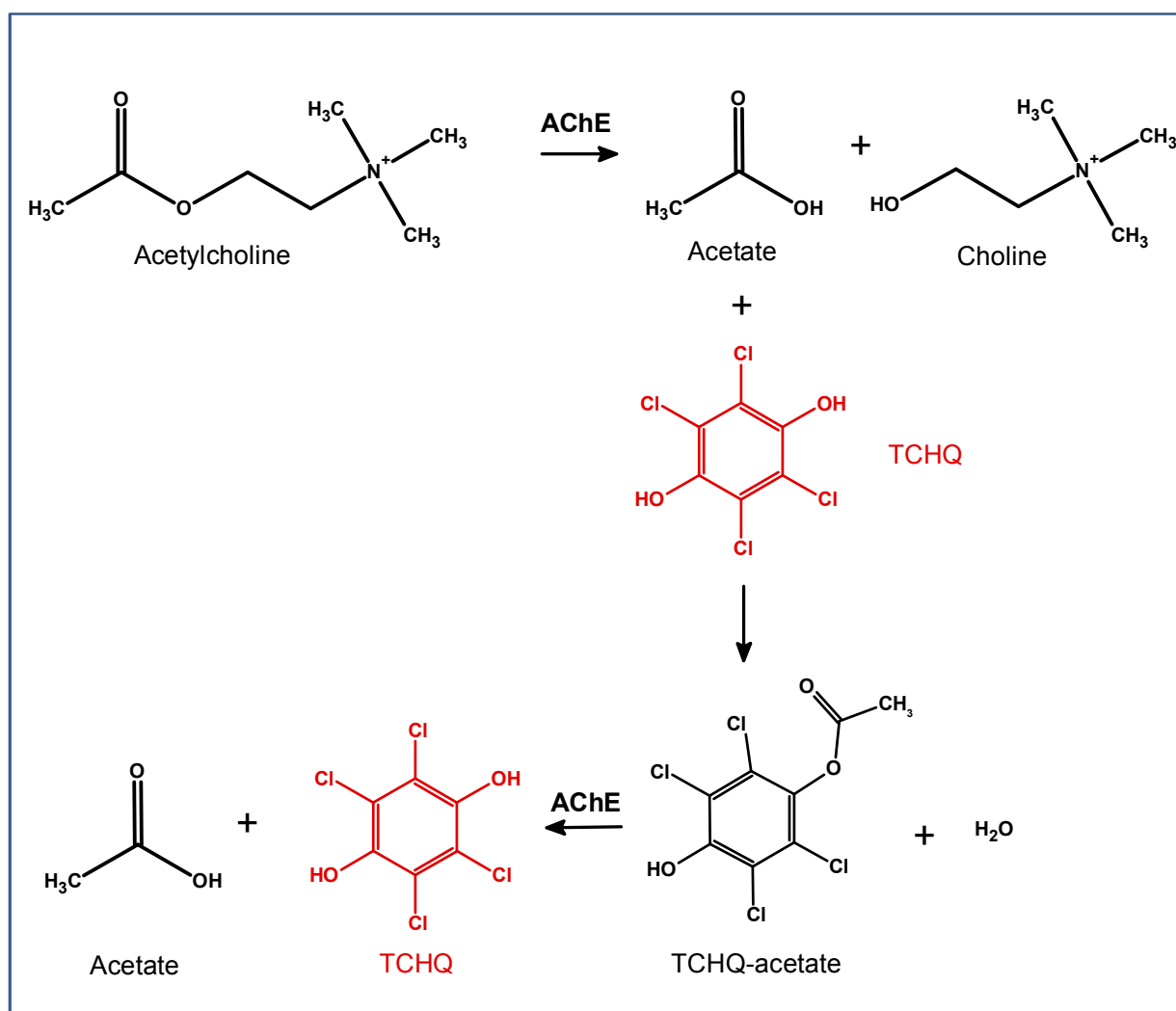


Figure 36: Theorised molecular mechanism of TCHQ inhibition of AChE.

The amino acids TRP 84, PHE 330, and TYR 334 appeared to play an integral role in the binding of docked ligands with lower binding energies. The docked ligands with the lowest binding energies were positioned in parallel with TRP 84 and PHE 330. Since these amino acids, as well as docked ligands contained aromatic moieties, pi-pi interactions likely constituted the primary binding effect.³⁶⁹ The central role of this interaction is further consolidated by docked ligands with higher binding energies being far removed from these moieties. Pi-pi interactions may occur in either parallel or t-shaped capacities,³⁷⁰ and the positioning of TYR 334 was representative of the latter. The conformation of the three mentioned amino acids appeared to form a pocket in which the docked ligands with lower binding energies resided, and was a similar molecular phenomenon to that of original bound ligands. TRP 84 has been identified as a critical amino acid in the binding specificity and function of AChE, and may confer not only pi-pi interactions, but also London and van der Waal interactions.³⁷¹ The binding of a compatible ligand in close proximity to TRP 84 provides a strong platform for AChE inhibition. The relationship between TRP 84 and AChE inhibitors was described for carbamates, where the more proximal the ligand to TRP 84, the higher the inhibition constant was, indicating greater potency.³⁷² Binding of ligands proximal to TRP 84 may also alter the orientation of its indole moiety, thereby modifying the cysteine loop of the active site, ultimately impeding ACh access.³⁷³ In addition, superposition of ACh with docked ligands of lower binding energies revealed overlap of the two molecules within the active site, suggesting mutual exclusivity. It is possible that this may account for inhibitory action of TCHQ (and PCP at high very concentrations), as inaccessibility of ACh to the AChE active site would disallow normal ACh cleavage. Docked ligands with higher binding energies did not overlap with ACh upon superimposition, but did reside at the entrance of the active site gorge, a pose which would also impair ACh access. These assumptions, however, require further confirmation of both the presence, and activity of the hypothesised structural analogues *in vitro* in order to attribute this mechanism to PCP and TCHQ AChE inhibitory activity with confidence.

A binding energy of less than -9 is generally considered a good binding energy, and the lower the binding energy, the greater binding affinity is assumed, indicating greater potency of the inhibitor.³⁷⁴ Although none of the docked ligands reached a binding energy of less than -9, this does not necessarily confer very low binding

affinity as the molecules assessed were small, and lower binding energies are more biased toward larger molecules.³⁷⁵ Consideration of ligand size lends to the inference of modest binding affinities for docked ligands with binding energies approaching -9. For TCHQ, a modest binding affinity of its structural analogue may correspond with the modest AChE inhibitory activity found in the Ellman esterase assay.

A surprising result of molecular docking was that PCP-Ac yielded relatively low binding energies despite no inhibitory activity of the original compound, PCP, in the Ellman esterase assay. As mentioned earlier, PCP is able to inhibit AChE activity at very high concentrations, thus it is possible for the discrepancy to be attributed to the likelihood of ligand formation. The present AChE inhibitory activity hypothesis relies on PCP or TCHQ binding acetate or choline. Such binding depends on collision theory and chemical kinetics, where molecules randomly collide with one another, and subsequent binding only occurring upon successful collision under favourable conditions.³⁷⁶ The presence of two hydroxyl groups in TCHQ increases the probability of acetate or choline successfully colliding with one of these groups when compared to that of PCP with only one hydroxyl group. Structural analogues of TCHQ hypothesised to inhibit AChE are therefore more likely to occur, thus lower concentrations of TCHQ would be required to give rise to the same AChE inhibitory capacity as PCP. The same concept may be applied to the lack of AChE inhibitory activity observed for TCBQ. This molecule contains no hydroxyl groups favourable of binding acetate or choline, but contains two carbonyl groups, the doubled bonded oxygen of which is more stable and unreactive. The probability of TCBQ binding acetate or choline without catalytic intervention is therefore extremely low, and the occurrence of structural analogues fitting with the proposed hypothesis of AChE inhibitory action would be implausible.

The use of PDB files with pre-bound ligands to direct ligand poses and binding has the potential to convey false positives, where in reality, binding may not actually occur.¹⁷² Although this potential exists, if the hypothesised structural analogues are indeed present, it is then unlikely to be the case for TCHQ as the experimental *in vitro* Ellman esterase assay indicated inhibitory activity toward AChE. If a false positive were the case, it is more likely that no activity would have been noted in experiment. No activity was observed for PCP in the present study, and while a false positive is possible, it is not thought likely due to the explanation in the previous

paragraph. The likelihood of false positives would be more robustly predicted upon further *in vitro* investigation of the docked analogues. This highlights the advantage of complimentary *in silico* and experimental assessment methods for the validation of results obtained.

While molecular docking provides an indication of binding affinity for a ligand to a receptor, it does not give insight into a ligand's behaviour within the receptor and surrounding environment. If a ligand is able to bind a receptor, but is not able to hold its position, the binding may not translate into activity in reality.³⁷⁷ An MD simulation was thus employed to assess the stability of selected docked ligands. PCP-Ac and Ac-TCHQ-Ac appeared to reside with fair stability within receptors 1ut6 and 1qti, respectively, indicating that binding would be maintained when solvent, temperature and pressure are accounted for. Despite this, their relative average binding energies were much lower than their original ligand counterparts. These original ligands were galanthamine and a tacrine derivative, which are much more potent AChE inhibitors than PCP and TCHQ based on concentrations required for inhibition,³⁷⁸ which may explain the lower binding energies. The higher average binding energies once again correspond with modest AChE inhibitory activity observed in experimental assessment. Overall, *in silico* assessment does not refute the hypothesised molecular mechanism of AChE inhibitory activity of TCHQ, but provides some preliminary support for it. First evidence for, or the lack of evidence against a new hypothesis does not however cement it to be true. The translation of results from the hypothesised structural analogues to the original pesticide compounds is limited, and as the presence of these analogues is not known, this renders the proposed mechanism somewhat speculative. This does, however, provide a basis for further research into the AChE inhibitory activity of PCP and TCHQ, and is the first known proposition of possible mechanisms at a molecular level.

Chapter 5: Conclusion

Each of the three compounds exhibited different mechanisms leading to different modes of cell death. The parent compound, PCP, was the least potent, while its metabolite TCBQ was the most potent. Pentachlorophenol induced necrotic cell death, which occurred due to an overload of apoptotic machinery as a result of mitochondrial dysfunction and oxidative stress. This was indicated by compromised cell membrane, slight increase in caspase-3 activity, an increase in ROS, and decreases in GSH and $\Delta\psi_m$. Compromised mitochondrial membrane integrity initiated oxidative stress leading to apoptosis in cells exposed to TCBQ, which was evident by PS presentation, increased ROS and caspase-3 activity, and decreased GSH and $\Delta\psi_m$. Treatment with TCHQ resulted in a few interesting findings, where one of two fates occurred. Either apoptosis or necrosis ensued, presumably depending on the extent of recovery of depleted $\Delta\psi_m$ and resultant sufficiency of ATP available for apoptosis completion, which may have been influenced by the switch from reductive to oxidative stress. Transient $\Delta\psi_m$ recovery was indicated by $\Delta\psi_m$ decreases at 4 and 48 h, while $\Delta\psi_m$ at 24 h was not depleted. Reductive stress was indicated by increased GSH, and subsequent oxidative stress by increased ROS. In addition, each compound exerted different effects on cell cycle, where PCP induced a G1 block, TCBQ an S-phase block, and TCHQ a G2/M block, with substantial cell death observed in the sub-G1 phase. A summary of pathways of toxicity for each compound is depicted in Figure 37. These results bring to light new evidence for neurotoxic effects of PCP and its metabolites *in vitro*, and highlight the importance of assessing metabolites in conjunction with the parent compound, as extrapolation of effects cannot be assumed from the parent alone. Acetylcholinesterase inhibitory activity was demonstrated for TCHQ, while no activity was observed for PCP and TCBQ at concentrations tested. *In silico* investigation gave first evidence for a new hypothesis of TCHQ AChE inhibition at a molecular level, and sets a platform for further investigation not only for the compounds of the present study, but for other pesticides as well. These results indicate the potential for neurotoxicity in chronically exposed populations, and indicate that greater environmental remediation of PCP should be undertaken in order to prevent exposure and adverse effects.

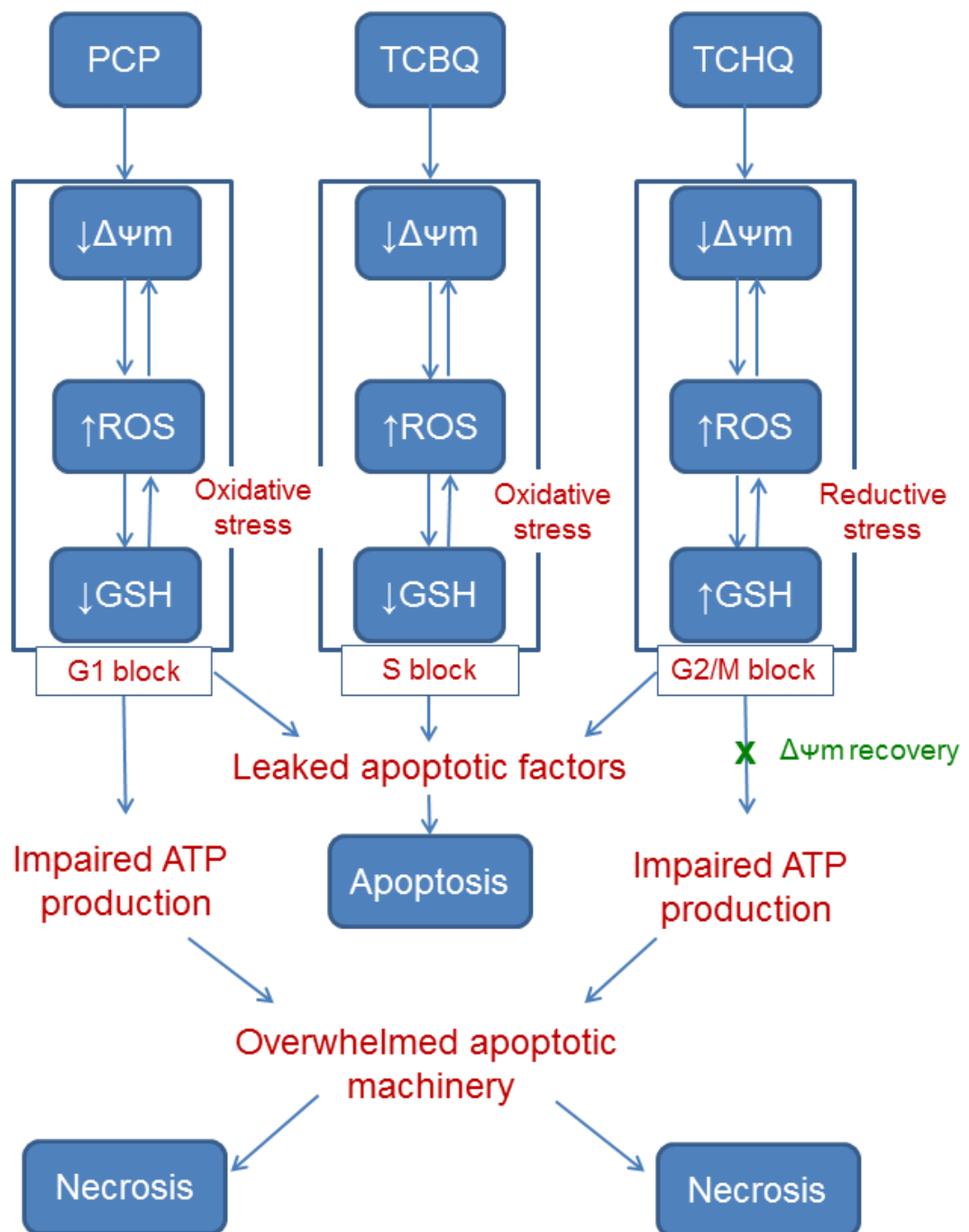


Figure 37: Summary of pathways of PCP, TCBQ and TCHQ.

Chapter 6: Limitations to the study and future research

While the present study provides valuable insight into mechanisms of toxicity in neuronal cells, the study was conducted *in vitro* and *in silico*, and the extent to which this data can be extrapolated to *in vivo* context is limited. In addition, the use of a cancerous cell line may further confound true representation of mechanisms, as there are distinct differences between cancerous and non-cancerous cells. Furthermore, the cell line used lacks maturity markers, 3D architecture, and synaptic connections found within a mature neuronal network. Further investigation *in vivo* is required to confirm these findings. The concept of autophagy as a mode of cell death was also not addressed in the present study. This could be a pertinent component of future work, as well as PCR based experiments to determine roles of specific genes and proteins. Inferences made, particularly regarding apoptosis-necrosis switch and the pathways thereof may be speculative, and therefore also require confirmation. Investigation on the effects of the compounds on cellular energetic would be helpful for clarification. It should also be noted that the relative ratios of each compound, particularly the metabolites, within the human body are currently unknown, and requires elucidation to determine the relative contribution of each compound to neurotoxic effects. A limitation regarding the *in silico* assessment conducted in this study was that the presence of the hypothesised structural analogues of PCP and TCHQ were not known. Confirmation of their presence is required, as well as further confirmation of the hypothesis via *in vitro* methods, additional *in silico* research, or x-ray crystallography among other research avenues. The techniques used for the assessment of this hypothesis may also be employed for investigation of other compounds implicated in AChE inhibitor poisoning.

References

1. Bocquet-Appel J-P. When the world's population took off: The springboard of the neolithic demographic transition. *Science*. 2011;333(6042):560-1.
2. Tilman D, Fargione J, Wolff B, D'Antonio C, Dobson A, Howarth R, Schindler D, Schlesinger WH, Simberloff D, Swackhamer D. Forecasting agriculturally driven global environmental change. *Science*. 2001;292(5515):281-4.
3. Smith AE, Secoy DM. A compendium of inorganic substances used in European pest control before 1850. *J Agric Food Chem*. 1976;24(6):1180-6.
4. Pimentel D. Green revolution agriculture and chemical hazards. *Sci Total Environ*. 1996;188 Suppl 1:S86-98.
5. Paranjape K, Gowariker V, Krishnamurthy VN, Gowariker S. *The Pesticide Encyclopedia*: CABI; 2014.
6. Kelce WR, Stone CR, Laws SC, Gray LE, Kemppainen JA, Wilson EM. Persistent DDT metabolite p,p'-DDE is a potent androgen receptor antagonist. *Nature*. 1995;375(6532):581-5.
7. Stockholm convention on persistent organic pollutants, (2004).
8. Convention on the prior informed consent procedure for certain hazardous chemicals and pesticides in international trade, 2244 UNTS 337; 38 ILM 1 (1999).
9. Gravance CG, Garner DL, Baumber J, Ball BA. Assessment of equine sperm mitochondrial function using JC-1. *Theriogenology*. 2000;53(9):1691-703.
10. Munoz-Quezada MT, Lucero BA, Iglesias VP, Munoz MP, Cornejo CA, Achu E, Baumert B, Hanchey A, Concha C, Brito AM, Villalobos M. Chronic exposure to organophosphate (OP) pesticides and neuropsychological functioning in farm workers: a review. *Int J Occup Environ Health*. 2016;22(1):68-79.
11. Freire C, Koifman RJ, Koifman S. Hematological and hepatic alterations in Brazilian population heavily exposed to organochlorine pesticides. *J Toxicol Environ Health A*. 2015;78(8):534-48.
12. Elliott M, editor *Synthetic pyrethroids: a symposium sponsored by the Division of Pesticide Chemistry at the 172nd meeting of the American Chemical Society, San Francisco, Calif., Aug. 30-31, 1976*. American Chemical Society ACS symposium series (USA); 1977: American Chemical Society.

13. Dawson RM. Oxime effects on the rate constants of carbamylation and decarbamylation of acetylcholinesterase for pyridostigmine, physostigmine and insecticidal carbamates. *Neurochem Int.* 1995;26(6):643-54.
14. Qaim M, Zilberman D. Yield effects of genetically modified crops in developing countries. *Science.* 2003;299(5608):900-2.
15. Phipps R, Park J. Environmental benefits of genetically modified crops: global and European perspectives on their ability to reduce pesticide use. *J Anim Feed Sci.* 2002;11(1):1-18.
16. Benbrook C. Do GM crops mean less pesticide use? *Pesticide outlook.* 2001;12(5):204-7.
17. Environmental Health Criteria 71: Pentachlorophenol. Geneva: International Programme on Chemical Safety, 1987. p. Report No.: 71.
18. Organisation WH. Pentachlorophenol Health and Safety Guide. Geneva: International Programme on Chemical Safety, 1989. p. Report No.: 19.
19. Decisions guidance documents: Pentachlorophenol and its salts and esters. Geneva: Operation of the prior informed consent procedure for banned or severely restricted chemicals in international trade Programme UNE, Organisation FaA, 1996.
20. Jones KC, de Voogt P. Persistent organic pollutants (POPs): state of the science. *Environ Pollut.* 1999;100(1-3):209-21.
21. Wandiga SO. Use and distribution of organochlorine pesticides. The future in Africa. *Pure Appl Chem.* 2001;73(7):1147-56.
22. Jorens PG, Schepens PJ. Human pentachlorophenol poisoning. *Hum Exp Toxicol.* 1993;12(6):479-95.
23. (IARC) IAfRoC. Polychlorophenols and their sodium salts (Group 2B). 1999. p. Report No.: 71.
24. Borysiewicz M, Kolsut W. Preliminary risk profile pentachlorophenol. Poland: Institute of Environmental Protection, 2005.
25. Arcand Y, Hawari J, Guiot SR. Solubility of pentachlorophenol in aqueous solutions: The pH effect. *Water Research.* 1995;29(1):131-6.
26. Weber R, Gaus C, Tysklind M, Johnston P, Forter M, Hollert H, Heinisch E, Holoubek I, Lloyd-Smith M, Masunaga S, Moccarelli P, Santillo D, Seike N, Symons R, Torres JP, Verta M, Varbelow G, Vijgen J, Watson A, Costner P, Woelz J, Wycisk P, Zennegg M. Dioxin- and POP-contaminated sites--contemporary and future

relevance and challenges: overview on background, aims and scope of the series. *Environ Sci Pollut Res Int.* 2008;15(5):363-93.

27. Nesakumar N, Sethuraman S, Krishnan UM, Rayappan JBB. Simultaneous detection of pentachlorophenol and 2,3,7,8-tetrachlorodibenzodioxin in guar gum— an electrochemical approach. *Journal of Applied Electrochemistry.* 2016;46(3):309-22.

28. Schroeder I. MSc dissertation: A mechanistic study of organochlorine hepatotoxicity [dissertation]: University of Pretoria; 2011.

29. Strategic Approach to International Chemicals Management (SAICM). Geneva: United Nations Environmental Programme, 2007. p. Report No.: GE. 06-01908.

30. Fischer D, Costley S, Moloï M, Jila X, Khaoué G. National implementation plan for the stockholm convention on persistent organic pollutants. In: Affairs E, editor. Republic of South Africa: Ministry of Water and Environmental Affairs; 2012.

31. Registration Review; Pesticide Dockets Opened for Review and Comment, EPA-HQ-OPP-2014-0763; FRL-9918-44 (2014).

32. Fernandes RS, Cotter TG. Apoptosis or necrosis: intracellular levels of glutathione influence mode of cell death. *Biochem Pharmacol.* 1994;48(4):675-81.

33. Annex XVII to REACH – Conditions of restriction. Helsinki: European Chemicals Agency, 2006. Contract No.: (EC) No 1907/2006.

34. Krishan A. Rapid flow cytofluorometric analysis of mammalian cell cycle by propidium iodide staining. *J Cell Biol.* 1975;66(1):188-93.

35. Eisler R. Eisler's Encyclopedia of Environmentally Hazardous Priority Chemicals: Elsevier Science; 2007.

36. Tsoufis T, Katsaros F, Kooi BJ, Bletsas E, Papageorgiou S, Deligiannakis Y, Panagiotopoulos I. Halloysite nanotube-magnetic iron oxide nanoparticle hybrids for the rapid catalytic decomposition of pentachlorophenol. *Chemical Engineering Journal.* 2017;313(Supplement C):466-74.

37. Rybnikova V, Singhal N, Hanna K. Remediation of an aged PCP-contaminated soil by chemical oxidation under flow-through conditions. *Chemical Engineering Journal.* 2017;314(Supplement C):202-11.

38. Moriwaki H, Akaishi Y, Akamine M, Usami H. Photodegradation of environmental pollutants using perylene adsorbed on silica gel as a visible-light photocatalyst. *Applied Catalysis B: Environmental.* 2017;204(Supplement C):456-64.

39. Proudfoot AT. Pentachlorophenol poisoning. *Toxicol Rev.* 2003;22(1):3-11.
40. Sullivan JB, Krieger GR. Clinical environmental health and toxic exposures: Lippincott Williams & Wilkins; 2001.
41. Gasiewicz TA. Nitro compounds and related phenolic pesticides. In: Hayes WJ, Jr. and Laws, E. R., Jr, editor. In *Handbook of Pesticide Toxicology*. New York: Academic Press; 1991. p. 6-70.
42. Qiao GL, Riviere JE. Systemic uptake and cutaneous disposition of pentachlorophenol in a sequential exposure scenario: effects of skin preexposure to benzo[a]pyrene. *J Toxicol Environ Health A.* 2002;65(18):1307-31.
43. Geyer HJ, Scheunert I, Korte F. Distribution and bioconcentration potential of the environmental chemical pentachlorophenol (PCP) in different tissues of humans. *Chemosphere.* 1987;16(4):887-99.
44. Juhl U, Witte I, Butte W. Metabolism of pentachlorophenol to tetrachlorohydroquinone by human liver homogenate. *Bull Environ Contam Toxicol.* 1985;35(5):596-601.
45. Uhl S, Schmid P, Schlatter C. Pharmacokinetics of pentachlorophenol in man. *Arch Toxicol.* 1986;58(3):182-6.
46. Ahlborg UG, Lindgren JE, Mercier M. Metabolism of pentachlorophenol. *Arch Toxicol.* 1974;32(4):271-81.
47. Reigner BG, Gungon RA, Hoag MK, Tozer TN. Pentachlorophenol toxicokinetics after intravenous and oral administration to rat. *Xenobiotica.* 1991;21(12):1547-58.
48. Reigner BG, Bois FY, Tozer TN. Assessment of pentachlorophenol exposure in humans using the clearance concept. *Hum Exp Toxicol.* 1992;11(1):17-26.
49. Miller L, Ingerman L. Toxicological profile for pentachlorophenol. Georgia: U.S. Department of health and human services, Registry AfTSaD; 2001.
50. Folch J, Yeste-Velasco M, Alvira D, de la Torre AV, Bordas M, Lopez M, Sureda FX, Rimbau V, Camins A, Pallas M. Evaluation of pathways involved in pentachlorophenol-induced apoptosis in rat neurons. *Neurotoxicology.* 2009;30(3):451-8.
51. Blakley BR, Yole MJ, Brousseau P, Boermans H, Fournier M. Effect of pentachlorophenol on immune function. *Toxicology.* 1998;125(2-3):141-8.
52. Guo Y, Zhou B. Thyroid endocrine system disruption by pentachlorophenol: an *in vitro* and *in vivo* assay. *Aquat Toxicol.* 2013;142-143:138-45.

53. Cooper GS, Jones S. Pentachlorophenol and cancer risk: focusing the lens on specific chlorophenols and contaminants. *Environ Health Perspect.* 2008;116(8):1001-8.
54. Guyton KZ, Loomis D, Grosse Y, El Ghissassi F, Bouvard V, Benbrahim-Tallaa L, Guha N, Mattock H, Straif K, International Agency for Research on Cancer Monograph Working G. Carcinogenicity of pentachlorophenol and some related compounds. *Lancet Oncol.* 2016;17(12):1637-8.
55. Ateeq B, Abul Farah M, Niamat Ali M, Ahmad W. Clastogenicity of pentachlorophenol, 2,4-D and butachlor evaluated by Allium root tip test. *Mutat Res.* 2002;514(1-2):105-13.
56. Orton F, Lutz I, Kloas W, Routledge EJ. Endocrine disrupting effects of herbicides and pentachlorophenol: *in vitro* and *in vivo* evidence. *Environ Sci Technol.* 2009;43(6):2144-50.
57. Debets FM, Strik JJ, Olie K. Effects of pentachlorophenol on rat liver changes induced by hexachlorobenzene, with special reference to porphyria, and alterations in mixed function oxygenases. *Toxicology.* 1980;15(3):181-95.
58. Schwetz BA, Keeler PA, Gehring PJ. The effect of purified and commercial grade pentachlorophenol on rat embryonal and fetal development. *Toxicol Appl Pharmacol.* 1974;28(1):151-61.
59. Bernard BK, Hoberman AM. A study of the developmental toxicity potential of pentachlorophenol in the rat. *Int J Toxicol.* 2001;20(6):353-62.
60. Kerkvliet NI, Baecher-Steppan L, Schmitz JA. Immunotoxicity of pentachlorophenol (PCP): increased susceptibility to tumor growth in adult mice fed technical PCP-contaminated diets. *Toxicol Appl Pharmacol.* 1982;62(1):55-64.
61. Kerkvliet NI, Baecher-Steppan L, Claycomb AT, Craig AM, Sheggeby GG. Immunotoxicity of technical pentachlorophenol (PCP-T): depressed humoral immune responses to T-dependent and T-independent antigen stimulation in PCP-T exposed mice. *Fundam Appl Toxicol.* 1982;2(2):90-9.
62. Lin PH, Nakamura J, Yamaguchi S, Upton PB, La DK, Swenberg JA. Oxidative damage and direct adducts in calf thymus DNA induced by the pentachlorophenol metabolites, tetrachlorohydroquinone and tetrachloro-1,4-benzoquinone. *Carcinogenesis.* 2001;22(4):627-34.
63. Purschke M, Jacobi H, Witte I. Differences in genotoxicity of H₂O₂ and tetrachlorohydroquinone in human fibroblasts. *Mutat Res.* 2002;513(1-2):159-67.

64. Fu J, Shi Q, Song X, Liu Z, Wang Y, Wang Y, Song E, Song Y. Tetrachlorobenzoquinone exerts neurological pro-inflammatory activity by promoting HMGB1 release, which induces TLR4 clustering within the lipid raft. *Toxicol Sci.* 2016.
65. Mosby's Medical Dictionary. 8 ed: Elsevier Health Sciences; 2013.
66. Polli JE. *In vitro* studies are sometimes better than conventional human pharmacokinetic *in vivo* studies in assessing bioequivalence of immediate-release solid oral dosage forms. *AAPS J.* 2008;10(2):289-99.
67. Slotkin TA, MacKillop EA, Ryde IT, Tate CA, Seidler FJ. Screening for developmental neurotoxicity using PC12 cells: comparisons of organophosphates with a carbamate, an organochlorine, and divalent nickel. *Environ Health Perspect.* 2007;115(1):93-101.
68. Xie HR, Hu LS, Li GY. SH-SY5Y human neuroblastoma cell line: *in vitro* cell model of dopaminergic neurons in Parkinson's disease. *Chin Med J (Engl).* 2010;123(8):1086-92.
69. Agholme L, Lindstrom T, Kagedal K, Marcusson J, Hallbeck M. An *in vitro* model for neuroscience: differentiation of SH-SY5Y cells into cells with morphological and biochemical characteristics of mature neurons. *J Alzheimers Dis.* 2010;20(4):1069-82.
70. Xun Z, Lee DY, Lim J, Canaria CA, Barnebey A, Yanonne SM, McMurray CT. Retinoic acid-induced differentiation increases the rate of oxygen consumption and enhances the spare respiratory capacity of mitochondria in SH-SY5Y cells. *Mech Ageing Dev.* 2012;133(4):176-85.
71. Forster JI, Koglsberger S, Trefois C, Boyd O, Baumuratov AS, Buck L, Balling R, Antony PM. Characterization of differentiated sh-sy5y as neuronal screening model reveals increased oxidative vulnerability. *J Biomol Screen.* 2016;21(5):496-509.
72. Ren M, Du C, Herrero Acero E, Tang-Schomer MD, Ozkucur N. A biofidelic 3D culture model to study the development of brain cellular systems. *Sci Rep.* 2016;6:24953.
73. Riss TL, Moravec RA, Niles AL. Cytotoxicity testing: measuring viable cells, dead cells, and detecting mechanism of cell death. *Methods Mol Biol.* 2011;740:103-14.

74. Kroemer G, Galluzzi L, Vandenabeele P, Abrams J, Alnemri ES, Baehrecke EH, Blagosklonny MV, El-Deiry WS, Golstein P, Green DR, Hengartner M, Knight RA, Kumar S, Lipton SA, Malorni W, Nunez G, Peter ME, Tschopp J, Yuan J, Piacentini M, Zhivotovsky B, Melino G, Nomenclature Committee on Cell D. Classification of cell death: recommendations of the Nomenclature Committee on Cell Death 2009. *Cell Death Differ.* 2009;16(1):3-11.
75. Orrenius S, Zhivotovsky B, Nicotera P. Regulation of cell death: the calcium-apoptosis link. *Nat Rev Mol Cell Biol.* 2003;4(7):552-65.
76. Kerr JF, Wyllie AH, Currie AR. Apoptosis: a basic biological phenomenon with wide-ranging implications in tissue kinetics. *Br J Cancer.* 1972;26(4):239-57.
77. Fadok VA, Bratton DL, Frasch SC, Warner ML, Henson PM. The role of phosphatidylserine in recognition of apoptotic cells by phagocytes. *Cell Death Differ.* 1998;5(7):551-62.
78. Taylor RC, Cullen SP, Martin SJ. Apoptosis: controlled demolition at the cellular level. *Nat Rev Mol Cell Biol.* 2008;9(3):231-41.
79. Adrain C, Creagh EM, Martin SJ. Apoptosis-associated release of Smac/DIABLO from mitochondria requires active caspases and is blocked by Bcl-2. *EMBO J.* 2001;20(23):6627-36.
80. Zhou LL, Zhou LY, Luo KQ, Chang DC. Smac/DIABLO and cytochrome c are released from mitochondria through a similar mechanism during UV-induced apoptosis. *Apoptosis.* 2005;10(2):289-99.
81. Du C, Fang M, Li Y, Li L, Wang X. Smac, a mitochondrial protein that promotes cytochrome c-dependent caspase activation by eliminating IAP inhibition. *Cell.* 2000;102(1):33-42.
82. McIlwain DR, Berger T, Mak TW. Caspase functions in cell death and disease. *Cold Spring Harb Perspect Biol.* 2013;5(4):a008656.
83. Li P, Nijhawan D, Budihardjo I, Srinivasula SM, Ahmad M, Alnemri ES, Wang X. Cytochrome c and dATP-dependent formation of Apaf-1/caspase-9 complex initiates an apoptotic protease cascade. *Cell.* 1997;91(4):479-89.
84. Boldin MP, Goncharov TM, Goltsev YV, Wallach D. Involvement of MACH, a novel MORT1/FADD-interacting protease, in Fas/APO-1- and TNF receptor-induced cell death. *Cell.* 1996;85(6):803-15.
85. Muzio M, Chinnaiyan AM, Kischkel FC, O'Rourke K, Shevchenko A, Ni J, Scaffidi C, Bretz JD, Zhang M, Gentz R, Mann M, Krammer PH, Peter ME, Dixit VM.

FLICE, a novel FADD-homologous ICE/CED-3-like protease, is recruited to the CD95 (Fas/APO-1) death--inducing signaling complex. *Cell*. 1996;85(6):817-27.

86. Harris SL, Levine AJ. The p53 pathway: positive and negative feedback loops. *Oncogene*. 2005;24(17):2899-908.

87. Proskuryakov SY, Konoplyannikov AG, Gabai VL. Necrosis: a specific form of programmed cell death? *Exp Cell Res*. 2003;283(1):1-16.

88. Rock KL, Kono H. The inflammatory response to cell death. *Annu Rev Pathol*. 2008;3:99-126.

89. Festjens N, Vanden Berghe T, Vandenabeele P. Necrosis, a well-orchestrated form of cell demise: signalling cascades, important mediators and concomitant immune response. *Biochim Biophys Acta*. 2006;1757(9-10):1371-87.

90. Alberts B, Johnson A, Lewis J, Raff M, Roberts K, Walter P. An overview of the cell cycle. *Molecular Biology of the Cell*. 4th ed. New York: Garland Science; 2002.

91. Cooper GM. The Eukaryotic Cell Cycle. *The Cell: A Molecular Approach*. 2nd ed. Sunderland (MA): Sinauer Associates; 2000.

92. Cheung TH, Rando TA. Molecular regulation of stem cell quiescence. *Nat Rev Mol Cell Biol*. 2013;14(6):329-40.

93. Morgan DO. *The Cell Cycle: Principles of Control*. London: New Science Press; 2007.

94. Wang Z, Fan M, Candas D, Zhang TQ, Qin L, Eldridge A, Wachsmann-Hogiu S, Ahmed KM, Chromy BA, Nantajit D, Duru N, He F, Chen M, Finkel T, Weinstein LS, Li JJ. Cyclin B1/Cdk1 coordinates mitochondrial respiration for cell-cycle G2/M progression. *Dev Cell*. 2014;29(2):217-32.

95. Taylor WR, Stark GR. Regulation of the G2/M transition by p53. *Oncogene*. 2001;20(15):1803-15.

96. Alberts B, Johnson A, Lewis J, Raff M, Roberts K, Walter P. Mitosis. *Molecular Biology of the Cell*. 4th ed. New York: Garland Science; 2002.

97. Blondel C, Melesan M, San Miguel A, Veyrenc S, Meresse P, Pezet M, Reynaud S, Raveton M. Cell cycle disruption and apoptosis as mechanisms of toxicity of organochlorines in *Zea mays* roots. *J Hazard Mater*. 2014;276:312-22.

98. Blagosklonny MV. Cell cycle arrest is not senescence. *Aging (Albany NY)*. 2011;3(2):94-101.

99. Di Leonardo A, Linke SP, Clarkin K, Wahl GM. DNA damage triggers a prolonged p53-dependent G1 arrest and long-term induction of Cip1 in normal human fibroblasts. *Genes Dev.* 1994;8(21):2540-51.
100. Murad H, Hawat M, Ekhtiar A, AlJapawe A, Abbas A, Darwish H, Sbenati O, Ghannam A. Induction of G1-phase cell cycle arrest and apoptosis pathway in MDA-MB-231 human breast cancer cells by sulfated polysaccharide extracted from *Laurencia papillosa*. *Cancer Cell Int.* 2016;16:39.
101. Giacinti C, Giordano A. RB and cell cycle progression. *Oncogene.* 2006;25(38):5220-7.
102. Hoffmann I, Draetta G, Karsenti E. Activation of the phosphatase activity of human cdc25A by a cdk2-cyclin E dependent phosphorylation at the G1/S transition. *EMBO J.* 1994;13(18):4302-10.
103. Willis N, Rhind N. Regulation of DNA replication by the S-phase DNA damage checkpoint. *Cell Div.* 2009;4:13.
104. Nguyen HD, Becker J, Thu YM, Costanzo M, Koch EN, Smith S, Myung K, Myers CL, Boone C, Bielinsky AK. Unligated okazaki fragments induce PCNA ubiquitination and a requirement for Rad59-dependent replication fork progression. *PLoS One.* 2013;8(6):e66379.
105. Ye X, Franco AA, Santos H, Nelson DM, Kaufman PD, Adams PD. Defective S phase chromatin assembly causes DNA damage, activation of the S phase checkpoint, and S phase arrest. *Mol Cell.* 2003;11(2):341-51.
106. Nagata S. Apoptotic DNA fragmentation. *Exp Cell Res.* 2000;256(1):12-8.
107. Zhou BB, Elledge SJ. The DNA damage response: putting checkpoints in perspective. *Nature.* 2000;408(6811):433-9.
108. Liu Q, Guntuku S, Cui XS, Matsuoka S, Cortez D, Tamai K, Luo G, Carattini-Rivera S, DeMayo F, Bradley A, Donehower LA, Elledge SJ. Chk1 is an essential kinase that is regulated by Atr and required for the G(2)/M DNA damage checkpoint. *Genes Dev.* 2000;14(12):1448-59.
109. Sanchez Y, Wong C, Thoma RS, Richman R, Wu Z, Piwnica-Worms H, Elledge SJ. Conservation of the Chk1 checkpoint pathway in mammals: linkage of DNA damage to Cdk regulation through Cdc25. *Science.* 1997;277(5331):1497-501.
110. Li F, Ambrosini G, Chu EY, Plescia J, Tognin S, Marchisio PC, Altieri DC. Control of apoptosis and mitotic spindle checkpoint by survivin. *Nature.* 1998;396(6711):580-4.

111. Musacchio A, Hardwick KG. The spindle checkpoint: structural insights into dynamic signalling. *Nat Rev Mol Cell Biol.* 2002;3(10):731-41.
112. Hauf S, Cole RW, LaTerra S, Zimmer C, Schnapp G, Walter R, Heckel A, van Meel J, Rieder CL, Peters JM. The small molecule Hesperadin reveals a role for Aurora B in correcting kinetochore-microtubule attachment and in maintaining the spindle assembly checkpoint. *J Cell Biol.* 2003;161(2):281-94.
113. Pucci B, Kasten M, Giordano A. Cell cycle and apoptosis. *Neoplasia.* 2000;2(4):291-9.
114. Frade JM, Ovejero-Benito MC. Neuronal cell cycle: the neuron itself and its circumstances. *Cell Cycle.* 2015;14(5):712-20.
115. Swiss VA, Casaccia P. Cell-context specific role of the E2F/Rb pathway in development and disease. *Glia.* 2010;58(4):377-90.
116. Cunningham JJ, Roussel MF. Cyclin-dependent kinase inhibitors in the development of the central nervous system. *Cell Growth Differ.* 2001;12(8):387-96.
117. Schwartz EI, Smilenov LB, Price MA, Osredkar T, Baker RA, Ghosh S, Shi FD, Vollmer TL, Lencinas A, Stearns DM, Gorospe M, Kruman, II. Cell cycle activation in postmitotic neurons is essential for DNA repair. *Cell Cycle.* 2007;6(3):318-29.
118. Herrup K, Yang Y. Cell cycle regulation in the postmitotic neuron: oxymoron or new biology? *Nat Rev Neurosci.* 2007;8(5):368-78.
119. van Leeuwen LA, Hoozemans JJ. Physiological and pathophysiological functions of cell cycle proteins in post-mitotic neurons: implications for Alzheimer's disease. *Acta Neuropathol.* 2015;129(4):511-25.
120. Sharma V, Collins LB, Chen TH, Herr N, Takeda S, Sun W, Swenberg JA, Nakamura J. Oxidative stress at low levels can induce clustered DNA lesions leading to NHEJ mediated mutations. *Oncotarget.* 2016;7(18):25377-90.
121. Hustedt N, Durocher D. The control of DNA repair by the cell cycle. *Nat Cell Biol.* 2017;19(1):1-9.
122. Narciso L, Parlanti E, Racaniello M, Simonelli V, Cardinale A, Merlo D, Dogliotti E. The response to oxidative DNA damage in neurons: Mechanisms and disease. *Neural Plast.* 2016;2016:3619274.
123. Casafont I, Palanca A, Lafarga V, Berciano MT, Lafarga M. Effect of ionizing radiation in sensory ganglion neurons: organization and dynamics of nuclear

compartments of DNA damage/repair and their relationship with transcription and cell cycle. *Acta Neuropathol.* 2011;122(4):481-93.

124. Khurana V, Merlo P, DuBoff B, Fulga TA, Sharp KA, Campbell SD, Gotz J, Feany MB. A neuroprotective role for the DNA damage checkpoint in tauopathy. *Aging Cell.* 2012;11(2):360-2.

125. Kruman, II, Wersto RP, Cardozo-Pelaez F, Smilenov L, Chan SL, Chrest FJ, Emokpae R, Jr., Gorospe M, Mattson MP. Cell cycle activation linked to neuronal cell death initiated by DNA damage. *Neuron.* 2004;41(4):549-61.

126. Fuchs E, Flugge G. Adult neuroplasticity: more than 40 years of research. *Neural Plast.* 2014;2014:541870.

127. Schmetsdorf S, Arnold E, Holzer M, Arendt T, Gartner U. A putative role for cell cycle-related proteins in microtubule-based neuroplasticity. *Eur J Neurosci.* 2009;29(6):1096-107.

128. Odajima J, Wills ZP, Ndassa YM, Terunuma M, Kretschmannova K, Deeb TZ, Geng Y, Gawrzak S, Quadros IM, Newman J, Das M, Jecrois ME, Yu Q, Li N, Bienvenu F, Moss SJ, Greenberg ME, Marto JA, Sicinski P. Cyclin E constrains Cdk5 activity to regulate synaptic plasticity and memory formation. *Dev Cell.* 2011;21(4):655-68.

129. Posada-Duque RA, Ramirez O, Hartel S, Inestrosa NC, Bodaleo F, Gonzalez-Billault C, Kirkwood A, Cardona-Gomez GP. CDK5 downregulation enhances synaptic plasticity. *Cell Mol Life Sci.* 2017;74(1):153-72.

130. Eriksson PS, Perfilieva E, Bjork-Eriksson T, Alborn AM, Nordborg C, Peterson DA, Gage FH. Neurogenesis in the adult human hippocampus. *Nat Med.* 1998;4(11):1313-7.

131. Ernst A, Alkass K, Bernard S, Salehpour M, Perl S, Tisdale J, Possnert G, Druid H, Frisen J. Neurogenesis in the striatum of the adult human brain. *Cell.* 2014;156(5):1072-83.

132. Patricio P, Mateus-Pinheiro A, Sousa N, Pinto L. Re-cycling paradigms: cell cycle regulation in adult hippocampal neurogenesis and implications for depression. *Mol Neurobiol.* 2013;48(1):84-96.

133. Spalding KL, Bergmann O, Alkass K, Bernard S, Salehpour M, Huttner HB, Bostrom E, Westerlund I, Vial C, Buchholz BA, Possnert G, Mash DC, Druid H, Frisen J. Dynamics of hippocampal neurogenesis in adult humans. *Cell.* 2013;153(6):1219-27.

134. Ribas V, Garcia-Ruiz C, Fernandez-Checa JC. Glutathione and mitochondria. *Front Pharmacol.* 2014;5:151.
135. Marchi S, Giorgi C, Suski JM, Agnoletto C, Bononi A, Bonora M, De Marchi E, Missiroli S, Patergnani S, Poletti F, Rimessi A, Duszynski J, Wieckowski MR, Pinton P. Mitochondria-ros crosstalk in the control of cell death and aging. *J Signal Transduct.* 2012;2012:329635.
136. Armstrong JS, Steinauer KK, Hornung B, Irish JM, Lecane P, Birrell GW, Peehl DM, Knox SJ. Role of glutathione depletion and reactive oxygen species generation in apoptotic signaling in a human B lymphoma cell line. *Cell Death Differ.* 2002;9(3):252-63.
137. Di Meo S, Reed TT, Venditti P, Victor VM. Role of ros and rns sources in physiological and pathological conditions. *Oxid Med Cell Longev.* 2016;2016:1245049.
138. Deavall DG, Martin EA, Horner JM, Roberts R. Drug-induced oxidative stress and toxicity. *J Toxicol.* 2012;2012:645460.
139. Kuter K, Nowak P, Golembiowska K, Ossowska K. Increased reactive oxygen species production in the brain after repeated low-dose pesticide paraquat exposure in rats. A comparison with peripheral tissues. *Neurochem Res.* 2010;35(8):1121-30.
140. Berlett BS, Stadtman ER. Protein oxidation in aging, disease, and oxidative stress. *J Biol Chem.* 1997;272(33):20313-6.
141. Itri R, Junqueira HC, Mertins O, Baptista MS. Membrane changes under oxidative stress: the impact of oxidized lipids. *Biophys Rev.* 2014;6(1):47-61.
142. Sinha K, Das J, Pal PB, Sil PC. Oxidative stress: the mitochondria-dependent and mitochondria-independent pathways of apoptosis. *Arch Toxicol.* 2013;87(7):1157-80.
143. Circu ML, Aw TY. Reactive oxygen species, cellular redox systems, and apoptosis. *Free Radic Biol Med.* 2010;48(6):749-62.
144. Kroemer G, Galluzzi L, Brenner C. Mitochondrial membrane permeabilization in cell death. *Physiol Rev.* 2007;87(1):99-163.
145. Weinbach EC. The effect of pentachlorophenol on oxidative phosphorylation. *J Biol Chem.* 1954;210(2):545-50.
146. Wang L, Azad N, Kongkaneramt L, Chen F, Lu Y, Jiang BH, Rojanasakul Y. The Fas death signaling pathway connecting reactive oxygen species generation and FLICE inhibitory protein down-regulation. *J Immunol.* 2008;180(5):3072-80.

147. Fiers W, Beyaert R, Declercq W, Vandenabeele P. More than one way to die: apoptosis, necrosis and reactive oxygen damage. *Oncogene*. 1999;18(54):7719-30.
148. Choi K, Kim J, Kim GW, Choi C. Oxidative stress-induced necrotic cell death via mitochondria-dependent burst of reactive oxygen species. *Curr Neurovasc Res*. 2009;6(4):213-22.
149. Klein JA, Ackerman SL. Oxidative stress, cell cycle, and neurodegeneration. *J Clin Invest*. 2003;111(6):785-93.
150. Mari M, Morales A, Colell A, Garcia-Ruiz C, Fernandez-Checa JC. Mitochondrial glutathione, a key survival antioxidant. *Antioxid Redox Signal*. 2009;11(11):2685-700.
151. Circu ML, Aw TY. Glutathione and modulation of cell apoptosis. *Biochim Biophys Acta*. 2012;1823(10):1767-77.
152. Lu SC. Regulation of glutathione synthesis. *Mol Aspects Med*. 2009;30(1-2):42-59.
153. Van Der Kloot W, Molgo J. Quantal acetylcholine release at the vertebrate neuromuscular junction. *Physiological reviews*. 1994;74(4):899-992.
154. Arvidsson U, Riedl M, Elde R, Meister B. Vesicular acetylcholine transporter (VAChT) protein: a novel and unique marker for cholinergic neurons in the central and peripheral nervous systems. *J Comp Neurol*. 1997;378(4):454-67.
155. Feldberg W. The role of acetylcholine in the central nervous system. *Br Med Bull*. 1950;6(4):312-21.
156. Colovic MB, Krstic DZ, Lazarevic-Pasti TD, Bondzic AM, Vasic VM. Acetylcholinesterase inhibitors: pharmacology and toxicology. *Curr Neuropharmacol*. 2013;11(3):315-35.
157. Ganesan K, Raza SK, Vijayaraghavan R. Chemical warfare agents. *J Pharm Bioallied Sci*. 2010;2(3):166-78.
158. Wiener SW, Hoffman RS. Nerve agents: a comprehensive review. *J Intensive Care Med*. 2004;19(1):22-37.
159. Jokanovic M. Medical treatment of acute poisoning with organophosphorus and carbamate pesticides. *Toxicol Lett*. 2009;190(2):107-15.
160. Dvir H, Silman I, Harel M, Rosenberry TL, Sussman JL. Acetylcholinesterase: from 3D structure to function. *Chem Biol Interact*. 2010;187(1-3):10-22.

161. Axelsen PH, Harel M, Silman I, Sussman JL. Structure and dynamics of the active site gorge of acetylcholinesterase: synergistic use of molecular dynamics simulation and X-ray crystallography. *Protein Sci.* 1994;3(2):188-97.
162. Bhagavan NV, Ha C-E. Chapter 6 - Enzymes and Enzyme Regulation. *Essentials of Medical Biochemistry*. San Diego: Academic Press; 2011. p. 47-58.
163. Galimberti D, Scarpini E. Old and new acetylcholinesterase inhibitors for Alzheimer's disease. *Expert Opin Investig Drugs.* 2016;25(10):1181-7.
164. Michaelis L, Menten ML, Johnson KA, Goody RS. The original Michaelis constant: translation of the 1913 Michaelis-Menten paper. *Biochemistry.* 2011;50(39):8264-9.
165. Engelking LR. Chapter 6 - Enzyme Kinetics. *Textbook of Veterinary Physiological Chemistry*. 3rd ed. Boston: Academic Press; 2015. p. 32-8.
166. Dougall IG, Unitt J. Chapter 2 - Evaluation of the Biological Activity of Compounds: Techniques and Mechanism of Action Studies. In: Aldous D, Raboisson P, Rognan D, editors. *The Practice of Medicinal Chemistry*. 4th ed. San Diego: Academic Press; 2015. p. 15-43.
167. Dudley JT, Butte AJ. *In silico* research in the era of cloud computing. *Nat Biotechnol.* 2010;28(11):1181-5.
168. Sanbonmatsu KY, Tung CS. High performance computing in biology: multimillion atom simulations of nanoscale systems. *J Struct Biol.* 2007;157(3):470-80.
169. Kitano H. Computational systems biology. *Nature.* 2002;420(6912):206-10.
170. Terstappen GC, Reggiani A. *In silico* research in drug discovery. *Trends Pharmacol Sci.* 2001;22(1):23-6.
171. Ekins S, Mestres J, Testa B. *In silico* pharmacology for drug discovery: applications to targets and beyond. *Br J Pharmacol.* 2007;152(1):21-37.
172. Raies AB, Bajic VB. *In silico* toxicology: computational methods for the prediction of chemical toxicity. *Wiley Interdiscip Rev Comput Mol Sci.* 2016;6(2):147-72.
173. Alves VM, Muratov EN, Capuzzi SJ, Politi R, Low Y, Braga RC, Zakharov AV, Sedykh A, Mokshyna E, Farag S, Andrade CH, Kuz'min VE, Fourches D, Tropsha A. Alarms about structural alerts. *Green Chemistry.* 2016;18(16):4348-60.
174. Benfenati E, Gini G. Computational predictive programs (expert systems) in toxicology. *Toxicology.* 1997;119(3):213-25.

175. Raunio H. *In silico* toxicology - non-testing methods. *Front Pharmacol.* 2011;2:33.
176. Rabinowitz JR, Goldsmith MR, Little SB, Pasquinelli MA. Computational molecular modeling for evaluating the toxicity of environmental chemicals: prioritizing bioassay requirements. *Environ Health Perspect.* 2008;116(5):573-7.
177. Cross JB, Thompson DC, Rai BK, Baber JC, Fan KY, Hu Y, Humblet C. Comparison of several molecular docking programs: pose prediction and virtual screening accuracy. *J Chem Inf Model.* 2009;49(6):1455-74.
178. Wang R, Lai L, Wang S. Further development and validation of empirical scoring functions for structure-based binding affinity prediction. *J Comput Aided Mol Des.* 2002;16(1):11-26.
179. Alder BJ, Wainwright TE. Studies in molecular dynamics. I. General method. *J Chem Phys.* 1959;31(2):459-66.
180. Liu K, Watanabe E, Kokubo H. Exploring the stability of ligand binding modes to proteins by molecular dynamics simulations. *J Comput Aided Mol Des.* 2017;31(2):201-11.
181. Karplus M, McCammon JA. Molecular dynamics simulations of biomolecules. *Nat Struct Biol.* 2002;9(9):646-52.
182. Selvaraj C, Sakkiah S, Tong W, Hong H. Molecular dynamics simulations and applications in computational toxicology and nanotoxicology. *Food Chem Toxicol.* 2017;Article in press.
183. Berendsen HJC, van der Spoel D, van Drunen R. GROMACS: a message-passing parallel molecular dynamics implementation. *Comput Phys Commun.* 1995;91(1-3):43-56.
184. Perez A, Marchan I, Svozil D, Sponer J, Cheatham TE, 3rd, Laughton CA, Orozco M. Refinement of the AMBER force field for nucleic acids: improving the description of alpha/gamma conformers. *Biophys J.* 2007;92(11):3817-29.
185. Payne MC, Teter MP, Allan DC, Arias TA, Joannopoulos JD. Iterative minimization techniques for ab initio total-energy calculations: molecular dynamics and conjugate gradients. *Rev Mod Phys.* 1992;64(4):1045.
186. Humphrey W, Dalke A, Schulten K. VMD: visual molecular dynamics. *J Mol Graph.* 1996;14(1):33-8, 27-8.
187. Vichai V, Kirtikara K. Sulforhodamine B colorimetric assay for cytotoxicity screening. *Nat Protoc.* 2006;1(3):1112-6.

188. Skehan P, Storeng R, Scudiero D, Monks A, McMahon J, Vistica D, Warren JT, Bokesch H, Kenney S, Boyd MR. New colorimetric cytotoxicity assay for anticancer-drug screening. *J Natl Cancer Inst.* 1990;82(13):1107-12.
189. Keepers YP, Pizao PE, Peters GJ, van Ark-Otte J, Winograd B, Pinedo HM. Comparison of the sulforhodamine B protein and tetrazolium (MTT) assays for *in vitro* chemosensitivity testing. *Eur J Cancer.* 1991;27(7):897-900.
190. Dalvie MA. DDT: Health Effects. Reference Module in Earth Systems and Environmental Sciences: Elsevier; 2013.
191. Kim JA, Aberg C, Salvati A, Dawson KA. Role of cell cycle on the cellular uptake and dilution of nanoparticles in a cell population. *Nat Nanotechnol.* 2011;7(1):62-8.
192. Rieger AM, Nelson KL, Konowalchuk JD, Barreda DR. Modified annexin V/propidium iodide apoptosis assay for accurate assessment of cell death. *J Vis Exp.* 2011(50).
193. Vermes I, Haanen C, Reutelingsperger C. Flow cytometry of apoptotic cell death. *J Immunol Methods.* 2000;243(1-2):167-90.
194. Porter AG, Janicke RU. Emerging roles of caspase-3 in apoptosis. *Cell Death Differ.* 1999;6(2):99-104.
195. Jänicke RU, Sprengart ML, Wati MR, Porter AG. Caspase-3 is required for DNA fragmentation and morphological changes associated with apoptosis. *Journal of Biological Chemistry.* 1998;273(16):9357-60.
196. Nicholson DW, Ali A, Thornberry NA, Vaillancourt JP, Ding CK, Gallant M, Gareau Y, Griffin PR, Labelle M, Lazebnik YA. Identification and inhibition of the ICE/CED-3 protease necessary for mammalian apoptosis. *Nature.* 1995;376(6535):37-43.
197. Garcia-Calvo M, Peterson EP, Rasper DM, Vaillancourt JP, Zamboni R, Nicholson DW, Thornberry NA. Purification and catalytic properties of human caspase family members. *Cell Death Differ.* 1999;6(4):362-9.
198. Belmokhtar CA, Hillion J, Ségal-Bendirdjian E. Staurosporine induces apoptosis through both caspase-dependent and caspase-independent mechanisms. *Oncogene.* 2001;20(26):3354-62.
199. Chazotte B. Labeling nuclear DNA with hoechst 33342. *Cold Spring Harb Protoc.* 2011;2011(1):pdb prot5557.

200. Robbins E, Marcus PI, Gonatas NK. Dynamics of acridine orange-cell interaction. II. Dye-induced ultrastructural changes in multivesicular bodies (acridine orange particles). *J Cell Biol.* 1964;21:49-62.
201. Foglieni C, Meoni C, Davalli AM. Fluorescent dyes for cell viability: an application on prefixed conditions. *Histochem Cell Biol.* 2001;115(3):223-9.
202. Orrenius S. Reactive oxygen species in mitochondria-mediated cell death. *Drug Metab Rev.* 2007;39(2-3):443-55.
203. Chen HM, Zhu BZ, Chen RJ, Wang BJ, Wang YJ. The pentachlorophenol metabolite tetrachlorohydroquinone induces massive ROS and prolonged p-ERK expression in splenocytes, leading to inhibition of apoptosis and necrotic cell death. *PLoS One.* 2014;9(2):e89483.
204. Kalyanaraman B, Darley-Usmar V, Davies KJ, Dennery PA, Forman HJ, Grisham MB, Mann GE, Moore K, Roberts LJ, 2nd, Ischiropoulos H. Measuring reactive oxygen and nitrogen species with fluorescent probes: challenges and limitations. *Free Radic Biol Med.* 2012;52(1):1-6.
205. Suski JM, Lebiezinska M, Bonora M, Pinton P, Duszynski J, Wieckowski MR. Relation between mitochondrial membrane potential and ROS formation. *Methods Mol Biol.* 2012;810:183-205.
206. Kamencic H, Lyon A, Paterson PG, Juurlink BH. Monochlorobimane fluorometric method to measure tissue glutathione. *Anal Biochem.* 2000;286(1):35-7.
207. Ellman GL, Courtney KD, Andres V, Jr., Feather-Stone RM. A new and rapid colorimetric determination of acetylcholinesterase activity. *Biochem Pharmacol.* 1961;7:88-95.
208. Badawy ME, El-Aswad AF. Bioactive paper sensor based on the acetylcholinesterase for the rapid detection of organophosphate and carbamate pesticides. *Int J Anal Chem.* 2014;2014:536823.
209. Sramek JJ, Frackiewicz EJ, Cutler NR. Review of the acetylcholinesterase inhibitor galanthamine. *Expert Opin Investig Drugs.* 2000;9(10):2393-402.
210. Santillo MF, Liu Y. A fluorescence assay for measuring acetylcholinesterase activity in rat blood and a human neuroblastoma cell line (SH-SY5Y). *J Pharmacol Toxicol Methods.* 2015;76:15-22.
211. ACD/ChemSketch, version C30E21, Advanced Chemistry Development, Inc., Toronto, ON, Canada, www.acdlabs.com, 2016.

212. Online SMILES Translator and Structure File Generator: National Cancer Institute; [updated 2017-10-16; cited 2018 24 January]. Available from: <https://cactus.nci.nih.gov/translate/>.
213. Pettersen EF, Goddard TD, Huang CC, Couch GS, Greenblatt DM, Meng EC, Ferrin TE. UCSF Chimera--a visualization system for exploratory research and analysis. *J Comput Chem*. 2004;25(13):1605-12.
214. Trott O, Olson AJ. AutoDock Vina: improving the speed and accuracy of docking with a new scoring function, efficient optimization, and multithreading. *J Comput Chem*. 2010;31(2):455-61.
215. Alhossary A, Handoko SD, Mu Y, Kwoh CK. Fast, accurate, and reliable molecular docking with QuickVina 2. *Bioinformatics*. 2015;31(13):2214-6.
216. Pronk S, Páll S, Schulz R, Larsson P, Bjelkmar P, Apostolov R, Shirts MR, Smith JC, Kasson PM, van der Spoel D. GROMACS 4.5: a high-throughput and highly parallel open source molecular simulation toolkit. *Bioinformatics*. 2013:btt055.
217. Lindorff-Larsen K, Piana S, Palmo K, Maragakis P, Klepeis JL, Dror RO, Shaw DE. Improved side-chain torsion potentials for the Amber ff99SB protein force field. *Proteins: Structure, Function, and Bioinformatics*. 2010;78(8):1950-8.
218. Nickolls J, Buck I, Garland M, Skadron K. Scalable parallel programming with CUDA. *Queue*. 2008;6(2):40-53.
219. da Silva AWS, Vranken WF. ACPYPE-Antechamber python parser interface. *BioMed Central research notes*. 2012;5(1):367.
220. Jämbeck JP, Lyubartsev AP. Update to the General Amber Force Field for small solutes with an emphasis on free energies of hydration. *The Journal of Physical Chemistry B*. 2014;118(14):3793-804.
221. Berendsen HJ, Postma JPM, van Gunsteren WF, DiNola A, Haak J. Molecular dynamics with coupling to an external bath. *The Journal of chemical physics*. 1984;81(8):3684-90.
222. Bussi G, Donadio D, Parrinello M. Canonical sampling through velocity rescaling. *The Journal of chemical physics*. 2007;126(1):014101.
223. Nosé S, Klein M. Constant pressure molecular dynamics for molecular systems. *Molecular Physics*. 1983;50(5):1055-76.
224. Darden T, York D, Pedersen L. Particle mesh Ewald: An $N \cdot \log(N)$ method for Ewald sums in large systems. *The Journal of chemical physics*. 1993;98(12):10089-92.

225. Hess B. P-LINCS: A parallel linear constraint solver for molecular simulation. *Journal of Chemical Theory and Computation*. 2008;4(1):116-22.
226. Kumari R, Kumar R, Lynn A. g_mmpbsa □ A GROMACS Tool for High-Throughput MM-PBSA Calculations. *Journal of chemical information and modeling*. 2014;54(7):1951-62.
227. Baker NA, Sept D, Joseph S, Holst MJ, McCammon JA. Electrostatics of nanosystems: application to microtubules and the ribosome. *Proceedings of the National Academy of Sciences*. 2001;98(18):10037-41.
228. Harel M, Schalk I, Ehret-Sabatier L, Bouet F, Goeldner M, Hirth C, Axelsen PH, Silman I, Sussman JL. Quaternary ligand binding to aromatic residues in the active-site gorge of acetylcholinesterase. *Proc Natl Acad Sci U S A*. 1993;90(19):9031-5.
229. Ravelli RB, Raves ML, Ren Z, Bourgeois D, Roth M, Kroon J, Silman I, Sussman JL. Static Laue diffraction studies on acetylcholinesterase. *Acta Crystallogr D Biol Crystallogr*. 1998;54(Pt 6 Pt 2):1359-66.
230. Millard CB, Kryger G, Ordentlich A, Greenblatt HM, Harel M, Raves ML, Segall Y, Barak D, Shafferman A, Silman I, Sussman JL. Crystal structures of aged phosphonylated acetylcholinesterase: nerve agent reaction products at the atomic level. *Biochemistry*. 1999;38(22):7032-9.
231. Harel M, Quinn DM, Nair HK, Silman I, Sussman JL. The X-ray structure of a transition state analog complex reveals the molecular origins of the catalytic power and substrate specificity of acetylcholinesterase. *JAmChemSoc*. 1996;118:2340-6.
232. Felder CE, Harel M, Silman I, Sussman JL. Structure of a complex of the potent and specific inhibitor BW284C51 with *Torpedo californica* acetylcholinesterase. *Acta Crystallogr D Biol Crystallogr*. 2002;58(Pt 10 Pt 2):1765-71.
233. Dvir H, Wong DM, Harel M, Barril X, Orozco M, Luque FJ, Munoz-Torrero D, Camps P, Rosenberry TL, Silman I, Sussman JL. 3D structure of *Torpedo californica* acetylcholinesterase complexed with huprine X at 2.1 Å resolution: kinetic and molecular dynamic correlates. *Biochemistry*. 2002;41(9):2970-81.
234. Kryger G, Silman I, Sussman JL. Structure of acetylcholinesterase complexed with E2020 (Aricept): implications for the design of new anti-Alzheimer drugs. *Structure*. 1999;7(3):297-307.

235. Dvir H, Jiang HL, Wong DM, Harel M, Chetrit M, He XC, Jin GY, Yu GL, Tang XC, Silman I, Bai DL, Sussman JL. X-ray structures of *Torpedo californica* acetylcholinesterase complexed with (+)-huperzine A and (-)-huperzine B: structural evidence for an active site rearrangement. *Biochemistry*. 2002;41(35):10810-8.
236. Harel M, Kleywegt GJ, Ravelli RB, Silman I, Sussman JL. Crystal structure of an acetylcholinesterase-fasciculin complex: interaction of a three-fingered toxin from snake venom with its target. *Structure*. 1995;3(12):1355-66.
237. Bar-On P, Millard CB, Harel M, Dvir H, Enz A, Sussman JL, Silman I. Kinetic and structural studies on the interaction of cholinesterases with the anti-Alzheimer drug rivastigmine. *Biochemistry*. 2002;41(11):3555-64.
238. Wong DM, Greenblatt HM, Dvir H, Carlier PR, Han YF, Pang YP, Silman I, Sussman JL. Acetylcholinesterase complexed with bivalent ligands related to huperzine a: experimental evidence for species-dependent protein-ligand complementarity. *J Am Chem Soc*. 2003;125(2):363-73.
239. Doucet-Personeni C, Bentley PD, Fletcher RJ, Kinkaid A, Kryger G, Pirard B, Taylor A, Taylor R, Taylor J, Viner R, Silman I, Sussman JL, Greenblatt HM, Lewis T. A structure-based design approach to the development of novel, reversible AChE inhibitors. *J Med Chem*. 2001;44(20):3203-15.
240. Rydberg EH, Brumshtein B, Greenblatt HM, Wong DM, Shaya D, Williams LD, Carlier PR, Pang YP, Silman I, Sussman JL. Complexes of alkylene-linked tacrine dimers with *Torpedo californica* acetylcholinesterase: Binding of Bis5-tacrine produces a dramatic rearrangement in the active-site gorge. *J Med Chem*. 2006;49(18):5491-500.
241. Bartolucci C, Perola E, Pilger C, Fels G, Lamba D. Three-dimensional structure of a complex of galanthamine (Nivalin) with acetylcholinesterase from *Torpedo californica*: implications for the design of new anti-Alzheimer drugs. *Proteins*. 2001;42(2):182-91.
242. Harel M, Hyatt JL, Brumshtein B, Morton CL, Yoon KJ, Wadkins RM, Silman I, Sussman JL, Potter PM. The crystal structure of the complex of the anticancer prodrug 7-ethyl-10-[4-(1-piperidino)-1-piperidino]-carbonyloxycamptothecin (CPT-11) with *Torpedo californica* acetylcholinesterase provides a molecular explanation for its cholinergic action. *Mol Pharmacol*. 2005;67(6):1874-81.

243. Raves ML, Harel M, Pang YP, Silman I, Kozikowski AP, Sussman JL. Structure of acetylcholinesterase complexed with the nootropic alkaloid, (-)-huperzine A. *Nat Struct Biol.* 1997;4(1):57-63.
244. Greenblatt HM, Guillou C, Guenard D, Argaman A, Botti S, Badet B, Thal C, Silman I, Sussman JL. The complex of a bivalent derivative of galanthamine with torpedo acetylcholinesterase displays drastic deformation of the active-site gorge: implications for structure-based drug design. *J Am Chem Soc.* 2004;126(47):15405-11.
245. Haviv H, Wong DM, Greenblatt HM, Carlier PR, Pang YP, Silman I, Sussman JL. Crystal packing mediates enantioselective ligand recognition at the peripheral site of acetylcholinesterase. *J Am Chem Soc.* 2005;127(31):11029-36.
246. Colletier JP, Sanson B, Nachon F, Gabellieri E, Fattorusso C, Campiani G, Weik M. Conformational flexibility in the peripheral site of *Torpedo californica* acetylcholinesterase revealed by the complex structure with a bifunctional inhibitor. *J Am Chem Soc.* 2006;128(14):4526-7.
247. Harel M, Sonoda LK, Silman I, Sussman JL, Rosenberry TL. Crystal structure of thioflavin T bound to the peripheral site of *Torpedo californica* acetylcholinesterase reveals how thioflavin T acts as a sensitive fluorescent reporter of ligand binding to the acylation site. *J Am Chem Soc.* 2008;130(25):7856-61.
248. Colletier JP, Royant A, Specht A, Sanson B, Nachon F, Masson P, Zaccai G, Sussman JL, Goeldner M, Silman I, Bourgeois D, Weik M. Use of a 'caged' analogue to study the traffic of choline within acetylcholinesterase by kinetic crystallography. *Acta Crystallogr D Biol Crystallogr.* 2007;63(Pt 11):1115-28.
249. Sanson B, Colletier JP, Xu Y, Lang PT, Jiang H, Silman I, Sussman JL, Weik M. Backdoor opening mechanism in acetylcholinesterase based on X-ray crystallography and molecular dynamics simulations. *Protein Sci.* 2011;20(7):1114-8.
250. Bartolucci C, Haller LA, Jordis U, Fels G, Lamba D. Probing *Torpedo californica* acetylcholinesterase catalytic gorge with two novel bis-functional galanthamine derivatives. *J Med Chem.* 2010;53(2):745-51.
251. Nepovimova E, Uliassi E, Korabecny J, Pena-Altamira LE, Samez S, Pesaresi A, Garcia GE, Bartolini M, Andrisano V, Bergamini C, Fato R, Lamba D, Roberti M, Kuca K, Monti B, Bolognesi ML. Multitarget drug design strategy: quinone-tacrine hybrids designed to block amyloid-beta aggregation and to exert anticholinesterase and antioxidant effects. *J Med Chem.* 2014;57(20):8576-89.

252. Pesaresi A, Samez S, Lamba D. Torpedo californica acetylcholinesterase in complex with a tacrine-benzofuran hybrid inhibitor. [To be published]. DOI: 10.2210/pdb4w63/pdb.
253. Pesaresi A, Lamba D. Torpedo californica acetylcholinesterase in complex with a tacrine-nicotinamide hybrid inhibitor. [To be published]. DOI: 10.2210/pdb4x3c/pdb.
254. Legler PM, Soojhawon I, Millard CB. A conformational change in the peripheral anionic site of Torpedo californica acetylcholinesterase induced by a bis-imidazolium oxime. *Acta Crystallogr D Biol Crystallogr*. 2015;71(Pt 9):1788-98.
255. Dym O, Song W, Felder C, Roth E, Shnyrov V, Ashani Y, Xu Y, Joosten RP, Weiner L, Sussman JL, Silman I. The impact of crystallization conditions on structure-based drug design: A case study on the methylene blue/acetylcholinesterase complex. *Protein Sci*. 2016;25(6):1096-114.
256. Pesaresi A, Lamba D. Torpedo californica acetylcholinesterase inhibited with msf. [To be published]. DOI: 10.2210/pdb5ehx/pdb.
257. Pesaresi A, Lamba D. Msf-aged torpedo californica acetylcholinesterase in complex with bistacrine. [To be published]. DOI: 10.2210/pdb5ei5/pdb.
258. Pesaresi A, Lamba D. Acetylcholinesterase of Torpedo californica in complex with the N-methyl-indoxylacetate hydrolysis products. [To be published]. DOI: 10.2210/pdb5ih7/pdb.
259. Parkinson A, Ogilvie BW. Chapter 6. Biotransformation of Xenobiotics In: Klaassen CD, Watkins JBI, editors. *Casarett & Doull's Essentials of Toxicology: The Basic Science of Poisons*. 2nd ed. New York: McGraw-Hill; 2001. p. 133-224.
260. Tang Y, Donnelly KC, Tiffany-Castiglioni E, Mumtaz MM. Neurotoxicity of polycyclic aromatic hydrocarbons and simple chemical mixtures. *J Toxicol Environ Health A*. 2003;66(10):919-40.
261. Wang YJ, Lee CC, Chang WC, Liou HB, Ho YS. Oxidative stress and liver toxicity in rats and human hepatoma cell line induced by pentachlorophenol and its major metabolite tetrachlorohydroquinone. *Toxicol Lett*. 2001;122(2):157-69.
262. Wispriyono B, Matsuoka M, Igisu H. Effects of pentachlorophenol and tetrachlorohydroquinone on mitogen-activated protein kinase pathways in Jurkat T cells. *Environ Health Perspect*. 2002;110(2):139-43.
263. Tanaka M, Ishizaka Y, Tosuji H, Kunimoto M, Hosoya N, Nishihara N, Kadono T, Kawano T, Kosaka T, Hosoya H. A new bioassay for toxic chemicals using green

- Paramecia, *Paramecium bursaria*. In: Lichtfouse E, Schwarzbauer J, Robert D, editors. Environmental Chemistry: Green Chemistry and Pollutants in Ecosystems. Berlin: Springer Science & Business Media; 2005. p. 676.
264. Fu J, Xia X, Liu Z, Wang Y, Wang Y, Shi Q, Song X, Song E, Song Y. The acute exposure of tetrachloro-p-benzoquinone (a.k.a. chloranil) triggers inflammation and neurological dysfunction via Toll-like receptor 4 signaling: The protective role of melatonin preconditioning. *Toxicology*. 2017;381:39-50.
265. Li C, Wang F, Wang H. Tetrachloro-1,4-benzoquinone induces apoptosis of mouse embryonic stem cells. *J Environ Sci (China)*. 2017;51:5-12.
266. Whitcomb EA, Dudek EJ, Liu Q, Taylor A. Novel control of S phase of the cell cycle by ubiquitin-conjugating enzyme H7. *Mol Biol Cell*. 2009;20(1):1-9.
267. Nakayama Y, Yamaguchi N. Multi-lobulation of the nucleus in prolonged S phase by nuclear expression of Chk tyrosine kinase. *Exp Cell Res*. 2005;304(2):570-81.
268. Cuddihy AR, O'Connell MJ. Cell-cycle responses to DNA damage in G2. *Int Rev Cytol*. 2003;222:99-140.
269. Bortner CD, Oldenburg NB, Cidlowski JA. The role of DNA fragmentation in apoptosis. *Trends Cell Biol*. 1995;5(1):21-6.
270. Higuchi Y. Chromosomal DNA fragmentation in apoptosis and necrosis induced by oxidative stress. *Biochem Pharmacol*. 2003;66(8):1527-35.
271. Warnes G. DNA fragmentation. London: Institute of Cell and Molecular Science, Queen Mary, University of London 2007 [updated 2016; cited 2017 29 December]. Available from: <http://www.icms.qmul.ac.uk/flowcytometry/uses/apoptosis/dnafragmentation/>.
272. Camps J, Wangsa D, Falke M, Brown M, Case CM, Erdos MR, Ried T. Loss of lamin B1 results in prolongation of S phase and decondensation of chromosome territories. *FASEB J*. 2014;28(8):3423-34.
273. Ma Y, Kanakousaki K, Buttitta L. How the cell cycle impacts chromatin architecture and influences cell fate. *Front Genet*. 2015;6:19.
274. Borel F, Lacroix FB, Margolis RL. Prolonged arrest of mammalian cells at the G1/S boundary results in permanent S phase stasis. *J Cell Sci*. 2002;115(Pt 14):2829-38.
275. Lobrich M, Jeggo PA. The impact of a negligent G2/M checkpoint on genomic instability and cancer induction. *Nat Rev Cancer*. 2007;7(11):861-9.

276. Gomez V, Hergovich A. Chapter 14 - Cell-Cycle Control and DNA-Damage Signaling in Mammals A2 - Kovalchuk, Igor. In: Kovalchuk O, editor. *Genome Stability*. Boston: Academic Press; 2016. p. 227-42.
277. Marechal A, Zou L. DNA damage sensing by the ATM and ATR kinases. *Cold Spring Harb Perspect Biol*. 2013;5(9):a012716.
278. Chow JP, Poon RY, Ma HT. Inhibitory phosphorylation of cyclin-dependent kinase 1 as a compensatory mechanism for mitosis exit. *Mol Cell Biol*. 2011;31(7):1478-91.
279. Xiong Y, Hannon GJ, Zhang H, Casso D, Kobayashi R, Beach D. p21 is a universal inhibitor of cyclin kinases. *Nature*. 1993;366(6456):701-4.
280. Hermeking H, Lengauer C, Polyak K, He TC, Zhang L, Thiagalingam S, Kinzler KW, Vogelstein B. 14-3-3sigma is a p53-regulated inhibitor of G2/M progression. *Mol Cell*. 1997;1(1):3-11.
281. Jin S, Antinore MJ, Lung FD, Dong X, Zhao H, Fan F, Colchagie AB, Blanck P, Roller PP, Fornace AJ, Jr., Zhan Q. The GADD45 inhibition of Cdc2 kinase correlates with GADD45-mediated growth suppression. *J Biol Chem*. 2000;275(22):16602-8.
282. Lolli G, Johnson LN. CAK-Cyclin-dependent Activating Kinase: a key kinase in cell cycle control and a target for drugs? *Cell Cycle*. 2005;4(4):572-7.
283. DiPaola RS. To arrest or not to g-m cell-cycle arrest. *Clinical Cancer Research*. 2002;8(11):3311.
284. Zeng X, Sigoillot F, Gaur S, Choi S, Pfaff KL, Oh DC, Hathaway N, Dimova N, Cuny GD, King RW. Pharmacologic inhibition of the anaphase-promoting complex induces a spindle checkpoint-dependent mitotic arrest in the absence of spindle damage. *Cancer Cell*. 2010;18(4):382-95.
285. Orth JD, Loewer A, Lahav G, Mitchison TJ. Prolonged mitotic arrest triggers partial activation of apoptosis, resulting in DNA damage and p53 induction. *Mol Biol Cell*. 2012;23(4):567-76.
286. Levine AJ. p53, the cellular gatekeeper for growth and division. *Cell*. 1997;88(3):323-31.
287. Abukhdeir AM, Park BH. P21 and p27: roles in carcinogenesis and drug resistance. *Expert Rev Mol Med*. 2008;10:e19.
288. Owen-Schaub LB, Zhang W, Cusack JC, Angelo LS, Santee SM, Fujiwara T, Roth JA, Deisseroth AB, Zhang WW, Kruzel E. Wild-type human p53 and a

temperature-sensitive mutant induce Fas/APO-1 expression. *Mol Cell Biol.* 1995;15(6):3032-40.

289. Guan B, Yue P, Clayman GL, Sun SY. Evidence that the death receptor DR4 is a DNA damage-inducible, p53-regulated gene. *J Cell Physiol.* 2001;188(1):98-105.

290. Hoeflerlin LA, Oleinik NV, Krupenko NI, Krupenko SA. Activation of p21-dependent G1/G2 Arrest in the absence of DNA damage as an antiapoptotic response to metabolic stress. *Genes Cancer.* 2011;2(9):889-99.

291. Yang S, Han X, Wei C, Chen J, Yin D. The toxic effects of pentachlorophenol on rat Sertoli cells *in vitro*. *Environ Toxicol Pharmacol.* 2005;20(1):182-7.

292. Diaz Vivancos P, Wolff T, Markovic J, Pallardo FV, Foyer CH. A nuclear glutathione cycle within the cell cycle. *Biochem J.* 2010;431(2):169-78.

293. Boonstra J, Post JA. Molecular events associated with reactive oxygen species and cell cycle progression in mammalian cells. *Gene.* 2004;337:1-13.

294. Upper D. The unsuccessful self-treatment of a case of "writer's block". *J Appl Behav Anal.* 1974;7(3):497.

295. Enari M, Sakahira H, Yokoyama H, Okawa K, Iwamatsu A, Nagata S. A caspase-activated DNase that degrades DNA during apoptosis, and its inhibitor ICAD. *Nature.* 1998;391(6662):43-50.

296. Schaefer S, Kreutzer JN, Issinger OG, Guerra B. Cytotoxic effects exerted by pentachlorophenol by targeting nodal pro-survival signaling pathways in human pancreatic cancer cells. *Toxicol Rep.* 2014;1:1162-74.

297. Chen J, Jiang J, Zhang F, Yu H, Zhang J. Cytotoxic effects of environmentally relevant chlorophenols on L929 cells and their mechanisms. *Cell Biol Toxicol.* 2004;20(3):183-96.

298. Dong YL, Zhou PJ, Jiang SY, Pan XW, Zhao XH. Induction of oxidative stress and apoptosis by pentachlorophenol in primary cultures of *Carassius carassius* hepatocytes. *Comp Biochem Physiol C Toxicol Pharmacol.* 2009;150(2):179-85.

299. Michalowicz J. Pentachlorophenol and its derivatives induce oxidative damage and morphological changes in human lymphocytes (*in vitro*). *Arch Toxicol.* 2010;84(5):379-87.

300. Wang YJ, Ho YS, Jeng JH, Su HJ, Lee CC. Different cell death mechanisms and gene expression in human cells induced by pentachlorophenol and its major metabolite, tetrachlorohydroquinone. *Chem Biol Interact.* 2000;128(3):173-88.

301. Kim D, Tsai LH. Linking cell cycle reentry and DNA damage in neurodegeneration. *Ann N Y Acad Sci.* 2009;1170:674-9.
302. Bonda DJ, Lee HP, Kudo W, Zhu X, Smith MA, Lee HG. Pathological implications of cell cycle re-entry in Alzheimer disease. *Expert Rev Mol Med.* 2010;12:e19.
303. Moh C, Kubiak JZ, Bajic VP, Zhu X, Smith MA, Lee HG. Cell cycle deregulation in the neurons of Alzheimer's disease. *Results Probl Cell Differ.* 2011;53:565-76.
304. Yan D, Zhang Y, Liu L, Yan H. Pesticide exposure and risk of Alzheimer's disease: a systematic review and meta-analysis. *Sci Rep.* 2016;6:32222.
305. Grumezescu AM. *New Pesticides and Soil Sensors.* Cambridge, Massachusetts: Academic Press, Elsevier; 2017. 792 p.
306. Nikolettou V, Markaki M, Palikaras K, Tavernarakis N. Crosstalk between apoptosis, necrosis and autophagy. *Biochim Biophys Acta.* 2013;1833(12):3448-59.
307. Abraham MC, Shaham S. Death without caspases, caspases without death. *Trends Cell Biol.* 2004;14(4):184-93.
308. Yuan J, Najafov A, Py BF. Roles of caspases in necrotic cell death. *Cell.* 2016;167(7):1693-704.
309. Luyet C, Schulze K, Sayar BS, Howald D, Muller EJ, Galichet A. Preclinical studies identify non-apoptotic low-level caspase-3 as therapeutic target in pemphigus vulgaris. *PLoS One.* 2015;10(3):e0119809.
310. Kushnareva Y, Newmeyer DD. Bioenergetics and cell death. *Ann N Y Acad Sci.* 2010;1201:50-7.
311. Skulachev VP. Bioenergetic aspects of apoptosis, necrosis and mitoptosis. *Apoptosis.* 2006;11(4):473-85.
312. Nicotera P, Melino G. Regulation of the apoptosis-necrosis switch. *Oncogene.* 2004;23(16):2757-65.
313. Racke MM, Mosior M, Kovacevic S, Chang CH, Glasebrook AL, Roehm NW, Na S. Activation of caspase-3 alone is insufficient for apoptotic morphological changes in human neuroblastoma cells. *J Neurochem.* 2002;80(6):1039-48.
314. Ricci JE, Munoz-Pinedo C, Fitzgerald P, Bailly-Maitre B, Perkins GA, Yadava N, Scheffler IE, Ellisman MH, Green DR. Disruption of mitochondrial function during apoptosis is mediated by caspase cleavage of the p75 subunit of complex I of the electron transport chain. *Cell.* 2004;117(6):773-86.

315. Ricci JE, Gottlieb RA, Green DR. Caspase-mediated loss of mitochondrial function and generation of reactive oxygen species during apoptosis. *J Cell Biol.* 2003;160(1):65-75.
316. Los M, Mozoluk M, Ferrari D, Stepczynska A, Stroh C, Renz A, Herceg Z, Wang ZQ, Schulze-Osthoff K. Activation and caspase-mediated inhibition of PARP: a molecular switch between fibroblast necrosis and apoptosis in death receptor signaling. *Mol Biol Cell.* 2002;13(3):978-88.
317. Fernandez Freire P, Labrador V, Perez Martin JM, Hazen MJ. Cytotoxic effects in mammalian Vero cells exposed to pentachlorophenol. *Toxicology.* 2005;210(1):37-44.
318. Villena F, Montoya G, Klaasen R, Fleckenstein R, Suwalsky M. Morphological changes on nerves and histopathological effects on liver and kidney of rats by pentachlorophenol (PCP). *Comp Biochem Physiol C.* 1992;101(2):353-63.
319. Umemura T, Kuroiwa Y, Kitamura Y, Ishii Y, Kanki K, Kodama Y, Itoh K, Yamamoto M, Nishikawa A, Hirose M. A crucial role of Nrf2 in *in vivo* defense against oxidative damage by an environmental pollutant, pentachlorophenol. *Toxicol Sci.* 2006;90(1):111-9.
320. Hu L, Su C, Song X, Shi Q, Fu J, Xia X, Xu D, Song E, Song Y. Tetrachlorobenzoquinone triggers the cleavage of Bid and promotes the cross-talk of extrinsic and intrinsic apoptotic signalings in pheochromocytoma (PC) 12 cells. *Neurotoxicology.* 2015;49:149-57.
321. Liu Z, Shi Q, Song X, Wang Y, Wang Y, Song E, Song Y. Activating transcription factor 4 (ATF4)-ATF3-C/EBP homologous protein (CHOP) cascade shows an essential role in the ER stress-induced sensitization of tetrachlorobenzoquinone-challenged PC12 cells to ROS-mediated apoptosis via death receptor 5 (DR5) signaling. *Chem Res Toxicol.* 2016;29(9):1510-8.
322. Liu Z, Wang Y, Wang Y, Dong W, Xia X, Song E, Song Y. Effect of subcellular translocation of protein disulfide isomerase on tetrachlorobenzoquinone-induced signaling shift from endoplasmic reticulum stress to apoptosis. *Chem Res Toxicol.* 2017;30(10):1804-14.
323. Fu J, Shi Q, Song X, Xia X, Su C, Liu Z, Song E, Song Y. Tetrachlorobenzoquinone exhibits neurotoxicity by inducing inflammatory responses through ROS-mediated IKK/IkappaB/NF-kappaB signaling. *Environ Toxicol Pharmacol.* 2016;41:241-50.

324. Albenzi BC, Mattson MP. Evidence for the involvement of TNF and NF-kappaB in hippocampal synaptic plasticity. *Synapse*. 2000;35(2):151-9.
325. Ling B, Gao B, Yang J. Evaluating the effects of tetrachloro-1,4-benzoquinone, an active metabolite of pentachlorophenol, on the growth of human breast cancer cells. *J Toxicol*. 2016;2016:8253726.
326. Eroglu M, Derry WB. Your neighbours matter - non-autonomous control of apoptosis in development and disease. *Cell Death Differ*. 2016;23(7):1110-8.
327. Erwig LP, Henson PM. Clearance of apoptotic cells by phagocytes. *Cell Death Differ*. 2008;15(2):243-50.
328. Chambard JC, Lefloch R, Pouyssegur J, Lenormand P. ERK implication in cell cycle regulation. *Biochim Biophys Acta*. 2007;1773(8):1299-310.
329. Weaver AN, Yang ES. Beyond DNA repair: Additional functions of PARP-1 in cancer. *Front Oncol*. 2013;3:290.
330. Yuan K, Sun Y, Zhou T, McDonald J, Chen Y. PARP-1 regulates resistance of pancreatic cancer to TRAIL therapy. *Clin Cancer Res*. 2013;19(17):4750-9.
331. Zorov DB, Juhaszova M, Sollott SJ. Mitochondrial reactive oxygen species (ROS) and ROS-induced ROS release. *Physiol Rev*. 2014;94(3):909-50.
332. Jastroch M, Divakaruni AS, Mookerjee S, Treberg JR, Brand MD. Mitochondrial proton and electron leaks. *Essays Biochem*. 2010;47:53-67.
333. Kadenbach B. Intrinsic and extrinsic uncoupling of oxidative phosphorylation. *Biochim Biophys Acta*. 2003;1604(2):77-94.
334. Guicciardi ME, Gores GJ. Complete lysosomal disruption: a route to necrosis, not to the inflammasome. *Cell Cycle*. 2013;12(13):1995.
335. Ruprecht J, Yankovskaya V, Maklashina E, Iwata S, Cecchini G. Structure of *Escherichia coli* succinate:quinone oxidoreductase with an occupied and empty quinone-binding site. *J Biol Chem*. 2009;284(43):29836-46.
336. Zhou Q, Zhai Y, Lou J, Liu M, Pang X, Sun F. Thiabendazole inhibits ubiquinone reduction activity of mitochondrial respiratory complex II via a water molecule mediated binding feature. *Protein Cell*. 2011;2(7):531-42.
337. Nnodu U, Whalen MM. Pentachlorophenol decreases ATP levels in human natural killer cells. *J Appl Toxicol*. 2008;28(8):1016-20.
338. Chen HM, Lee YH, Wang YJ. ROS-triggered signaling pathways involved in the cytotoxicity and tumor promotion effects of pentachlorophenol and tetrachlorohydroquinone. *Chem Res Toxicol*. 2015;28(3):339-50.

339. Gravance CG, Garner DL, Miller MG, Berger T. Flow cytometric assessment of changes in rat sperm mitochondrial function after treatment with pentachlorophenol. *Toxicol In Vitro*. 2003;17(3):253-7.
340. Afonso V, Champy R, Mitrovic D, Collin P, Lomri A. Reactive oxygen species and superoxide dismutases: role in joint diseases. *Joint Bone Spine*. 2007;74(4):324-9.
341. Keyer K, Gort AS, Imlay JA. Superoxide and the production of oxidative DNA damage. *J Bacteriol*. 1995;177(23):6782-90.
342. Pietsch C, Hollender J, Dorusch F, Burkhardt-Holm P. Cytotoxic effects of pentachlorophenol (PCP) and its metabolite tetrachlorohydroquinone (TCHQ) on liver cells are modulated by antioxidants. *Cell Biol Toxicol*. 2014;30(4):233-52.
343. Jiang P, Wang J, Zhang J, Dai J. Effects of pentachlorophenol on the detoxification system in white-rumped munia (*Lonchura striata*). *J Environ Sci (China)*. 2016;44:224-34.
344. Meyer AJ. The integration of glutathione homeostasis and redox signaling. *J Plant Physiol*. 2008;165(13):1390-403.
345. Lu JM, Lin PH, Yao Q, Chen C. Chemical and molecular mechanisms of antioxidants: experimental approaches and model systems. *J Cell Mol Med*. 2010;14(4):840-60.
346. Jiang P, Wang J, Sheng N, Wei D, Dai J. Effects of pentachlorophenol on the quail (*Coturnix japonica*) liver detoxification pathway. *Chemosphere*. 2017;177:44-50.
347. Poot M, Teubert H, Rabinovitch PS, Kavanagh TJ. De novo synthesis of glutathione is required for both entry into and progression through the cell cycle. *J Cell Physiol*. 1995;163(3):555-60.
348. Havens CG, Ho A, Yoshioka N, Dowdy SF. Regulation of late G1/S phase transition and APC Cdh1 by reactive oxygen species. *Mol Cell Biol*. 2006;26(12):4701-11.
349. Su C, Shi Q, Song X, Fu J, Liu Z, Wang Y, Wang Y, Xia X, Song E, Song Y. Tetrachlorobenzoquinone induces Nrf2 activation via rapid Bach1 nuclear export/ubiquitination and JNK-P62 signaling. *Toxicology*. 2016;363-364:48-57.
350. Ma Q. Role of nrf2 in oxidative stress and toxicity. *Annu Rev Pharmacol Toxicol*. 2013;53:401-26.
351. Sunaga D, Tanno M, Kuno A, Ishikawa S, Ogasawara M, Yano T, Miki T, Miura T. Accelerated recovery of mitochondrial membrane potential by GSK-3beta

inactivation affords cardiomyocytes protection from oxidant-induced necrosis. *PLoS One*. 2014;9(11):e112529.

352. Lin YP, Zhu BZ, Yang MC, Frei B, Pan MH, Lin JK, Wang YJ. Bcl-2 overexpression inhibits tetrachlorohydroquinone-induced apoptosis in NIH3T3 cells: a possible mechanism for tumor promotion. *Mol Carcinog*. 2004;40(1):24-33.

353. Traverso N, Ricciarelli R, Nitti M, Marengo B, Furfaro AL, Pronzato MA, Marinari UM, Domenicotti C. Role of glutathione in cancer progression and chemoresistance. *Oxid Med Cell Longev*. 2013;2013:972913.

354. Zhang H, Limphong P, Pieper J, Liu Q, Rodesch CK, Christians E, Benjamin IJ. Glutathione-dependent reductive stress triggers mitochondrial oxidation and cytotoxicity. *FASEB J*. 2012;26(4):1442-51.

355. Lemasters JJ, Nieminen AL. Mitochondrial oxygen radical formation during reductive and oxidative stress to intact hepatocytes. *Biosci Rep*. 1997;17(3):281-91.

356. Lu SC. Glutathione synthesis. *Biochim Biophys Acta*. 2013;1830(5):3143-53.

357. Korge P, Calmettes G, Weiss JN. Increased reactive oxygen species production during reductive stress: The roles of mitochondrial glutathione and thioredoxin reductases. *Biochim Biophys Acta*. 2015;1847(6-7):514-25.

358. Pervaiz S, Clement MV. Hydrogen peroxide-induced apoptosis: oxidative or reductive stress? *Methods Enzymol*. 2002;352:150-9.

359. Green RM, Graham M, O'Donovan MR, Chipman JK, Hodges NJ. Subcellular compartmentalization of glutathione: correlations with parameters of oxidative stress related to genotoxicity. *Mutagenesis*. 2006;21(6):383-90.

360. Circu ML, Aw TY. Glutathione and apoptosis. *Free Radic Res*. 2008;42(8):689-706.

361. Kumar A, Darreh-Shori T. DMSO: A mixed-competitive inhibitor of human acetylcholinesterase. *ACS Chem Neurosci*. 2017;8(12):2618-25.

362. Groner E, Ashani Y, Schorer-Apelbaum D, Sterling J, Herzig Y, Weinstock M. The kinetics of inhibition of human acetylcholinesterase and butyrylcholinesterase by two series of novel carbamates. *Mol Pharmacol*. 2007;71(6):1610-7.

363. Lotti M, Moretto A. Promotion of organophosphate induced delayed polyneuropathy by certain esterase inhibitors. *Chem Biol Interact*. 1999;119-120:519-24.

364. Parron T, Requena M, Hernandez AF, Alarcon R. Association between environmental exposure to pesticides and neurodegenerative diseases. *Toxicol Appl Pharmacol.* 2011;256(3):379-85.
365. Pentachlorophenyl acetate: Pubchem; [cited 2017 25 October]. Compound Summary for CID 15041]. Available from: https://pubchem.ncbi.nlm.nih.gov/compound/pentachlorophenyl_acetate#section=To p.
366. Acheson SA, Quinn DM. Anatomy of acetylcholinesterase catalysis: reaction dynamics analogy for human erythrocyte and electric eel enzymes. *Biochim Biophys Acta.* 1990;1040(2):199-205.
367. Sussman JL, Harel M, Frolow F, Oefner C, Goldman A, Toker L, Silman I. Atomic structure of acetylcholinesterase from *Torpedo californica*: a prototypic acetylcholine-binding protein. *Science.* 1991;253(5022):872-9.
368. Igisu H, Hamasaki N, Ikeda M. Highly cooperative inhibition of acetylcholinesterase by pentachlorophenol in human erythrocytes. *Biochem Pharmacol.* 1993;46(1):175-7.
369. McGaughey GB, Gagne M, Rappe AK. pi-Stacking interactions. Alive and well in proteins. *J Biol Chem.* 1998;273(25):15458-63.
370. Sinnokrot MO, Valeev EF, Sherrill CD. Estimates of the ab initio limit for pi-pi interactions: the benzene dimer. *J Am Chem Soc.* 2002;124(36):10887-93.
371. Pomponi M, Sacchi S, Colella A, Patamia M, Marta M. The role of TRP84 in catalytic power and the specificity of AChE. *Biophys Chem.* 1998;72(3):239-46.
372. Bertoni C, Marta M, Patamia M, Colella A, Pomponi M. Inhibition of AChE: structure-activity relationship among conformational transition of Trp84 and biomolecular rate constant. *J Enzyme Inhib.* 2000;15(6):547-56.
373. Velan B, Barak D, Ariel N, Leitner M, Bino T, Ordentlich A, Shafferman A. Structural modifications of the omega loop in human acetylcholinesterase. *FEBS Lett.* 1996;395(1):22-8.
374. Guedes IA, de Magalhaes CS, Dardenne LE. Receptor-ligand molecular docking. *Biophys Rev.* 2014;6(1):75-87.
375. Mobley DL, Dill KA. Binding of small-molecule ligands to proteins: "what you see" is not always "what you get". *Structure.* 2009;17(4):489-98.

376. McNaught AD, Wilkinson A. Compendium of chemical terminology: International Union of Pure and Applied Chemistry. 2nd ed. Oxford: Blackwell Science 1997.
377. Du X, Li Y, Xia YL, Ai SM, Liang J, Sang P, Ji XL, Liu SQ. Insights into protein-ligand interactions: Mechanisms, models, and methods. *Int J Mol Sci.* 2016;17(2).
378. Thomsen T, Kaden B, Fischer JP, Bickel U, Barz H, Gusztony G, Cervos-Navarro J, Kewitz H. Inhibition of acetylcholinesterase activity in human brain tissue and erythrocytes by galanthamine, physostigmine and tacrine. *Eur J Clin Chem Clin Biochem.* 1991;29(8):487-92.

Appendix I: Ethical approval

The Research Ethics Committee, Faculty Health Sciences, University of Pretoria complies with ICH-GCP guidelines and has US Federal wide Assurance.

- FWA 00022557, Approved dt 22 May 2002 and Expires 29 August 2018.
- IRB 0000 7235 IO-RG000732 Approved dt 22/04/2014 and Expires 22/04/2017.



UNIVERSITEIT VAN PRETORIA
UNIVERSITY OF PRETORIA
YUNIBESITHI YA PRETORIA

Faculty of Health Sciences Research Ethics Committee

24/11/2016

Approval Certificate New Application

Ethics Reference No.: 464/2016

Title: Evaluation of the neurotoxicity of pentachlorophenol and its active metabolites on SH-SY5Y neuroblastoma cells

Dear Miss Desiree Fraser

The **New Application** as supported by documents specific in your cover letter dated 17/10/2016 for your research received on the 17/10/2016, was approved by the Faculty of Health Sciences Research Ethics Committee on its quorate meeting of 23/11/2016.

Please note the following about your ethics approval:

- Ethics Approval is valid for 2 years
- Please remember to use your protocol number (**464/2016**) on any documents or correspondence with the Research Ethics Committee regarding your research.
- Please note that the Research Ethics Committee may ask further questions, seek additional information, require further modification or monitor the conduct of your research.

Ethics approval is subject to the following:

- The ethics approval is conditional on the receipt of **6 monthly written Progress Reports**, and
- The ethics approval is conditional on the research being conducted as stipulated by the details of all documents submitted to the Committee. In the event that a further need arises to change who the investigators are, the methods or any other aspect such changes must be submitted as an Amendment for approval by the Committee.

We wish you the best with your research.

Yours sincerely

Dr R Sommers; MChB, MMed (Int); MPharmD.PhD

Deputy Chairperson of the Faculty of Health Sciences Research Ethics Committee, University of Pretoria

The Faculty of Health Sciences Research Ethics Committee complies with the SA National Act 61 of 2003 as it pertains to health research and the United States Code of Federal Regulations Title 45 and 46. This committee abides by the ethical norms and principles for research, established by the Declaration of Helsinki, the South African Medical Research Council Guidelines as well as the Guidelines for Ethical Research: Principles Structures and Processes, Second Edition 2015 (Department of Health).

☎ 012 356 3084 ✉ deespeka.beheri@up.ac.za / frsethics@up.ac.za 🌐 <http://www.up.ac.za/healthethics>
📍 Private Bag X325, Arcadia, 0007 - Tswelopele Building, Level 4, Room 60, Gazina, Pretoria

Appendix II: Reagents and preparation

2,2'-Azobis(2-amidinopropane) dihydrochloride (AAPH)

AAPH was purchased from Sigma-Aldrich (St. Louis, USA), and a 400 mM stock solution was prepared by dissolving 10.8 mg in 0.1 mL DMSO. Stock was aliquoted and stored at -80°C.

2,7-Dichlorofluorescein diacetate (DCFDA)

DCFDA was purchased from Sigma-Aldrich (St. Louis, USA). A 10 mM stock solution was prepared by dissolving 4.9 mg powder in 1 mL DMSO. Stock was aliquoted and stored at -80°C.

Acetic acid

Glacial acetic acid was purchased from Saarchem (Gauteng, South Africa), and prepared to 1% by adding 10 mL with 1000 mL distilled water.

Acetylthiocholine iodide (ATChI)

Acetylthiocholine iodide was purchased from Sigma-Aldrich (St. Louis, USA). A fresh 15 mM stock was prepared before the start of each experiment by adding 9.8 mg to 2.25 mL water. Powder ATChI was stored at -20°C.

Acetylcholinesterase (AChE)

Acetylcholinesterase from *Electrophorus electricus* (electric eel) type VI-S was purchased from Sigma-Aldrich (St. Louis, USA). A 200 U/mL stock solution was prepared by dissolving 120 µg AChE in 100 µL distilled water. Stock was aliquoted and stored at -20°C.

Annexin V-FITC

Annexin V-FITC stain was purchased in liquid form from Sigma-Aldrich (St. Louis, USA). No dilutions of stock were made.

Annexin V-FITC binding buffer

Annexin V-FITC binding buffer comprised of 10 mM 4-(2-hydroxyethyl)-1-piperazineethanesulfonic acid (Hepes) (pH 7.4), 150 mM NaCl, 5 mM potassium

chloride (KCl), 5 mM MgCl₂.6H₂O and 2,5 mM calcium chloride (CaCl₂), which were purchased from Sigma-Aldrich (St. Louis, USA). The buffer was prepared by dissolving 238.3 mg HEPES, 876.6 mg NaCl, 37.2 mg KCl, 47.6 mg MgCl₂.6H₂O, and 27.7 mg CaCl₂ in 100 mL distilled water. The buffer was adjusted to pH 7.4 using sodium hydroxide (NaOH) and stored at 4°C.

Caspase-3 assay buffer

The caspase-3 assay buffer was prepared from an incomplete assay buffer containing 20 µM HEPES (pH 7.5) and 2 mM ethylenediaminetetraacetic acid (EDTA). For every 10 mL of incomplete assay buffer, 4 µl 2-mercaptoethanol, 100 µl 50 µM phenylmethane sulfonyl fluoride (PMSF) and 5 µl 10 mM caspase-3 substrate was added. These products were purchased from Sigma-Aldrich (St. Louis, USA).

Caspase-3 substrate

N-Acetyl-Asp-Glu-Val-Asp-7-amido-4-Methylcoumarin (Ac-DEVD-AMC) was purchased from Sigma-Aldrich (St. Louis, USA). A 5 mM stock solution was prepared by dissolving 3.4 mg in 1 mL DMSO. Stock was aliquoted and stored at -80°C.

Cell culture medium

Ham's F-12 nutrient mixture and DMEM were purchased from Sigma-Aldrich (St. Louis, USA), and mixed at a 1:1 ratio. The cell culture medium contained 1% antibiotics (fungizone, streptomycin and penicillin G). Medium was supplemented with 10% FCS from The Scientific Group (Gauteng, South Africa) by adding 10 mL FCS for every 90 mL medium.

Dimethyl sulfoxide (DMSO)

DMSO was purchased from Merck Millipore (Darmstadt, Germany), and stored at room temperature.

5,5'-dithiobis(2-nitrobenzoic acid) (DTNB)

A fresh 3 mM DTNB solution was prepared before each experiment by adding 13.4 mg to 11.25 mL of Ellman esterase assay buffer C.

Ellman esterase assay buffers

Three buffers were prepared for the Ellman esterase assay:

- Buffer A: 50 mM Tris-HCl was prepared by dissolving 63.04 mg Tris-HCl in 8 mL distilled water. The buffer was adjusted to pH 8 with hydrochloric acid (HCl).
- Buffer B: Consisted of Buffer A with and added 0.1% bovine serum albumin (BSA) (Sigma-Aldrich (St. Louis, USA)).
- Buffer C: Consisted of buffer A with the following salts added: 0.1 mM NaCl, and 0.02 M MgCl₂.6H₂O. The buffer was prepared by adding 26.9 mg NaCl and 18.7 mg MgCl₂.6H₂O to 4.6 mL buffer A. All buffers were stored at 4°C.

Galanthamine

Galanthamine was purchased from Sigma-Aldrich (St. Louis, USA), and a 25 mM stock solution was prepared by dissolving 7.2 mg powder in 1 mL DMSO. Stock was aliquoted and stored at -20°C.

JC-1 dye (5,5,'6,6'-tetrachloro-1,1,3,3'- tetraethylbenzimidazolylcarbocyanine iodide)

JC-1 dye was purchased from Sigma-Aldrich (St. Louis, USA), and a 5 mg/mL solution prepared by dissolving 5 mg in 1 mL DMSO

Caspase-3 lysis buffer

The caspase-3 lysis buffer was prepared from an incomplete lysis buffer containing 10 mM HEPES (pH 7.5), 2 mM EDTA and 5 mM CHAPS. For every 10 mL of incomplete buffer, 100 µL of 50 mM phenylmethane sulfonyl fluoride (PMSF), and 4 µl 2-mecaptoethanol was added. These products were purchased from Sigma-Aldrich (St. Louis, USA).

Monochlorobimane (MCB)

Monochlorobimane was purchased from Sigma-Aldrich (St. Louis, USA). A 25 mM solution was prepared by dissolving 5 mg powder in 880 µL DMSO, and stored at -80°C

n-Ethylmaleimide (NEM)

n-Ethylmaleimide was purchased from Sigma-Aldrich (St. Louis, USA). A 50 mM solution was prepared by 6.3 mg in 1 mL DMSO. Stock was aliquoted and stored at -80°C.

Phosphate Buffered Saline (PBS)

Phosphate Buffered Saline was prepared from BBL™ FTA hemagglutination powder purchased from BD Biosciences (Le Pont de Claix, France). One litre of distilled water had 9.23 g of the powder added to it.

Pentachlorophenol (PCP)

Pentachlorophenol was purchased from Chem Service (West Chester, USA) Lot: 401-98B. A 100 mM stock solution was prepared by adding 40 mg powder to 1.5 mL of 5% DMSO. Stock was aliquoted into silanized glass tubes and stored at -20°C, shielded from light.

Phenylmethane sulfonyl fluoride (PMSF)

Phenylmethane sulfonyl fluoride was purchased from Sigma-Aldrich (St. Louis, USA). A 100 mM stock solution was prepared by dissolving 17.4 mg in 1 mL DMSO. Stock was aliquoted and stored at -80°C.

Propidium iodide (PI)

Propidium iodide powder was purchased from Sigma-Aldrich (St. Louis, USA). A stock of 100 µg/mL was prepared.

Rotenone

Rotenone was purchased from Sigma-Aldrich (St. Louis, USA), and a 600 µM stock was prepared by dissolving 4.7 mg in 2 mL DMSO. Stock was aliquoted and stored at -20°C.

Staurosporine

Staurosporine was purchased from Sigma-Aldrich (St. Louis, USA), and a 2.14 mM stock solution was prepared by adding 1 mg to 1 mL DMSO.

Sulforhodamine B

Sulforhodamine B stain was purchased from Sigma-Aldrich (St. Louis, USA). A 0.057% solution was prepared by dissolving 57 mg in 100 mL 1% acetic acid.

Tetrachloro-1,4-benzoquinone (TCBQ) (AKA P-Chloranil)

TCBQ was purchased from Sigma-Aldrich (St. Louis, USA). A 100 mM stock solution was prepared by adding 36.9 mg powder to 1.5 mL DMSO. Stock was aliquoted into silanized glass tubes and stored at -20°C, shielded from light.

Tetrachlorohydroquinone (TCHQ)

TCHQ was purchased from Dr Ehrenstorfer, (Augsburg, Germany) via Industrial Analytical (PTY) LTD. A 100 mM stock solution was prepared by adding 37.2 mg powder to 1.5 mL DMSO. Stock was aliquoted into silanized glass tubes and stored at -20°C, shielded from light.

Trichloroacetic acid (TCA)

Trichloroacetic acid was purchased from Merck Millipore (Darmstadt, Germany). A 50% solution was prepared by dissolving 5 g in 10 mL distilled water

Tris-base

Tris-base powder was purchased from Merck Millipore (Darmstadt, Germany) and, for the purpose of the SRB assay, a solution was prepared by dissolving 2.42 g powder in a litre of distilled water

TrypLE Express Enzyme

TrypLE Express enzyme was purchased as a liquid from Thermo Fisher Scientific (Massachusetts, United States). No dilutions were performed.